Coherence approach to neutron propagation in spin echo instruments

V.-O. de Haan

Cover photograph:

Interference pattern of a wave traveling to the right through two small openings at a distance of 10 wavelengths.

CIP-DATA KONINKLIJKE BIBLIOTHEEK, DEN HAAG

Haan, V.-O. de

Coherence approach to neutron propagation in spin echo instruments

Delft: Department Radiation, Radionuclides & Reactors,
Faculty of Applied Sciences,
Delft University of Technology, Mekelweg 15,
2629 JB Delft, The Netherlands

Puttershoek: BonPhysics Research and Investigations B.V.
Laan van Heemstede 38 · P.O. Box 5629,
3297 ZG Puttershoek, The Netherlands

Publication: BonPhysics Research and Investigations B.V. - With ref.
ISBN 978-90-811708-1-9

NUR 926 Experimentele natuurkunde
Subject headings: neutrons; coherence; propagation; small angle neutron scattering; neutron reflectometry; spin echo technique; polarization analysis.

To Lisette Anna,

Esther Petra and Jan Joost,

with love

The White Queens Riddle

'First, the fish must be caught.'
That is easy: a baby, I think, could have caught it.
'Next, the fish must be bought.'
That is easy: a peny, I think, would have bought it.

'Now cook me the fish!'
That is easy, and will not take more than a minute.
'Let it lie in a dish!'
That is easy, because it already is in it.

'Bring it here! Let me sup!'
It is easy to set such a dish on the table.
'Take the dish-cover up!'
Ah! that *is so hard that I fear I'm unable!*

For it holds it like glue -
Holds the lid to the dish, while it lies in the middle:
Which is easiest to do,
Un-dish-cover the fish, or dishcover the riddle?

from: *Through the Looking Glass*
and what Alice found there.

Lewis Carrol, 1896

Contents

Fundamental Constants

symbol	description	quantity[†]	unit
N_a	Avogadro constant	$6.0221415(10) \times 10^{23}$	mol^{-1}
k_B	Boltzmann constant	$1.3806505(24) \times 10^{-23}$	JK^{-1}
e	elementary charge	$1.60217653(14) \times 10^{-19}$	C
g_r	gyro magnetic ratio neutron	$-1.91304273(45)$	
m	neutron mass	$1.67492728(29) \times 10^{-27}$	kg
μ_N	nuclear magneton	$5.05078343(43) \times 10^{-27}$	JT^{-1}
μ_o	permeability of vacuum	$4\pi \times 10^{-7}$	NA^{-2}
h	Planck constant	$6.6260693(11) \times 10^{-34}$	Js
$\hbar$	Planck constant divided by 2π	$1.05457168(18) \times 10^{-34}$	Js

[†] Source: Reviews of Modern Physics **77** (2005) 1-107.

Glossary

A_0	source area or aperture	10
A_b	beam area or aperture	67
A_d	detector area or aperture	11
A_s	sample area or aperture	11
$C(x,z)$	height-height correlation function of sample surface	105
D_y	width detector diaphragm in y-direction	55
D_z	width detector diaphragm in z-direction	55
$G(\vec{r},t)$	time-dependent Green function	5
$G^{(+)}(\vec{r},\vec{r}_s)$	specialized (potential dependent) Green function	16
$G_0(\vec{r})$	Green function for a monochromatic free particle	9
$G_c(y,z)$	two dimensional correlation function	23
$G_r(\vec{r})$	sample correlation function	23
$G_s(\vec{r})$	sample correlation function	17
$G_{s,d}(\vec{r})$	diffuse component of sample correlation function	65
$G_{s,s}(\vec{r})$	specular component of sample correlation function	65
H	height diaphragm above sample surface	55
$H(x,z)$	height of the surface above the xz-plane	105
H_d	height detector diaphragm above sample surface	55
I_d	detector count rate	11
$J_0(\vec{r})$	isotropic neutron source flux	10
P_A	polarizing power of analyser	38
P_P	polarizing power of polarizer	38
$R(p_y)$	reflectivity scattered beam	74
$R^{FT}(\vec{q})$	Momentum space instrumental resolution function	18
$R_{out}(\vec{r}_1,\vec{r}_2)$	Real space instrumental resolution function	17
$S(\vec{r})$	extra phase shift acquired due to the material properties of the sample	20
$S_d(\vec{q})$	diffuse component of sample structure factor	65
$S_k(\vec{q})$	sample structure factor	18
$S_s(\vec{q})$	specular component of sample structure factor	65
$T(k_y)$	transmission factor incident beam	74
$T(p_y)$	transmission factor scattered beam	74

T_A	neutron transmission of analyser	38
T_P	neutron transmission of polarizer	38
$V(\vec{r})$	complex optical potential	7
$V^{(0)}(y)$	potential of smooth surface	69
$V^{(1)}(\vec{r})$	potential due to interface roughness or structure	69
W_y	width diaphragm in y-direction	55
W_z	width diaphragm in z-direction	55
$W_{in}(\vec{r}_s, \vec{k})$	wavevector distribution of incident beam	73
$W_{sc}(\vec{r}_s, \vec{k})$	wavevector distribution of scattered beam	80
$\Gamma(\vec{r}_1, \vec{r}_2, \tau)$	mutual coherence function	4
$\Gamma_0(\vec{r}_1, \vec{r}_2, \tau)$	mutual coherence function for the non-magnetic wave function	33
$\Gamma_{in}(\vec{r}_1, \vec{r}_2, \tau)$	mutual coherence function of direct beam	17
$\Gamma_{sc}(\vec{r}_1, \vec{r}_2, \tau)$	mutual coherence function of scattered beam	17
$\Psi(\vec{r})$	time-independent part of wave function	15
$\Psi(\vec{r}, t)$	neutron wave function at point $\vec{r}$ at time t	3
$\Psi_{in}(\vec{r})$	channel state or incident-wave function	15
$\Psi_{sc}(\vec{r})$	scattered state or scattered-wave function	15
$\gamma(\vec{r}_1, \vec{r}_2, \tau)$	complex degree of coherence	4
$\gamma_H(\vec{r})$	van Hove contrast correlation function	19
$\gamma_{2D}(y, z)$	projection of the scattering length density	23
ω_k	frequency of neutron function or total energy divided by $\hbar$	3
$\phi(\vec{r'}, \vec{r})$	extra phase acquired due to the interaction with the magnetic flux density	35
$\psi_{\vec{k}}(\vec{r})$	neutron wave function at point $\vec{r}$ with wavevector $\vec{k}$	3
$\psi_{sc}^{(0)}(\vec{k}, \vec{r})$	undisturbed scattered-wave function from the perfectly flat sample surface	70
$\psi_{sc}^{(1)}(\vec{k}, \vec{r})$	scattered-wave function from the surface structure or roughness	70
$\rho(\vec{r})$	neutron density	3
$\rho(q)$	transmission amplitude	63
$\rho_b(\vec{r})$	scattering length density	19
σ	surface roughness	105
τ	time difference between two events	4
$\tau(q)$	reflection amplitude	63
$\vec{B}(\vec{r})$	magnetic flux density	33
$\vec{J}(\vec{r})$	neutron flux or current density	3
$\vec{P}(\vec{r})$	polarization vector	32
$\vec{p}$	wavevector of the scattered neutron	71
$\vec{r}_d$	position of detector	11
$\vec{r}_s$	position of sample	11

$\vec{r}_{s0}$	average position of sample	11
$\widehat{\Gamma}(\vec{r}_1, \vec{r}_2, \tau)$	2×2 coherence matrix	32
$\widehat{\gamma}_B(\vec{r}_1, \vec{r}_2, \tau)$	reduced coherence matrix	33
l_c	longitudinal coherence length	5
l_{se}	spin echo length	46
$n(x, y, z)$	local refraction index	19
r_c	coherence length	5
$t_c(\vec{r})$	coherence time	4
v_p	phase velocity	3
$g(p_y, y, y_s)$	one-dimensional Green function perpendicular to the surface	111
$\bar{k}$	average length of wavevector	3
$\vec{k}$	wavevector or propagation vector	3
k	length of wavevector or propagation vector	3
k'_y	y component in the sample material of the wavevector of the incident neutron	71
k_c	critical wavevector	20
k_y	y component of the wavevector of the incident neutron	71
$\bar{\lambda}$	average wavelength	3
λ	wavelength	3
p'_y	y component in the sample material of the wavevector of the scattered neutron	71
p_y	y component of the wavevector of the scattered neutron	71
$\vec{Q}$	wavevector transfer	72, 115
κ_y	wavevector transfer inside the sample	74
$\vec{q}$	wavevector transfer	18

Preface

Delft University of Technology participates in a project for instrument development at the second target station of the neutron spallation source ISIS, Rutherford Appleton Laboratory. This project consists of the construction of a neutron reflectometer *OffSpec*, optimized for off-specular neutron scattering. Delft is responsible for the development and implementation of spin-echo angular labeling to determine the off-specular reflection, which in turn yields information about in-plane inhomogeneities. This novel technique, developed in Delft, is already successfully applied in spin echo small-angle neutron scattering (SESANS).

In contrast to conventional off-specular methods, where experiments are performed in reciprocal space, the spin-echo method probes directly in real space (on length scales from approximately 50 nm to 50 μm). The main object of this book will be the theoretical description and interpretation of small angular neutron scattering and off-specular reflection in real space as obtained by the spin echo technique.

Chapter 1

Introduction

When general properties are assigned to functions governed by a wave equation, coherence theory can be applied. Then, it is possible to find general formulations for the propagation of wave functions despite their physical background might be different. Coherence theory is widely used in optical [1] scattering phenomena but is still fairly new in X-ray [2], [3], [4] or neutron scattering. Textbooks briefly discuss the coherence properties of neutron beams [5] but do not apply it to neutron scattering. Rauch and collaborators [6] are using the results of coherence theory to explain their neutron-interferometry measurements.

Recently Gähler used a space-time approach to derive the neutron scattering formulas for many body systems [7] in the kinematic approximation. In the following this approach is followed and extended to the phase-object approximation [8] and neutron reflectometry. Here, it is assumed that all wave functions are *statistically stationary* (an ensemble average is independent of the origin of time) and ergodic (an ensemble average is time-independent and equal to a time average) [1] and only second-order coherence effects are discussed. Further coherence theory is used to describe neutron polarization effects [9] and the way a polarized beam is transported through an instrument. This enables a coherent approach to these effects without the need for some ad-hoc definition on beam polarization and analysis.

Coherence theory can be interpreted as a shorthand notation for the description of ensemble averages of wave functions and their (mathematical) properties. In general coherence theory does not give new insight in the involved physics. Worse, it complicates the classical view of a neutron as a small magnet moving through the instrument performing Larmor precession in magnetic flux density regions. However, it gives possibilities to apply insight from one field of physics to another. The main advantage of coherence theory is that it gives the possibility to calculate the results of the propagation of the wave function through the instrument directly. No ad-hoc folding of theoretical results with instrumental resolution is needed, but direct computation of measurable data is possible. Coherence theory seems to be quite complicated and unnecessary to describe the neutron propagation through an instrument. But after getting used to the concepts of the mutual coherence function and the way this function is propagated through free-space and space with magnetic flux density it can give a more thorough account of the important effects before and after the scattering process.

Chapter 2

Coherence theory

2.1 Definitions

Let $\Psi(\vec{r},t)$ denote a neutron wave function characterizing the field at point $\vec{r}$ at time t. For a realistic neutron source it will be a fluctuating function of time and may be regarded as a typical member of an ensemble consisting of all possible neutron generating events. It consists of a large number of Fourier components independent of each other, so that their superposition gives rise to a fluctuating field only describable in statistical terms. For a statistically stationary beam it can be constructed from its constituting monochromatic waves:

$$\Psi(\vec{r},t) = \int \psi_{\vec{k}}(\vec{r}) e^{-i\omega_k t} d^3k, \tag{2.1}$$

where $\vec{k}$ is the *wavevector* or *propagation vector*, $\omega_k = v_p k$ where $v_p = \hbar k/2m$ equals the *phase velocity*[1] of the wave function and m equals the neutron mass. Note that $\hbar\omega_k$ is determined by the total energy of the neutron (the sum of kinetic and potential energy) and is constant for a statistically stationary beam. The wavevector is related to the wavelength, λ of the neutron wave by $k = 2\pi/\lambda$. Statistical stationarity is related to the frequency, ω_k of the neutrons wave function. Hence, processes with relevant time constants much larger than ω_k^{-1} can still be treated.

Knowing the wave function, the neutron density can be calculated by:

$$\rho(\vec{r}) = \left\langle \Psi^*(\vec{r},t)\Psi(\vec{r},t) \right\rangle_t, \tag{2.2}$$

where $\langle x(t) \rangle_t$ denotes the time average of $x(t)$ and X^* the complex conjugated value of the function X. The neutron flux (or neutron current density) is given by

$$\vec{J}(\vec{r}) = \Re\left\{ \left\langle \Psi^*(\vec{r},t) \frac{\hbar}{im} \vec{\nabla} \Psi(\vec{r},t) \right\rangle_t \right\}, \tag{2.3}$$

where $\Re\{a\}$ denotes the real part of a.

[1] The phase velocity is the velocity at which a *phase change* is propagated through the medium. For light this is the speed of light, which in vacuum does not depend on the wavelength of the waves. For neutrons, the phase velocity is inversely proportional to the wavelength and half of the velocity of a classical neutron. In a medium it is determined by the neutron scattering properties of the constituting particles.

When the wave function is quasi monochromatic, for instance a Gaussian distribution with an average wavevector of $\bar{k}$ and an effective spread of Δk :

$$\psi_{\vec{k}}(\vec{r}) = \hat{\psi}\frac{e^{-(k-\bar{k})^2/2\Delta k^2}}{\Delta k\sqrt{2\pi}}e^{i\vec{k}\cdot\vec{r}}, \tag{2.4}$$

equation (2.3) reduces to:

$$\vec{J}(\vec{r}) = 2\vec{v}_p\rho(\vec{r}), \tag{2.5}$$

where $\vec{v}_p = \vec{k}v_p/\bar{k}$. Note that this equation holds exactly only for a beam in the direction $\vec{v}_p$. If the divergence of the beam becomes too large this approximation is not allowed. The time dependence of the density and the flux disappears as only statistically stationary fields are taken into account. Further it is assumed that all fields are ergodic, indicating that time average and ensemble average yield the same results.

The neutron density itself is not sufficient to describe the field completely, since it does not contain information on the propagation of the waves. Therefore the *mutual coherence function* is introduced and defined as:

$$\Gamma(\vec{r}_1, \vec{r}_2, \tau) = \langle \Psi^*(\vec{r}_1, t)\Psi(\vec{r}_2, t+\tau)\rangle_t \,. \tag{2.6}$$

It represents the correlation between the field at a point $\vec{r}_1$ and the complex conjugated field at a point $\vec{r}_2$ at time moments t and $t+\tau$ respectively. As the considered field is statistically stationary the ensemble average is independent of time t and only the time difference between two point influences the mutual coherence. Note that the density of the wave function can be determined from the mutual coherence function as:

$$\rho(\vec{r}) = \Gamma(\vec{r}, \vec{r}, 0). \tag{2.7}$$

The mutual coherence function can be normalized resulting in the *complex degree of coherence*:

$$\gamma(\vec{r}_1, \vec{r}_2, \tau) = \frac{\Gamma(\vec{r}_1, \vec{r}_2, \tau)}{\sqrt{\rho(\vec{r}_1)\rho(\vec{r}_2)}}. \tag{2.8}$$

It can be shown [1] that $|\gamma(\vec{r}_1, \vec{r}_2, \tau)| \leq 1$.

2.2 Coherence time and lengths

The coherence time, t_c of a wave function is a measure of the time interval in which appreciable amplitude and wave correlations of the wave function at a particular point P in a fluctuating field will persist. The mutual coherence function can be used to define the coherence time of a wave function. A definition of the coherence time [1] can be:

$$t_c(\vec{r})^2 = \frac{\int_{-\infty}^{\infty}\tau^2\left|\Gamma(\vec{r}, \vec{r}, \tau)\right|^2 d\tau}{\int_{-\infty}^{\infty}\left|\Gamma(\vec{r}, \vec{r}, \tau)\right|^2 d\tau}. \tag{2.9}$$

For a quasi-monochromatic beam the coherence time can be related to the effective spectral width of the wave function at point P:

$$t_c \geq \frac{1}{2\Delta k v_p}, \tag{2.10}$$

where the equal sign holds for a Gaussian distribution. This definition of coherence time is useful when the wave function is quasi-monochromatic and the spectrum has a single reasonable well-defined peak. In other situations other definitions can be applied [1].

In non-dispersive media[2] (and statistically stationary fields) the temporal coherence can be expressed in terms of the spatial coherence $\Gamma(\vec{r}, \vec{r'}, 0)$ [1]:

$$\Gamma(\vec{r}, \vec{r}, \tau) = \int \Gamma(\vec{r}, \vec{r'}, 0) G(\vec{r} - \vec{r'}, \tau) d\vec{r'}, \tag{2.11}$$

where $G(\vec{r}, t)$ is the time-dependent Green function:

$$G(\vec{r}, t) = \frac{1}{(2\pi)^2} \int e^{i(\vec{k}\cdot\vec{r} - k v_p t)} d\vec{k}. \tag{2.12}$$

This means that under such conditions the coherence time is related to the longitudinal coherence length, l_c which is the distance traveled by the wave function during the coherence time. As the neutron phase velocity depends on the neutron wavelength this limits the applicability of general coherence theory to quasi-monochromatic beams. For a quasi monochromatic wave function the phase velocity can be taken constant, so the longitudinal coherence length is given by:

$$l_c = v_p t_c \geq \frac{1}{2\Delta k} = \frac{\bar{\lambda}^2}{4\pi\Delta\lambda}, \tag{2.13}$$

where $\bar{\lambda}$ is the average wavelength of the wave function and $\Delta\lambda$ the effective wavelength spread equal to $\Delta k \bar{\lambda}^2 / 2\pi$.

The general coherence length, r_c can be defined in a similar way as the coherence time, but this does not lead to a finite value for the coherence length at some distance from a pure incoherent source. In this case one can define the coherence length as:

$$r_c(\vec{r}) = \frac{\int_{-\infty}^{\infty} |r_1| \left|\Gamma(\vec{r}, \vec{r} + \vec{r}_1, 0)\right|^2 dr_1}{\int_{-\infty}^{\infty} \left|\Gamma(\vec{r}, \vec{r} + \vec{r}_1, 0)\right|^2 dr_1}. \tag{2.14}$$

Note that the term *longitudinal* applies to the direction of the propagation of the wave function. Only if the wave function can be regarded as a beam the term becomes useful. However, one must keep in mind the conceptual difference between the longitudinal coherence length as derived from the time dependence of the mutual coherence function and the general coherence length as derived from the spatial dependence of the mutual coherence function. In a directed quasi-monochromatic statistically stationary wave function the longitudinal coherence length is the same as the general coherence length taken along the beam direction. Then the general coherence lengths in directions perpendicular to the beam are referred to as *transversal* coherence lengths.

[2] A non-dispersive medium, is a medium in which the phase velocity does not depend on the wavelength of the wave function. Here, it is assumed that for quasi monochromatic neutron beams this condition is full-filled.

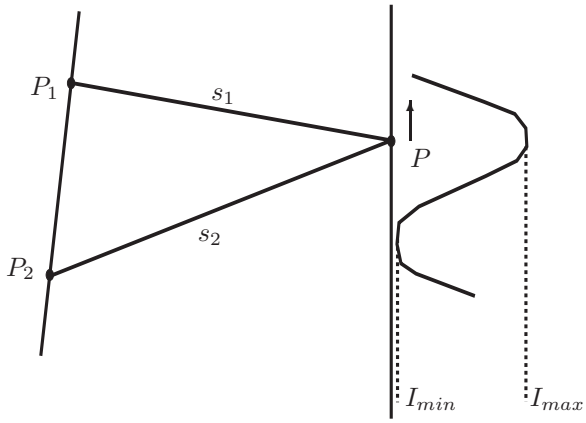

Figure 2.1: Visibility of interference fringes illustrated with the help of a two-beam interference experiment.

2.3 Visibility of fringes

The modulus of the complex degree of coherence can be understood as the visibility of the fringes created by two points P_1 and P_2 as shown in figure 2.1. Scanning the screen with point P the intensity of the sum of the wave functions expanding from points P_1 and P_2 varies between a maximum (I_{max}) and minimum (I_{min}) value. The visibility defined by Michelson in 1890 [10] is given by:

$$v = \frac{I_{max} - I_{min}}{I_{max} + I_{min}} = \frac{2\sqrt{\rho(\vec{r}_1)\rho(\vec{r}_2)}}{\rho(\vec{r}_1) + \rho(\vec{r}_2)} \left|\gamma(\vec{r}_1, \vec{r}_2, \tau)\right| . \tag{2.15}$$

τ can be interpreted as the phase traveling-time difference for path P_1P (s_1) and P_2P (s_2) equal to $(s_1 - s_2)/v_p$. In the extreme case that $v = 1$, the average intensity around any point P in the fringe pattern undergoes the greatest possible variation. This represents *complete coherence*. In the other extreme case $v = 0$, no interference fringes are formed at all. This is called *complete incoherence*. The intermediate values $0 < v < 1$ represent *partial coherence*. The phase of the complex degree of coherence determines the exact position of the minima and maxima of the intensity while scanning with P.

The complex degree of coherence is associated with points P_1 and P_2 of the wave function. It can be interpreted as the effective retardation of the wave function as P_1 with respect to the wave function at P_2. The complex degree of coherence contains an ambiguity, as also $s_1 - s_2$ influences the value. However, when the wave function is quasi-monochromatic and τ is restricted to a small enough range of values which is usually the case, this influence can be approximated by

$$\gamma(\vec{r}_1, \vec{r}_2, \tau_1) \approx \gamma(\vec{r}_1, \vec{r}_2, \tau_2) e^{-i\bar{k}v_p(\tau_1 - \tau_2)} \tag{2.16}$$

and

$$\Gamma(\vec{r}_1, \vec{r}_2, \tau_1) \approx \Gamma(\vec{r}_1, \vec{r}_2, \tau_2) e^{-i\bar{k}v_p(\tau_1 - \tau_2)}, \tag{2.17}$$

under the condition that

$$|\tau_1 - \tau_2| << t_c. \tag{2.18}$$

Over a τ range satisfying this condition γ and also Γ are periodic in τ with a period equal to the mid period $2\pi/\bar{k}v_p$ of the wave function.

2.4 Propagation of mutual coherence function

It can be shown [1] that the mutual coherence function is subject to the same differential equation as the wave function itself, with respect to co-ordinates $\vec{r}_1$ and $\vec{r}_2$. The time-dependent Schrödinger equation [5],

$$i\hbar\frac{\partial\Psi(\vec{r},t)}{\partial t} = -\frac{\hbar^2}{2m}\nabla^2\Psi(\vec{r},t) + V(\vec{r})\Psi(\vec{r},t), \tag{2.19}$$

where $V(\vec{r})$ is the complex optical potential, can directly be used to calculate that

$$\nabla_1^2\Gamma(\vec{r}_1,\vec{r}_2,\tau) = -i\frac{2m}{\hbar}\frac{\partial\Gamma(\vec{r}_1,\vec{r}_2,\tau)}{\partial\tau} + \frac{2mV^*(\vec{r}_1)}{\hbar^2}\Gamma(\vec{r}_1,\vec{r}_2,\tau), \tag{2.20}$$

and

$$\nabla_2^2\Gamma(\vec{r}_1,\vec{r}_2,\tau) = -i\frac{2m}{\hbar}\frac{\partial\Gamma(\vec{r}_1,\vec{r}_2,\tau)}{\partial\tau} + \frac{2mV(\vec{r}_2)}{\hbar^2}\Gamma(\vec{r}_1,\vec{r}_2,\tau), \tag{2.21}$$

where ∇_j^2 is the Laplace operator taken with respect to the point $\vec{r}_j$. Under the conditions of a quasi-monochromatic beam as introduced in the previous section:

$$\Gamma\left(\vec{r}_1,\vec{r}_2,\tau\right) = \Gamma(\vec{r}_1,\vec{r}_2,0)e^{-i\bar{k}v_p\tau} \tag{2.22}$$

then

$$\frac{\partial\Gamma(\vec{r}_1,\vec{r}_2,\tau)}{\partial\tau} = -iv_p\bar{k}\Gamma(\vec{r}_1,\vec{r}_2,\tau), \tag{2.23}$$

so that the wave equations reduce to:

$$\nabla_1^2\Gamma(\vec{r}_1,\vec{r}_2,\tau) = \left(\frac{2mV^*(\vec{r}_1)}{\hbar^2} - \bar{k}^2\right)\Gamma(\vec{r}_1,\vec{r}_2,\tau), \tag{2.24}$$

and

$$\nabla_2^2\Gamma(\vec{r}_1,\vec{r}_2,\tau) = \left(\frac{2mV(\vec{r}_2)}{\hbar^2} - \bar{k}^2\right)\Gamma(\vec{r}_1,\vec{r}_2,\tau). \tag{2.25}$$

2.5 Propagation in free space

The solution of equations (2.20) and (2.21) in free space ($V(\vec{r}) = 0$) when the mutual coherence function propagates into the half-space $x > 0$ yields the coherence propagation law. It can be derived by applying the Rayleigh diffraction formula of the first kind to the wave function. The Rayleigh diffraction formula just describes the wave function in the half-space $x > 0$ given its value and derivative at $x = 0$. Hence, it does not really describe a propagation. It is just a solution of the wave equation with the correct boundary conditions. However, within certain limits, the solution of a wave equation can be understood as the propagation of a ray [5].

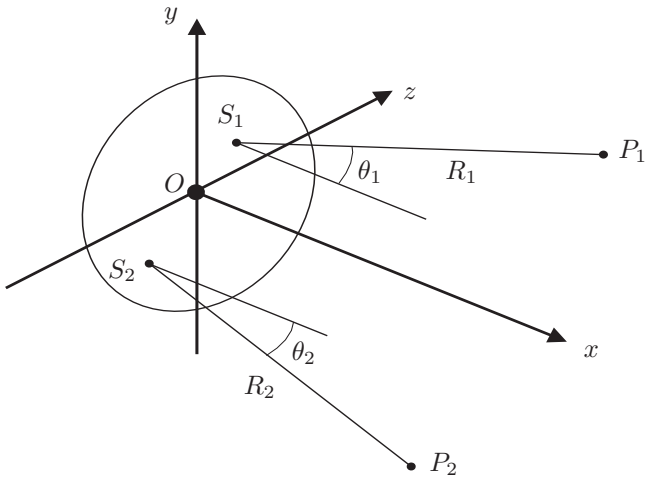

Figure 2.2: Notation relating to the propagation of the mutual coherence from plane $x = 0$ into the half-space $x > 0$.

Applying the definition of the mutual coherence function [1] and using the Rayleigh diffraction formula twice, the propagation of the mutual coherence function can be described by:

$$\Gamma(\vec{r}_1, \vec{r}_2, \tau) = \frac{1}{4\pi^2} \int\int_{x=0} \frac{\cos\theta_1 \cos\theta_2}{R_1^2 R_2^2} \wp\Gamma\left(\vec{r_1'}, \vec{r_2'}, \tau - \frac{R_2 - R_1}{v_p}\right) d^2r_1' d^2r_2', \quad (2.26)$$

where $\wp$ is the differential operator

$$\wp = 1 + \frac{R_2 - R_1}{v_p}\frac{\partial}{\partial\tau} - \frac{R_1 R_2}{v_p^2}\frac{\partial^2}{\partial\tau^2}. \quad (2.27)$$

The integral is taken over points $\vec{r_1'}$ and $\vec{r_2'}$ of plane $x = 0$, $\vec{R}_i = \vec{r}_i - \vec{r_i'}$ and θ_i is the angle between the line $P_i S_i$ and the x-axis as shown in figure 2.2. Under the conditions of a quasi-monochromatic beam:

$$\Gamma\left(\vec{r_1'}, \vec{r_2'}, \tau - \frac{R_2 - R_1}{v_p}\right) = \Gamma(\vec{r_1'}, \vec{r_2'}, \tau) e^{i\bar{k}(R_2 - R_1)}, \quad (2.28)$$

$$\frac{\partial\Gamma(\vec{r_1'}, \vec{r_2'}, \tau)}{\partial\tau} = -iv_p\bar{k}\Gamma(\vec{r_1'}, \vec{r_2'}, \tau) \quad (2.29)$$

and

$$\frac{\partial^2\Gamma(\vec{r_1'}, \vec{r_2'}, \tau)}{\partial\tau^2} = -v_p^2\bar{k}^2\Gamma(\vec{r_1'}, \vec{r_2'}, \tau). \quad (2.30)$$

If further $R_i >> 2\pi/\bar{k}$ then the first two terms of the differential operator can be neglected and equation (2.26) reduces to:

$$\Gamma(\vec{r}_1, \vec{r}_2, \tau) = \int\int_{x=0} \frac{\cos\theta_1 \cos\theta_2 e^{i\bar{k}(R_2 - R_1)}}{R_1 R_2 \bar{\lambda}^2} \Gamma(\vec{r_1'}, \vec{r_2'}, \tau) d^2r_1' d^2r_2'. \quad (2.31)$$

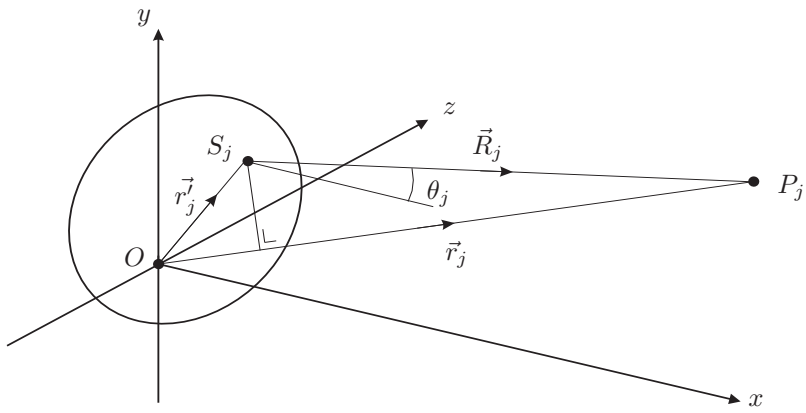

Figure 2.3: Illustrating the notation relating to the far-zone form of the propagation law.

One should realize that the propagated mutual coherence function is calculated by two integrals. One can be interpreted as the propagation of the incident-wave function reaching point $\vec{r}_1$ integrated over the source-wave function at $\vec{r'}_1$. The other integral does the same for the incident-wave function reaching point $\vec{r}_2$ from $\vec{r'}_2$. This can be stressed by re-writing the above integral as:

$$\Gamma(\vec{r}_1, \vec{r}_2, \tau) = 4\bar{k}^2 \int\int_{x=0} \cos\theta_1 \cos\theta_2 G_0(\vec{R}_1)^* G_0(\vec{R}_2) \Gamma(\vec{r'_1}, \vec{r'_2}, \tau) d^2r'_1 d^2r'_2, \quad (2.32)$$

where again $\vec{R}_i = \vec{r}_i - \vec{r'_i}$ and

$$G_0(\vec{r}) = \frac{e^{i\bar{k}r}}{4\pi r} \quad (2.33)$$

is the Green function for a monochromatic free particle with wavevector $\bar{k}$, describing the propagation of a converging spherical wave in vacuum toward the origin at $\vec{r} = 0$ in each half-space ($x > 0$ and $x < 0$). The complex conjugated Green function describes the propagation of a diverging spherical wave in vacuum from the origin. Note that the Green function is only applicable for $r >> \bar{\lambda}$ (see also appendix D). The cosine factors represent the fact that the solid angle in the field of vision of the observer of a surface area when seen under an angle scales with the cosine of that angle.

In most cases of practical interest the points P_1 and P_2 are situated in the *far-zone* of the source as illustrated in figure 2.3. As previously $\vec{R}_j = \vec{r}_j - \vec{r'_j}$ and $\cos\theta_j = \vec{r}_j \cdot \vec{e_x}/R_j$, where $\vec{e_x}$ is the unit vector in the x-direction. In the far-zone $\cos\theta_1 \approx \cos\theta_2$, $R_j \approx r_j - \vec{r}_j \cdot \vec{r'_j}/r_j$ so that:

$$R_2 - R_1 = r_2 - r_1 - r_{12}, \quad (2.34)$$

where $r_{12} = \vec{r}_2 \cdot \vec{r'_2}/r_2 - \vec{r}_1 \cdot \vec{r'_1}/r_1$. Also R_j can be replaced by r_j in the cosine factor and in the denominator of equation (2.31), giving

$$\Gamma(\vec{r}_1, \vec{r}_2, \tau) = \frac{\cos\theta_1 \cos\theta_2 e^{i\bar{k}(r_2 - r_1)}}{r_1 r_2 \bar{\lambda}^2} \int\int_{x=0} e^{-i\bar{k}r_{12}} \Gamma(\vec{r'_1}, \vec{r'_2}, \tau) d^2r'_1 d^2r'_2. \quad (2.35)$$

This equation enables the calculation of the propagation of the mutual coherence function from neutron source to sample and from sample to detector.

2.6 Propagation from source to sample

A typical neutron source consists of unrelated neutron generating events and limiting the case to statistically stationary phenomena the mutual coherence function at the source position ($x = 0$) is given by [1]:

$$\Gamma(\vec{r_1'}, \vec{r_2'}, \tau) = \frac{1}{2v_p} \frac{J_0(\vec{r_1'})}{4\pi} \bar{\lambda}^2 \delta^{(2)}(\vec{r_1'} - \vec{r_2'}) e^{-i\bar{k}v_p\tau}, \tag{2.36}$$

where $J_0(\vec{r})$ is the isotropic neutron source flux in neutrons per second per squared meter at $\vec{r}$. $\delta^{(2)}(\vec{r})$ is the two-dimensional Dirac-delta function, expressing the mutually uncorrelated source elements. The normalization factors are introduced to transform the neutron flux to the density of the wave function. Although this is an idealization it will hold if the correlations extends only over distances of the same order as the neutron wavelength and the source dimensions are much larger. Substituting this in equation (2.35) yields for the mutual coherence function

$$\Gamma(\vec{r}_1, \vec{r}_2, \tau) = \frac{1}{2v_p} \frac{e^{i\bar{k}(r_2 - r_1 - v_p\tau)} \cos\theta_1 \cos\theta_2}{4\pi r_1 r_2} \int_{x=0} e^{-i\vec{q}_{12}\cdot\vec{r'}} J_0(\vec{r'}) d^2r' \tag{2.37}$$

and for the complex degree of coherence

$$\gamma(\vec{r}_1, \vec{r}_2, \tau) = e^{i\bar{k}(r_2 - r_1 - v_p\tau)} \frac{\int_{x=0} e^{-i\vec{q}_{12}\cdot\vec{r'}} J_0(\vec{r'}) d^2r'}{\int_{x=0} J_0(\vec{r'}) d^2r'}, \tag{2.38}$$

where $\vec{q}_{12} = \bar{k}\left(\frac{\vec{r}_2}{r_2} - \frac{\vec{r}_1}{r_1}\right)$. If the source intensity is constant over some aperture the integral over $x = 0$ is limited to the area A_0 of the source and the integral containing the exponential in equation (2.38) reduces to a shape transform of the aperture:

$$\gamma(\vec{r}_1, \vec{r}_2, \tau) = e^{i\bar{k}(r_2 - r_1 - v_p\tau)} \frac{\int_{A_0} e^{-i\vec{q}_{12}\cdot\vec{r'}} d^2r'}{A_0}. \tag{2.39}$$

This equation can be used to calculate the transversal coherence length at a distance L of a circular homogeneous completely incoherent quasi-monochromatic source with radius a with it surface perpendicular to the x-axis. Then $\vec{r}_1 = (L, y_1, z_1)^{\mathrm{T}}$, $\vec{r}_2 = (L, y_2, z_2)^{\mathrm{T}}$ and the above becomes:

$$\gamma(\vec{r}_1, \vec{r}_2, \tau) = e^{i\bar{k}(r_2 - r_1 - v_p\tau)} \frac{2\mathrm{J}_1(\nu)}{\nu}, \tag{2.40}$$

where $\nu = \bar{k}ar/L$ and $r = \sqrt{(y_2 - y_1)^2 + (z_2 - z_1)^2}$ the distance between the two points. The amplitude of this function is shown in figure 2.4. Using this result in equation (2.14) yields:

$$r_c = \frac{L}{\bar{k}a} \frac{\int_0^\infty u^{-1}\mathrm{J}_1(u)^2 du}{\int_0^\infty u^{-2}\mathrm{J}_1(u)^2 du}, \tag{2.41}$$

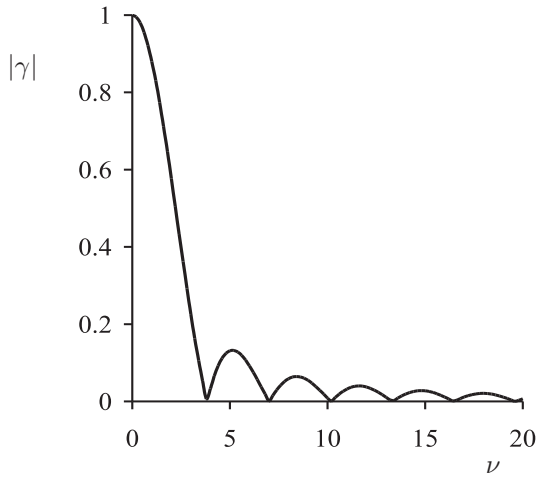

Figure 2.4: Amplitude of the normalized mutual coherence function or complex degree of coherence, $|\gamma|$ as function of the normalized distance, ν (see text).

so that

$$r_c = \frac{L}{\bar{k}a}\frac{3\pi}{8} \approx 1.178\frac{L}{\bar{k}a}. \tag{2.42}$$

If the source area is 1 mm^2 and the distance is 4 m then the coherence length for 0.2 nm neutrons is about 250 nm. Sometimes the transversal coherence length is defined as the distance over which the modulus of the complex degree of coherence is reduced from its maximum value 1 for r=0 to 0.88 at $r = r_c$. This value is reached for $\nu = 1$, hence $r_c = L/\bar{k}a$. Another possibility is to use the first zero of J_1 for $\nu = 3.83$ as a measure for the coherence length. All definitions are a bit different from each other, but clearly have the same order of magnitude.

This example helps to understand, how it is possible to create a (partly) coherent neutron beam from a (purely) incoherent source. The coherence length increases as the distance from the source increases. Hence, the limited size of the source and the distance between source and observation point creates the partly coherent beam. If the source would not be limited (viz. $a \to \infty$) the neutrons emerging from this source never would become (partly) coherent. Hence, the propagation of the radiation from a finite size source is a sufficient condition to create partly coherent beams.

2.7 Propagation from sample to detector

In the detector the count rate is determined as an integral of the neutron flux $\vec{J}(\vec{r}_d)$ over the detector area, A_d at a position $\vec{r}_d$:

$$I_d = \int_{A_d} \vec{J}(\vec{r_d}) \cdot \vec{n}_{A_d} d^2 r_d, \tag{2.43}$$

where $\vec{n}_{A_d}$ is a unit vector perpendicular to the detector area. Using equations (2.5) and (2.7) and assuming $\vec{v}_p \cdot \vec{n}_{A_d} = v_p$ this reduces to:

$$I_d = 2v_p \int_{A_d} \Gamma(\vec{r_d}, \vec{r_d}, 0) d^2 r_d. \tag{2.44}$$

Assume that the whole sample is in the half-space $x < 0$, then the mutual coherence function at $x = 0$ is propagated to the detector. One can use equation (2.35) to calculate $\Gamma(\vec{r_d}, \vec{r_d}, 0)$:

$$\Gamma(\vec{r_d}, \vec{r_d}, 0) = \frac{\cos^2\theta_d}{r_d^2 \bar{\lambda}^2} \int\int_{x=0} e^{-i\vec{p}\cdot(\vec{r_2'} - \vec{r_1'})} \Gamma(\vec{r_1'}, \vec{r_2'}, 0) d^2 r_1' d^2 r_2', \tag{2.45}$$

where $\vec{p} = \bar{k}\vec{r}_d / r_d$. Here, it is assumed that the detector is in the far-zone of the sample. If further the spatial coherence is much smaller than the sample area equation (2.45) can be reduced to

$$\Gamma(\vec{r_d}, \vec{r_d}, 0) = \frac{\cos^2\theta_d}{r_d^2} \int_{x=0} e^{-i\vec{p}\cdot\vec{r'}} F(\vec{r'}, 0) d^2 r'. \tag{2.46}$$

where

$$F(\vec{r'}, \tau) = \bar{\lambda}^{-2} \int_{x=0} \Gamma(\vec{r_1'}, \vec{r'} + \vec{r_1'}, \tau) d^2 r_1'. \tag{2.47}$$

Note that for a homogeneous beam at the sample position this reduces to:

$$F(\vec{r'}, \tau) = \bar{\lambda}^{-2} A_s \Gamma(\vec{r}_{s0}, \vec{r'} + \vec{r}_{s0}, \tau), \tag{2.48}$$

where A_s is the sample aperture and $\vec{r}_{s0}$ the average sample position. If the detector area is small and $\cos\theta_d$ and $\vec{r_d}$ can be taken constant the detector count rate is:

$$I_d(\vec{r_d}) = 2v_p \frac{A_d \cos^2\theta_d}{r_d^2} \int_{x=0} e^{-i\vec{p}\cdot\vec{r'}} F(\vec{r'}, 0) d^2 r', \tag{2.49}$$

Equation (2.49) describes the detector count rate as a two-dimensional Fourier transform of the mutual coherence function at $x = 0$ integrated over the yz-plane. Otherwise if the detector area is large and the scattering is mainly in some preferential direction so that $\cos\theta_d$ can be taken constant the total count rate in the detector is given by:

$$I_d = 2v_p \cos^2\theta_d \int_{x=0} \Gamma(\vec{r_1'}, \vec{r_1'}, 0) d^2 r_1', \tag{2.50}$$

which can be interpreted as the count rate in a detector placed under an angle θ_d at the sample position with an area equal to the cross section of the beam.

2.8 Beam divergence

The relation between beam divergence and the mutual coherence function can be underlined using the results of the previous section. Assume the beam is created from an incoherent source. The mutual coherence at the source position is given by equation (2.36). For the divergence of the beam at $x = r_d$ the spread in angles is used, being defined as:

$$\Delta\theta^2 = \left\langle \theta^2 \right\rangle - \langle\theta\rangle^2 = \frac{\int_{A_d} \theta^2 \Gamma(\vec{r_d}, \vec{r_d}, 0) d^2 r_d}{\int_{A_d} \Gamma(\vec{r_d}, \vec{r_d}, 0) d^2 r_d} - \left(\frac{\int_{A_d} \theta \Gamma(\vec{r_d}, \vec{r_d}, 0) d^2 r_d}{\int_{A_d} \Gamma(\vec{r_d}, \vec{r_d}, 0) d^2 r_d} \right)^2 \tag{2.51}$$

where the beam propagates along the x-axis and the angles are assumed to be small compared to 1. Note that $\int_{A_d} \Gamma(\vec{r}_d, \vec{r}_d, 0) d^2 r_d$ is just the total number of neutrons per second moving through the detector aperture, A_d. Assume that at $x = 0$ the mutual coherence function is given by equation (2.40), then $\Gamma(\vec{r}_d, \vec{r}_d, 0)$ is given by:

$$\Gamma(\vec{r}_d, \vec{r}_d, 0) = \frac{J_0 A_0 A_d r_c^2}{8 v_p r_d^2 L^2 \bar{\lambda}^2} \int_0^\infty e^{-i q_r r_c \nu} \mathrm{J}_1(\nu) d\nu, \tag{2.52}$$

where q_r is the radial component of $\vec{p}$ and $r_c = L/\bar{k}a$, the transversal coherence length at $x = 0$ due to a incoherent source with radius a at position $x = -L$. As $\theta = q_r/\bar{k}$ and $\langle\theta\rangle = 0$ equation (2.51) becomes:

$$\Delta\theta^2 = \frac{1}{\bar{k}^2 r_c^2} \frac{\int_0^\infty \eta^2 \int_0^\infty e^{-i\eta\nu} \mathrm{J}_1(\nu) d\nu d\eta}{\int_0^\infty \int_0^\infty e^{-i\eta\nu} \mathrm{J}_1(\nu) d\nu d\eta} \tag{2.53}$$

or

$$\Delta\theta = \frac{1}{\bar{k} r_c} = \frac{a}{L}. \tag{2.54}$$

Hence, the beam divergence is inversely proportional to the wavevector and the coherence length.

2.9 Propagation from source to detector

For a good understanding the propagation of the mutual coherence function from source to detector is discussed. This is the same as from sample to detector, except now the mutual coherence function at the sample position is that for an incoherence source according to equation (2.36). The count rate in the detector can be determined by using equation (2.45) (or equation (2.37) can be used with equation (2.44)) so that:

$$I_d = \int_{A_d} \frac{\cos^2\theta_d}{4\pi r_d^2} d^2 r_d \int_{x=0} J_0(\vec{r_1'}) d^2 r_1'. \tag{2.55}$$

If the detector area is small, so that r_d and $\cos\theta_d$ can be taken constant this reduces to:

$$I_d = \frac{A_d \cos^2\theta_d}{4\pi r_d^2} \int_{x=0} J_0(\vec{r_1'}) d^2 r_1'. \tag{2.56}$$

Further if the source is homogeneous and limited to an area A_0:

$$I_d = J_0 A_0 \frac{A_d \cos^2\theta_d}{4\pi r_d^2}. \tag{2.57}$$

$J_0 A_0$ is the total number of neutrons emitted from the source, $A_d \cos^2\theta_d / 4\pi r_d^2$ is the total fraction of source neutrons traveling through the detector area and θ_d is the angle between detector surface and the line between source and detector.

Chapter 3

Propagation in the sample

Propagation in free space was elaborately discussed in the previous chapter. However, the use of wave equations for the mutual coherence function to solve the propagation through some material has no advantage over normal solution methods. Further, one should realize that according to quantum mechanics the wave function itself is scattered by the interaction potential. The effect on the mutual coherence function is derived from its definition. That is why for propagation through a sample the solutions of the Schrödinger equation for the wave function are used. By applying the definition of the mutual coherence function these solutions can be transformed to a form where the mutual coherence function directly after the sample or in the detector is expressed in a sample correlation function and the mutual coherence function just before the sample or in the source.

3.1 Scattering

The equations in the previous chapter were derived for the propagation of the mutual coherence function in free space. This does not include the scattering process. In the most general case for elastic scattering, propagation of the wave function itself in the sample is governed by the stationary Lippmann-Swinger equation [5]:

$$\Psi_{sc}(\vec{r}) = \Psi_{in}(\vec{r}) - \frac{2m}{\hbar^2} \int G_0(\vec{r} - \vec{r}_s) V(\vec{r}_s) \Psi_{sc}(\vec{r}_s) d^3 r_s, \tag{3.1}$$

where $\Psi_{in}(\vec{r})$ represents the channel state or incident wave function, $\Psi_{sc}(\vec{r})$ the scattered state or function, $V(\vec{r}_s)$ the scattering potential of the sample and $G_0(\vec{r})$ is the free particle Green function given by equation (2.33). Strictly speaking this Green function is only valid for a mono-chromatic beam in vacuum. Here, it is assumed that the wavevector spread Δk is sufficiently small not to impart this equation. The time dependence of the wave functions is given by:

$$\Psi(\vec{r}, t) = \Psi(\vec{r}) e^{-i\omega_k t}. \tag{3.2}$$

The basis of the Lippmann-Schwinger equation is the time-dependent Schrödinger equation applied to a time-dependent potential. The potential can be factorized in a time-dependent

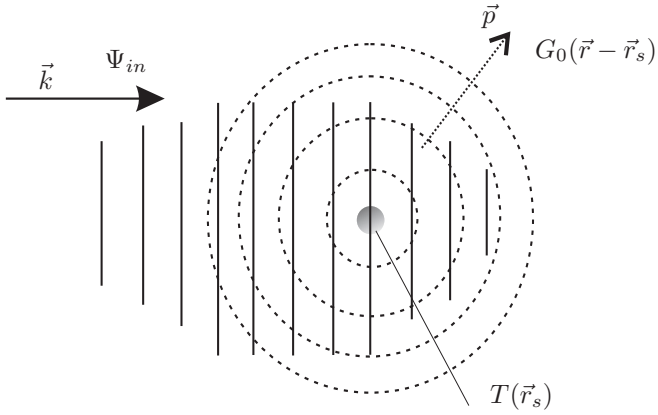

Figure 3.1: Scattering geometry.

part and a space-dependent part: $V(\vec{r},t) = V_r(\vec{r})V_t(t)$. By varying $V_t(t)$ in a specific way (0 for $t \to \pm\infty$ and 1 during the scattering process), the channel state can be identified as the solution for the Schrödinger equation before the scattering process and the scattered state as the solution after the scattering process [11]. It can also be derived from the stationary Schrödinger equation assuming appropriate boundary conditions (an incident plane wave and an scattered spherical wave at the sample position).

Normally the scattered-wave function is unknown. However, the Lippmann-Schwinger equation can be iterated resulting in an infinite series for $\Psi_{sc}(\vec{r})$:

$$\Psi_{sc}(\vec{r}) = \Psi_{in}(\vec{r}) - \frac{2m}{\hbar^2}\int G_0(\vec{r}-\vec{r}_{s1})V(\vec{r}_{s1})\Psi_{in}(\vec{r}_{s1})d^3r_{s1} + \tag{3.3}$$

$$\left(\frac{2m}{\hbar^2}\right)^2 \int\int G_0(\vec{r}-\vec{r}_{s1})V(\vec{r}_{s1})G_0(\vec{r}_{s1}-\vec{r}_{s2})V(\vec{r}_{s2})\Psi_{in}(\vec{r}_{s2})d^3r_{s2}d^3r_{s1} - \cdots,$$

which can be rewritten in the form:

$$\Psi_{sc}(\vec{r}) = \Psi_{in}(\vec{r}) - \frac{2m}{\hbar^2}\int G^{(+)}(\vec{r},\vec{r}_s)V(\vec{r}_s)\Psi_{in}(\vec{r}_s)d^3r_s, \tag{3.4}$$

where $G^{(+)}(\vec{r},\vec{r}_s)$ is a specialized (potential dependent) Green function describing the scattering into on scattered-wave function and defined by the solution of the following Schrödinger equation:

$$\left(\nabla^2 + \bar{k}^2 - \frac{2mV(\vec{r}_s)}{\hbar^2}\right) G^{(+)}(\vec{r},\vec{r}_s) = \delta(\vec{r}-\vec{r}_s), \tag{3.5}$$

where the ∇^2 operator represents the derivatives to $\vec{r}_s$. This equation describes the scattered wave as a superposition of waves produced by many scattering events occurring at different elements of the sample (see figure 3.1). From this equation the propagation of the mutual coherence function through the sample can be derived.

Introducing the scattering operator, $T_{\bar{k}}$ equation (3.1) can also be transformed to:

$$\Psi_{sc}(\vec{r}) = \Psi_{in}(\vec{r}) - \frac{2m}{\hbar^2}\int G_0(\vec{r}-\vec{r}_s)T_{\bar{k}}(\vec{r}_s)\Psi_{in}(\vec{r}_s)d^3r_s. \tag{3.6}$$

The mutual coherence function of the scattered state can be expressed in the mutual coherence function of the channel state. This can be calculated using the definition (2.6) and the Lippmann-Swinger equation (3.1) yielding:

$$\Gamma_{sc}(\vec{r}_1,\vec{r}_2,\tau) = \Gamma_{in}(\vec{r}_1,\vec{r}_2,\tau) \tag{3.7}$$
$$-\frac{2m}{\hbar^2}\int G_0^*(\vec{r}_1-\vec{r}_s)T_{\bar{k}}(\vec{r}_s)\Gamma_{in}(\vec{r}_s,\vec{r}_2,\tau)+G_0(\vec{r}_2-\vec{r}_s)T_{\bar{k}}^*(\vec{r}_s)\Gamma_{in}^*(\vec{r}_s,\vec{r}_1,-\tau)d^3r_s$$
$$+\left[\frac{2m}{\hbar^2}\right]^2\int\int G_0(\vec{r}_2-\vec{r'}_s)G_0^*(\vec{r}_1-\vec{r}_s)T_{\bar{k}}(\vec{r}_s)T_{\bar{k}}^*(\vec{r'}_s)\Gamma_{in}(\vec{r}_s,\vec{r'}_s,\tau)d^3r'_sd^3r_s.$$

The first term of this equation can be understood as the mutual coherence function of the direct beam, the second term as an interference term between the direct and scattered beam and the last term the mutual coherence function of the scattered beam. However, in general the mutual coherence function at the detector position is needed. Using equation (2.44) and $\vec{r}=\vec{r'}_s-\vec{r}_s$ the count rate at the detector due to the scattered beam becomes:

$$I_d = 2v_p\int\int R_{out}(\vec{r}_s,\vec{r}_s+\vec{r})\left[\frac{m}{4\pi\hbar^2}\right]^2 T_{\bar{k}}(\vec{r}_s)T_{\bar{k}}^*(\vec{r}_s+\vec{r})\Gamma_{in}(\vec{r}_s,\vec{r}_s+\vec{r},0)d^3r_sd^3r, \tag{3.8}$$

where

$$R_{out}(\vec{r}_1,\vec{r}_2) = (4\pi)^2\int_{A_d} G_0^*(\vec{r}_d-\vec{r}_2)G_0(\vec{r}_d-\vec{r}_1)d^2r_d. \tag{3.9}$$

If it is assumed that the direct beam is spatial homogeneous over the sample-beam cross section and the same holds for R_{out} the count rate at the detector position becomes

$$I_d = 2v_p\int R_{out}(\vec{r}_{s0},\vec{r}_{s0}+\vec{r})G_s(\vec{r})\Gamma_{in}(\vec{r}_{s0},\vec{r}_{s0}+\vec{r},0)d^3r, \tag{3.10}$$

where $\vec{r}_{s0}$ is the average sample position and

$$G_s(\vec{r}) = \left[\frac{m}{2\pi\hbar^2}\right]^2\int T_{\bar{k}}(\vec{r}_s)T_{\bar{k}}^*(\vec{r}_s+\vec{r})d^3r_s \tag{3.11}$$

is a sample correlation function comparable to the scattering length density correlation function. Note that equation (3.10) holds for any scattering angle and for any scattering operator function. Hence, the count rate in the detector is determined by an integral over the sample correlation function and two functions that are determined by the instrument details. These two functions together constitute the resolution of the instrument under consideration.

The interpretation of this equation can be understood by looking at figure 3.2. Γ_{in} represents the effect of the phase differences between path 1 and 2 on the coherence function of the incident beam. R_{out} represents the same for the scattered beam. Only paths which comes from within the coherence volume contribute to the interference at the detector position.

In general R_{out} and Γ_{in} are complicated functions depending on the full instrumental details. Under certain conditions these functions can be determined approximately. Equation (2.31) and equation (2.36) can be used to calculate the incident mutual coherence function for a completely homogeneous and incoherent source with area A_0:

$$\Gamma_{in}(\vec{r}_1,\vec{r}_1+\vec{r},0) = \frac{J_0}{2v_p}\int_{A_0}\frac{e^{i\vec{k}\cdot\vec{r}}}{4\pi\left|\vec{r}_1-\vec{r'}\right|^2}d^2r', \tag{3.12}$$

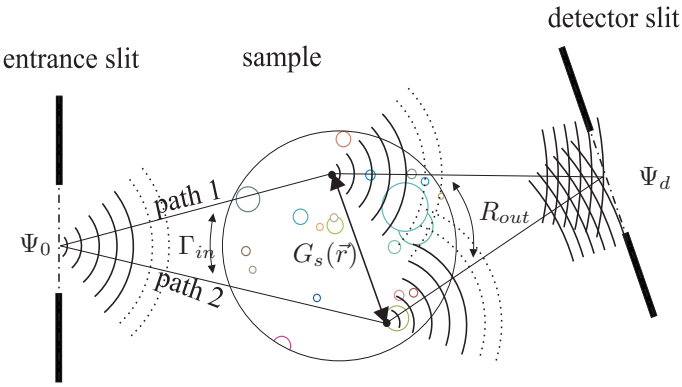

Figure 3.2: Scattering geometry.

where $\vec{k} = \bar{k}(\vec{r}_1 - \vec{r'})/\left|\vec{r}_1 - \vec{r'}\right|$. If it is assumed that the mutual coherence function of the incident beam, Γ_{in} is only different from 0 for small values of $\vec{r}$ (i.e. the coherence length of the incident beam is much smaller than the sample dimensions) the conjugated Green function in the expression for R_{out} can be approximated by

$$G_0(\vec{r}_d - \vec{r}_2) \approx G_0(\vec{r}_d - \vec{r}_1)e^{i\vec{p}\cdot\vec{r}}, \tag{3.13}$$

where $\vec{r} = \vec{r}_2 - \vec{r}_1$ and $\vec{p} = \bar{k}(\vec{r}_d - \vec{r}_1)/\left|\vec{r}_d - \vec{r}_1\right|$ so that

$$R_{out}(\vec{r}_1, \vec{r}_2) \approx \int_{A_d} \frac{e^{-\vec{p}\cdot\vec{r}}}{\left|\vec{r}_d - \vec{r}_1\right|^2} d^2 r_d. \tag{3.14}$$

If the source, sample and detector dimensions are small compared to the distance between the source and sample at the one hand and sample and detector at the other, r_1 can be replaced by r_{s0}, the average sample position. The count rate in the detector due to the scattered beam becomes:

$$I_d = J_0 \int\int_{A_0}\int_{A_d} \frac{e^{-\vec{q}\cdot\vec{r}}}{4\pi\left|\vec{r}_d - \vec{r}_{s0}\right|^2\left|\vec{r}_{s0} - \vec{r'}\right|^2} d^2 r_d d^2 r' G_s(\vec{r}) d^3 r, \tag{3.15}$$

where $\vec{q} = \vec{p} - \vec{k}$ is also known as the wavevector transfer. The argument of the outer integral is proportional to the number of neutrons scattered by the coherence volume d^3r at the sample position reaching the detector. In this view the sample correlation function is comparable to a scattering amplitude. To stress the resolution effect this equation is rewritten as a convolution:

$$I_d(\vec{r}_d) = R^{FT}(\vec{q}) * S_k(\vec{q}), \tag{3.16}$$

where

$$R^{FT}(\vec{q}) = J_0 \int\int_{A_0}\int_{A_d} \frac{e^{-\vec{q}\cdot\vec{r}}}{4\pi\left|\vec{r}_d - \vec{r}_{s0}\right|^2\left|\vec{r}_{s0} - \vec{r'}\right|^2} d^2 r_d d^2 r' d^3 r \tag{3.17}$$

can be interpreted as the instrumental resolution function and

$$S_k(\vec{q}) = \int e^{-i\vec{q}\cdot\vec{r}} G_s(\vec{r}) d^3r \tag{3.18}$$

is called the *sample structure factor* and equals the Fourier transform of the sample correlation function.

Note that this interpretation of the scattered detector count rate as a convolution of sample structure factor and instrumental resolution is only valid if the detector area and sample dimensions are small compared to the distance between sample and detector. If this is the case, the mutual coherence function at the sample position can be considered to be *homogeneous*. It only depends on the difference between the two position vectors (see also appendix C). If it is assumed that after scattering at the sample the scattered mutual coherence function is also homogeneous, then the coherence approach to scattering yields the same results as the stationary collision theory [11], describing the scattering of a wave function by means of transition matrices, scattering amplitudes and differential scattering cross sections.

3.2 Born approximation

In the kinematic or first Born approximation it is assumed that the scattered beam is only a fraction of the incident beam. In this case the transition operator $T_{\bar{k}}$ can be replaced by the Fermi pseudo potential [5]:

$$T_{\bar{k}}(\vec{r}) = V(\vec{r}) = -\frac{2\pi\hbar^2}{m}\rho_b(\vec{r}), \tag{3.19}$$

where $\rho_b(\vec{r})$ equals the scattering length density of the sample defined as

$$\rho_b(\vec{r}) = \sum_i b_i \delta(\vec{r} - \vec{r}_i) \tag{3.20}$$

and b_i is the bound scattering length of the ith atom. The sample correlation function $G_s(\vec{r})$ as defined in equation (3.11) becomes the three-dimensional van Hove contrast correlation function, $\gamma_H(\vec{r})$ [12]:

$$G_s(\vec{r}) \approx \gamma_H(\vec{r}) = \int_{V_s} \rho_b(\vec{r}_s)\rho_b(\vec{r}_s + \vec{r}) d^3r_s. \tag{3.21}$$

3.3 Phase-object approximation

De Haan et al. [8] showed that for small angle neutrons scattering and thin samples it is possible to directly relate the mutual coherence function behind the sample to the one before the sample using Feynmann path integrals [13]. An example of such a scattering process is shown in figure 3.3. In the small angle approximation the wave function can be calculated by estimating the phase acquired by the neutron wave if it had followed the classical path through the sample. Hence, the wave function behind the sample becomes:

$$\Psi_{sc}(x_1, y, z) = \Psi_{in}(x_0, y, z) e^{i\bar{k}\int_{x_0}^{x_1} n(x,y,z)dx} \quad , \tag{3.22}$$

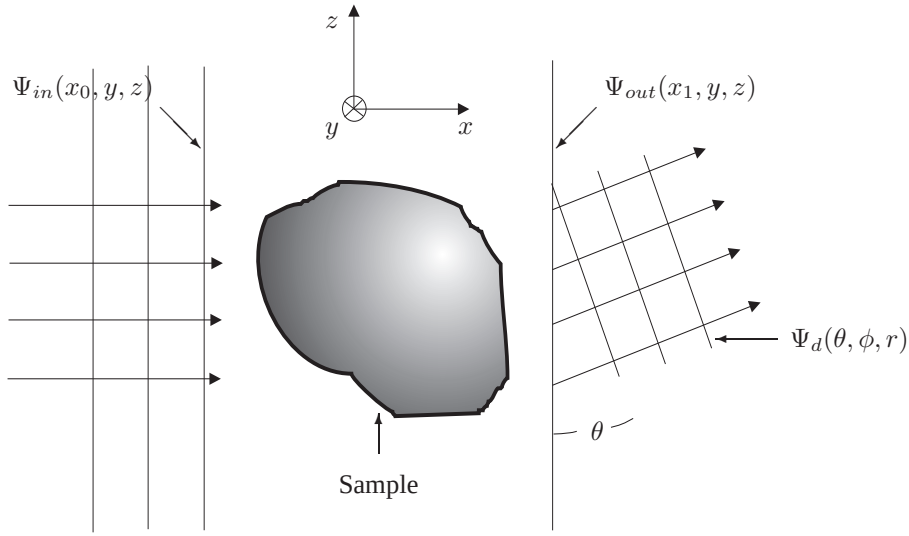

Figure 3.3: Scattering geometry projected on a plane with constant y.

where x is the incident beam direction, $x = x_0$ a plane just before the sample, $x = x_1$ a plane just behind the sample and $n(x, y, z)$ is the local refraction index of the sample. The integral in the exponent is known as the optical path length. As it is assumed the scattering object only influences the phase of the neutron wave function this is called the phase-object approximation. This approximation can also be derived using the *Eikonal approximation* [5], [11] and holds for $|\nabla V(\vec{r})| \ll \left|\bar{k}V(\vec{r})\right|$, which is valid as long as two conditions are fulfilled [14]. First, the difference in optical path length between the classical-line path for straight lines through the sample with a small angle (θ) between them should be much smaller than the neutron wavelength, hence $(x_1 - x_0)\theta^2 \ll 2\bar{\lambda}$ or $x_1 - x_0 \ll 8\pi^2/q^2\bar{\lambda}$, where $q = \theta\bar{k}$. For instance if $q \leq 0.01$ nm^{-1} and $\bar{\lambda} \approx 0.2$ nm then $x_1 - x_0 \ll 4$ mm. Second, the local refractive index does not change appreciably from one path to the other. If these conditions are not satisfied it is possible to make a second order correction or to break up the calculation in slices of small enough pieces [14].

The refraction index is related to the potential $V(x, y, z)$ given by the Fermi pseudo potential:

$$n^2 = 1 - \frac{V(x, y, z)}{\hbar\omega_k} = 1 - \frac{\lambda^2\rho_b(x, y, z)}{\pi} = 1 - \frac{\lambda^2 k_c^2}{4\pi^2}, \tag{3.23}$$

where $\hbar\omega_k$ equals the total energy of the neutron, λ its wavelength, $\rho_b(x, y, z)$ the coherent scattering length density and k_c the critical wavevector defined by $\sqrt{4\pi\rho_b}$ (see also section 6.2). Incoherent scattering, large angle coherent scattering or absorption can be taken into account by a suitable imaginary part of the refraction index [5]. The approximation is valid for thermal neutrons as used in SESANS (spin echo small angle neutron scattering) [15], [16], [17], [18] or USANS (ultra small angle neutron scattering) [19], [20], [21] as the refractive index is close to unity. Note that the deviation from unity of the refractive index is proportional to the square of the wavelength so it increases rapidly for increasing wavelength.

Propagation of the mutual coherence function through the sample (from $x = x_0$ to $x = x_1$) can be calculated using equation (3.22) and the definition of the mutual coherence function (2.6):

$$\Gamma_{sc}(\vec{r}_1, \vec{r}_2, \tau) = \Gamma_{in}(\vec{r}_1 - \vec{d}_x, \vec{r}_2 - \vec{d}_x, \tau) e^{iS(\vec{r}_2 - \vec{d}_x) - iS^*(\vec{r}_1 - \vec{d}_x)}, \tag{3.24}$$

where $\vec{d}_x = (x_1 - x_0)\vec{e}_x$ and

$$S(\vec{r}) = \bar{k} \int_0^{d_x} (n(\vec{r} + x\vec{e}_x) - 1) dx \tag{3.25}$$

is the *extra* phase shift acquired by the neutron wave function due to the material properties of the sample. Note that S can be complex due to a complex refraction index. In principle the subtraction of 1 from the refractive index is not needed and it has no influence on the results. However, because the refractive index only differs from 1 by a small amount, the extra acquired phase shift is much smaller than the total phase shift acquired after traveling through the sample. The use of the extra acquired phase shift enables series expansion of the equation for small values of S.

These equations can be used together with equation (2.49) to determine the count rate at the detector. By realizing that $\cos\theta_d \approx 1$ for small angle neutron scattering the result is:

$$I_d = 2v_p \frac{A_d}{r_d^2} \int_{x=x_1} e^{-i\vec{p}\cdot\vec{r}} F(\vec{r}) d^2 r, \tag{3.26}$$

where

$$F(\vec{r}) = \bar{\lambda}^{-2} \int_{x=x_0} \Gamma_{in}(\vec{r}_1, \vec{r} + \vec{r_1}, 0) e^{iS(\vec{r} + \vec{r}_1) - iS^*(\vec{r_1})} d^2 r_1. \tag{3.27}$$

An important feature of this equation is it describes what normally in SANS is called the scattered neutron intensity *and* the direct beam. In the above formalism there is no difference any more: the direct beam is also refracted or in other words: there is no direct beam. Another important feature is that in general the coherence function (3.24) does not have to be a real valued function so that the scattering profile can be different for positive and negative wavevectors.

Assume that the incident beam has a homogeneous intensity over the sample cross section, then equation (3.26) reduces to:

$$I_d = \frac{2v_p A_d}{r_d^2 \bar{\lambda}^2} \int_{x=x_1} G_r(\vec{r}) e^{-i\vec{p}\cdot\vec{r}} \Gamma_{in}(\vec{r}_{s0}, \vec{r} + \vec{r}_{s0}, 0) d^2 r, \tag{3.28}$$

where $G_r(\vec{r})$ is the sample correlation function:

$$G_r(\vec{r}) = \int_{x=x_0} e^{iS(\vec{r} + \vec{r}_1) - iS^*(\vec{r_1})} d^2 r_1. \tag{3.29}$$

Again by using equation (3.12) equation (3.28) can be rewritten as a convolution of the instrumental resolution and the two-dimensional Fourier transform of the sample correlation function:

$$I_d = R^{FT}(\vec{q}) * S_k(\vec{q}), \tag{3.30}$$

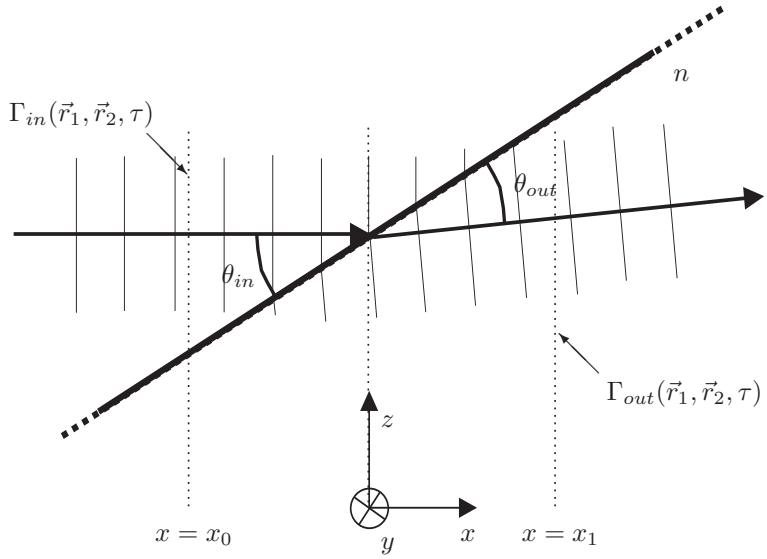

Figure 3.4: Refraction geometry projected on a plane with constant y.

where the instrumental resolution is given by

$$R^{FT}(\vec{q}) = \frac{J_0 A_d}{r_d^2 \bar{\lambda}^2} \int_{x=x_1} \int_{A_0} e^{-i\vec{q}\cdot\vec{r}} \frac{1}{4\pi \left|\vec{r}_{s0} - \vec{r'}\right|^2} d^2r' d^2r \tag{3.31}$$

and

$$S_k(\vec{q}) = \int_{x=x_1} e^{-i\vec{q}\cdot\vec{r}} G_r(\vec{r}) d^2r. \tag{3.32}$$

3.4 Refraction

Refraction and diffraction occur when a neutron beam travels through a medium where the optical potential of the medium depends on the position. In general diffraction can be seen as an interference phenomena of coherent parts of the scattered beam. Refraction can be understood as the interference phenomena of the coherent direct beam. However, as was shown in the previous section the differentiation in direct and scattered beam is somewhat arbitrary. Here, refraction is defined as small angle scattering at macroscopic surfaces. An example of refraction is shown in figure 3.4.

Let space be divided into two half-spaces with a boundary making an angle of θ_{in} with the incident neutron beam parallel to the x-axis. The refractive index of the left half-space is 1 and of the right n. Assume a neutron wave function, described by the mutual coherence function, Γ_{in} is known at a plane for $x = x_0$, and the y dependence is ignored. The mutual coherence function at the position $x = x_1$ can be calculated using the results of equations (3.24) and (3.25) from the previous section. The propagation of the mutual coherence function from $x = x_1$ to the detector position is given by equation (3.30). Ignoring

resolution effects and absorption or scattering (the refractive index of the medium is real) the count rate in the detector position is proportional to S_k, which in this case is given by

$$S_k(\vec{q}) = \int_{x=x_1} e^{-i\vec{q}\cdot\vec{r}} \int_{x=x_0} e^{iS(\vec{r}+\vec{r}_1) - iS(\vec{r_1})} d^2r_1 d^2r, \tag{3.33}$$

where

$$S(\vec{r}+\vec{r}_1) - S(\vec{r}_1) = \bar{k}(1-n)\cot\theta_{in}(\vec{r}\cdot\vec{e}_z) \tag{3.34}$$

only depends on $\vec{r}$, so that equation (3.33) reduces to:

$$S_k(\vec{q}) = \int_{x=x_0} \int_{x=x_1} e^{i\left\{\bar{k}(1-n)\cot\theta_{in}(\vec{r}\cdot\vec{e}_z) - \vec{q}\cdot\vec{r}\right\}} d^2r d^2r_1, \tag{3.35}$$

The inner integral of equation (3.35) is taken over the whole $x = x_1$ plane and only gives a non-zero result when the exponent is 0. In this case $\vec{q} = \bar{k}\vec{r}_d/r_d$, where $\vec{r}_d$ is the detector position. Hence:

$$((1-n)\cot\theta_{in}\vec{e}_y - \vec{r}_d/r_d)\cdot\vec{r} = 0, \tag{3.36}$$

where it was used that the y-component of $\vec{r}_d$ is zero, the z-component is $r_d\sin(\theta_{in}-\theta_{out})$ and the x-component $r_d\cos(\theta_{in}-\theta_{out})$. θ_{out} is the refraction angle and is determined by the direction in which the detector is seen at the sample position. Realizing that $\vec{r}$ has no y-component this reduces to:

$$(1-n)\cot\theta_{in} = \sin(\theta_{in}-\theta_{out}), \tag{3.37}$$

which under the condition that $\tan\theta_{in} \gg |1-n|$ is the same as:

$$\frac{\cos\theta_{out}}{\cos\theta_{in}} = n, \tag{3.38}$$

known as Snells law.

One should realize that the Phase-object approximation only holds if $(x_1-x_0)(\theta_{in}-\theta_{out})^2 \ll 2\bar{\lambda}$. This gives an indication of the maximum length of the transition zone between the two media for equation (3.37) or (3.38) to hold: $x_1 - x_0 \ll 2\bar{\lambda}\tan^2\theta_{in}/(1-n)^2$. Using equation (3.23) this is equal to $x_1 - x_0 \ll 8\tan^2\theta_{in}(2\pi/k_c)^4/\bar{\lambda}^3$. For silicon ($k_c = 0.051$ nm^{-1}), $\theta_{in} = 45^o$ and an average neutron wavelength of 0.2 nm: $x_1 - x_0 \ll 230$ m ! For the region of total reflection $\theta_{in} \approx |1-n|$. Then $x_1 - x_0 \ll 2\bar{\lambda}$, which is not the case and the above derivation is not applicable. The region where (partial) reflection is occurring is subject of chapter 6.

3.5 Born approximation for SANS

Kinematic or first Born approximation is the neutron scattering theory for weak scattering. In the weak scattering limit, the difference $|S(\vec{r}+\vec{r}_1) - S^*(\vec{r}_1)|$ is much smaller than 1. The above equation (3.29) reduces to the kinematic or first Born approximation by a series expansion. The zeroth order term represents the incident beam. The first order term is 0. And the second order term represents the reduction of the incident beam and the scattered intensity:

$$G_r(\vec{r}) = A_s T + \int_{x=x_0} S(\vec{r}+\vec{r}_1)S^*(\vec{r}_1)d^2r_1, \tag{3.39}$$

where

$$T = 1 - \frac{2}{A_s}\int_{x=x_0} \Im\{S(\vec{r}_1)\} d^2 r_1 - \frac{1}{A_s}\int_{x=x_0} \Re\{S(\vec{r}_1)^2\} d^2 r_1 \ , \tag{3.40}$$

where $\Re\{a\}$ is the real part of a, $\Im\{a\}$ the imaginary part of a and A_s is the beam-lightened sample area. Note that the transmission, T is independent of y and z as it should. By substituting equation (3.25) the integral at the right hand side of these equations can be interpreted using the two dimensional correlation function [22]:

$$G_c(y,z) = \frac{\bar{\lambda}^2}{A_s}\int_{A_s} \gamma_{2D}(y_1,z_1)\gamma_{2D}(y+y_1, z+z_1) dy_1 dz_1 \ , \tag{3.41}$$

where the projection of the scattering length density along the neutron beam is given by:

$$\gamma_{2D}(y,z) = \int_{x_0}^{x_1} \rho_b(x,y,z) dz. \tag{3.42}$$

Equation (3.39) then reduces to

$$G_r(\vec{r}) = A_s \left(1 - G_c(0) + G_c(\vec{r})\right). \tag{3.43}$$

3.6 Multiple scattering for SANS

Interestingly the phase-object approximation also describes a multiple scattering effect as derived by Schelten and Schmatz in the first Born approximation [23]. This can be understood by investigating equation (3.29), relating the sample correlation function to the extra phase shift acquired by the neutron wave function while traversing the sample:

$$G_r(\vec{r}) = \int_{A_s} e^{iS(\vec{r}+\vec{r}_s) - iS^*(\vec{r_s})} d^2 r_s, \tag{3.44}$$

where the integration is over the sample surface area, A_s. This equation is an average of the exponential over the sample area and can be rewritten as the sample area times the expectation value:

$$G_r(\vec{r}) = A_s E[e^{iS(\vec{r}+\vec{r}_s) - iS^*(\vec{r_s})}]. \tag{3.45}$$

Now, if $S(\vec{r}_s)$ is real and has a Gaussian random distribution, a correlation function can be defined as:

$$C(\vec{r}) = \frac{1}{A_s}\int_{A_s} (S(\vec{r}+\vec{r}_s) - S_0)(S(\vec{r}_s) - S_0) d^2 r_s, \tag{3.46}$$

where S_0 is the first moment (or average or expectation value) of $S(\vec{r}_s)$. This correlation function can be expressed in the 2D-correlation function given in equation (3.41):

$$C(\vec{r}) = G_c(\vec{r}) - S_0^2. \tag{3.47}$$

The second moment (or variance) of $S(\vec{r}_s) - S_0$ is defined as $\sigma^2 = C(0)$. Then, the expectation value of $e^{iS(\vec{r}_s)}$, known as the *characteristic function* of $S(\vec{r}_s)$, is given by:

$$E[e^{iS(\vec{r}_s)}] = e^{iS_0} e^{-\sigma^2/2}. \tag{3.48}$$

Further it is assumed that $S(\vec{r}_1) - S(\vec{r}_2)$ has a Gaussian random distribution with zero mean too and its variance only depends on $\vec{r}_2 - \vec{r}_1$:

$$g(\vec{r}) = \left\langle [S(\vec{r}_s) - S(\vec{r}_s + \vec{r})]^2 \right\rangle_{A_s}, \tag{3.49}$$

where the average is taken over the whole sample area. Note that $g(\vec{r})$ can be reduced to $g(\vec{r}) = 2(G_c(0) - G_c(\vec{r}))$. Further

$$E[e^{i(S(\vec{r}_s) - S(\vec{r}_s + \vec{r}))}] = e^{-g(\vec{r})/2}, \tag{3.50}$$

can be reduced to:

$$E[e^{i(S(\vec{r}_s) - S(\vec{r}_s + \vec{r}))}] = e^{G_c(\vec{r}) - G_c(0)}, \tag{3.51}$$

so that

$$G_r(\vec{r}) = A_s e^{G_c(\vec{r}) - G_c(0)}, \tag{3.52}$$

the same as given by Rekveldt et al. [17]. This was also found by Muller in case of high resolution electron microscopy [24].

3.7 Sample correlation function for a sphere

As an example scattering from a sphere is considered. For a sphere $S(\vec{r})$, given by equation (3.25) becomes:

$$S(y, z) = 2\bar{k}(n-1)\Re\left\{\sqrt{R^2 - y^2 - z^2}\right\}, \tag{3.53}$$

where R is the radius of the sphere, n the index of refraction of the homogeneous sphere material, $\bar{k}$ the average neutron wavevector in vacuum and $\Re\{a\}$ denotes the real part of a. It was used that $\vec{r} = y\vec{e}_y + z\vec{e}_z$. The sample correlation function (3.29) for a sphere becomes:

$$G_r(0, \delta) = \int_{A_s} e^{iS(y, z+\delta) - iS^*(y,z)} dydz, \tag{3.54}$$

where A_s is the beam cross section assuming the beam totally envelops the sphere and δ is in the z-direction. In the following the correlation in the y direction is ignored. The reason for this is that SESANS or USANS techniques only determine one correlation direction and the other direction is averaged (see chapter 5). The so-called *form factor* can be calculated as:

$$F(\delta) = \frac{\Re\{G_r(\delta) - G_r(\infty)\}}{\Re\{G_r(0) - G_r(\infty)\}} = 1 - \frac{\Re\{G_r(0) - G_r(\delta)\}}{\Re\{G_r(0) - G_r(\infty)\}}, \tag{3.55}$$

which is 1 for $\delta = 0$ and 0 for $\delta = \infty$. Only the real part is taken because in practice only the real part is measured (see section 5.2). Note that $G_r(0) = A_s$, here equal to πR^2. From the above equation (3.54) and assuming the imaginary part of the index of refraction can be neglected, it can be shown that:

$$\Re\{G_r(0) - G_r(\delta)\} = \int_{A_s} 1 - \cos(S(y, z+\delta) - S(y, z)) dydz. \tag{3.56}$$

Note that in the (y, z)-range where both $S(y, z+\delta)$ and $S(y, z)$ are 0 the integrand is 0. Hence, the integration only has to be taken over the area where one or both are non-zero (see the shaded area of figure 3.5). As soon as $\delta \geq 2R$ this equation reduces to:

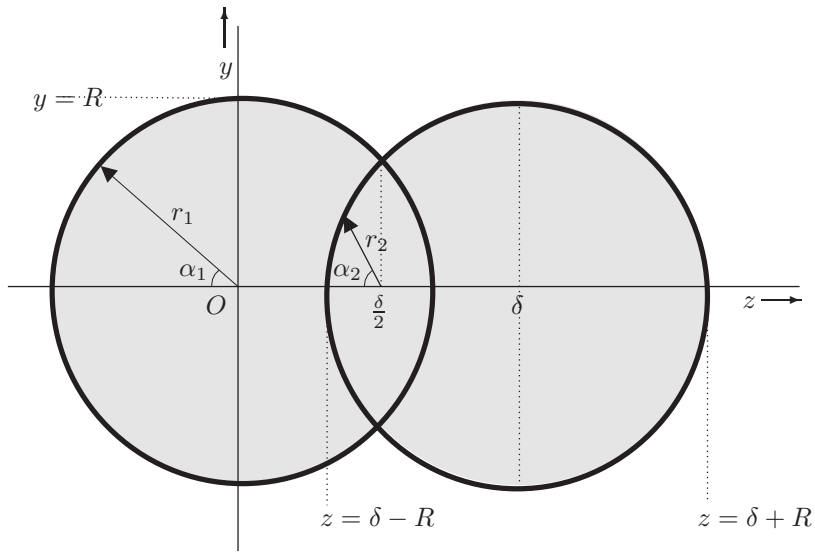

Figure 3.5: Correlation geometry projected on a yz-plane for the calculation of the form factor of a sphere. R is the radius of the sphere and δ the probed correlation length. The variables r_1, α_1 and r_2, α_2 are used to describe the integrals over the shaded area's.

$$\Re\{G_r(0) - G_r(\delta)\} = G_r(0) - G_r(\infty) = 2\int_{A_s} 1 - \cos\{S(y,z)\}dydz. \tag{3.57}$$

This equation can be rewritten as (see also figure 3.5) :

$$\Re\{G_r(0) - G_r(\infty)\} = 2\int_0^{2\pi}\int_0^R r_1\left(1 - \cos\left\{2(n-1)\bar{k}\sqrt{R^2 - r_1^2}\right\}\right)dr_1 d\alpha_1. \tag{3.58}$$

Solving this integral results in:

$$\Re\{G_r(0) - G_r(\infty)\} = \frac{\pi}{2}R^2\eta^2\zeta(\eta), \tag{3.59}$$

where $\eta = \left|2(n-1)R\bar{k}\right|$ and $\zeta(\eta) = 4(2 + \eta^2 - 2\eta\sin\eta - 2\cos\eta)/\eta^4$. η is the phase acquired by a neutron passing through a distance of $2R$ through a material with refractive index n compared to a neutron traveling the same distance through vacuum. For neutrons of 0.2 nm passing through aluminum or silicon the distance to acquire a phase difference of π is about 76 μm, for copper 24 μm. If $\eta \ll 1$ then $\zeta(\eta) \approx 1 - \eta^2/18 + O(\eta^4)$ and if $\eta \gg 1$ then $\zeta(\eta) \approx 4/\eta^2 + O(\eta^{-3})$. This is shown in figure 3.6. The index of refraction is given by equation (3.23) so that $\eta \approx 2R\bar{\lambda}\rho_b$. Hence, in the kinematic limit the above equation reduces to:

$$\Re\{G_r(0) - G_r(\infty)\} \approx 2\pi R^4\bar{\lambda}^2\rho_b^2\left(1 - \frac{\eta^2}{18} + O(\eta^4)\right). \tag{3.60}$$

Note that in the limit of very large η the dependence on the refractive index and the neutron wavelength vanishes: $\Re\{G_r(0) - G_r(\infty)\} = 2\pi R^2$. As soon as $\delta < 2R$ the two sphere's in

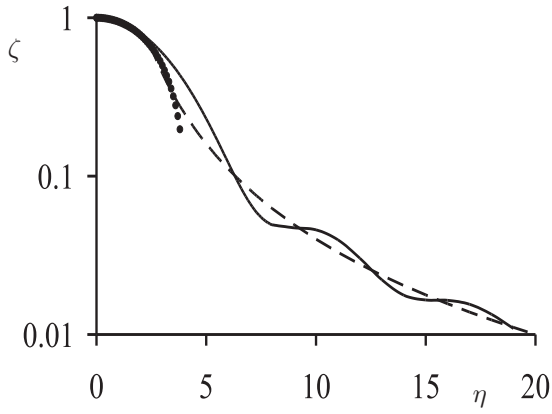

Figure 3.6: Normalized scattering function $\zeta(\eta)$, describing the change in the amplitude of the form factor as function of the phase acquired by a neutron passing through a sphere diameter of sphere material, η (full line). The dotted line is the approximation in the kinematic limit (small η) and the dashed line the approximation in the refraction limit (large η).

figure 3.5 start to overlap and equation (3.56) can only be calculated numerically. However for small η it can be expanded into a series:

$$\Re\{G_r(0) - G_r(\delta)\} = \int_{A_s} \frac{(S(y,z+\delta) - S(y,z))^2}{2} + O((S(y,z+\delta) - S(y,z))^4) dydz. \tag{3.61}$$

Ignoring fourth and higher order terms this reduces to:

$$\Re\{G_r(0) - G_r(\delta)\} = \int_{A_s} S(y,z)^2 dydz - \int_{A_s} S(y,z+\delta)S(y,z) dydz. \tag{3.62}$$

After substituting equation (3.53) for $S(y,z)$ the first term at the right hand side reduces to $\pi R^2\eta^2/2$. The second term can be converted to a solvable double integral by changing the integration variables to r_2 and α_2 (see figure 3.5). This gives for the second term:

$$-\frac{4\eta^2}{R^2}\int_0^{\frac{\pi}{2}}\int_0^{r_{max}} r_2\sqrt{r_2^4 - 2\left(2z^2\cos^2\alpha_2 + 1 - z^2\right)R^2r_2^2 + \left(1-z^2\right)^2R^4}dr_2d\alpha_2, \tag{3.63}$$

where $z = \delta/2R$ and $r_{max} = R\sqrt{1 - z^2\sin^2\alpha_2} - Rz\cos\alpha_2$. This can be rewritten as $-\eta^2R^2f(\delta/2R)$ where:

$$f(z) = 4\int_0^{\frac{\pi}{2}}\int_0^{\sqrt{1-z^2\sin^2\alpha}-z\cos\alpha} r\sqrt{r^4 - 2(2z^2\cos^2\alpha + 1 - z^2)r^2 + \left(1-z^2\right)^2}drd\alpha. \tag{3.64}$$

The inner integral can be solved by changing the integral variable to r^2 and realizing that the integration over r^2 can be extended to $1 - z^2$ if the real value of the result is taken. This yields:

$$f(z) = \frac{\pi}{2}(1-z^2) - z^2\int_0^{\frac{\pi}{2}} 2\cos^2\alpha\left(1 - z^2 + z^2\cos^2\alpha\right)\ln\left\{1 + \frac{1-z^2}{z^2\cos^2\alpha}\right\}d\alpha. \tag{3.65}$$

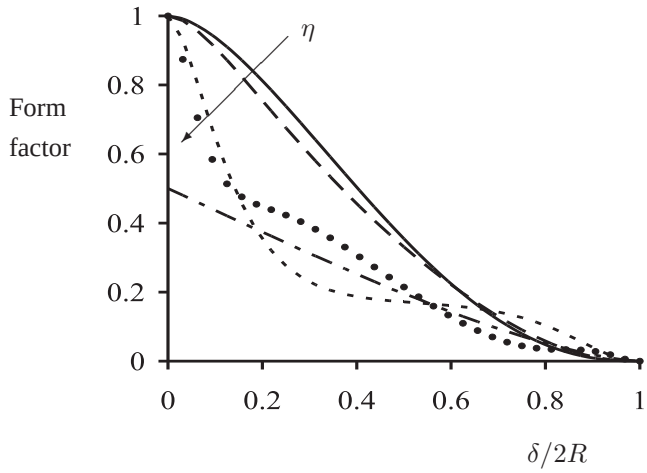

Figure 3.7: Real space form factor of a sphere as function of the reduced probing distance $\delta/2R$ for several values the phase acquired by a neutron passing through a sphere diameter of sphere material, η. Full line: $\eta \ll 1$; long-dashed line: $\eta = \pi$; short-dashed line: $\eta = 2\pi$; dotted line: $\eta = 3\pi$ and dashed-dotted line: $\eta \gg 1$.

This integral can be solved by splitting is into its terms and changing the integral variable to 2α or 4α. After some lengthy calculations this yields:

$$f(z) = \pi \left\{ \left(\frac{z^2}{4} + \frac{1}{2} \right) \sqrt{1 - z^2} - \left(1 - \frac{z^2}{4} \right) z^2 \ln \left(\frac{1 + \sqrt{1 - z^2}}{z} \right) \right\}, \tag{3.66}$$

so that the form factor equation (3.55) in the kinematic limit becomes:

$$F_{kin}(\delta) = \frac{2}{\pi} f(\delta/2R), \tag{3.67}$$

the same as was given by Krouglov [25]. In the kinematic limit the form factor does not depend on η, only on the radius of the sphere. This is shown as the full line in figure 3.7. With increasing η the form factor is decreasing shown as the dashed lines in the figure. If η is of the order of 2π it starts to oscillate around its value for $\eta \gg 1$, represented by the dashed-dotted line. The oscillation is shown for two values of η in the figure. Hence, when η becomes of the order of π or higher significant deviations occur from the kinematic limit. For large value's of η it can be shown that the form factor reduces to:

$$F_{ref}(\delta) = \frac{1 + 2\eta z K_1(2\eta z)}{2} - \frac{\text{asin}(z) + z\sqrt{1 - z^2}}{\pi}, \tag{3.68}$$

where $z = \delta/2R$ and $K_1(x)$ is the first order Bessel function of the second kind [26]. This equation describes the form factor quite well except for the oscillations in the tail. This function is shown as the dashed-dotted line in figure 3.7. Note that for large radius of the sphere z will in general be much smaller than 1 and the last two terms can be ignored. In

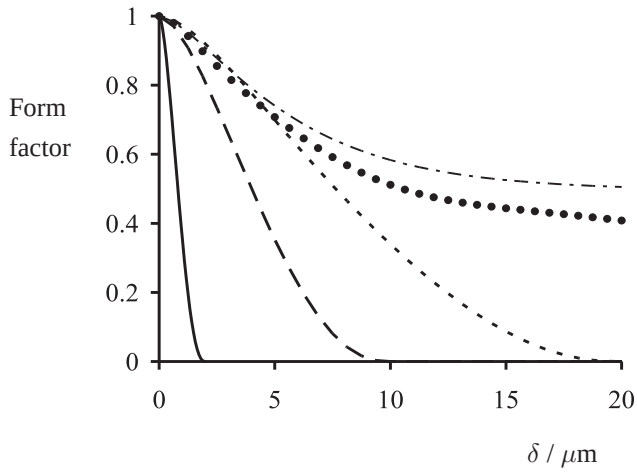

Figure 3.8: Real space form factor of a copper sphere as function of the probing distance δ for several values of its radius. Full line: 1 μm; long-dashed line: 5 μm; short-dashed line: 10 μm; dotted line: 100 μm and dashed-dotted line: 1000 μm.

figure 3.8 the form factor of a homogeneous copper sphere is shown for several values of its radius. Within the shown range the form factor is constant for large radii of the sphere. The form factor is then determined by refraction at the sphere's surface only. One can use Snells law to determine the refraction of neutrons at the surface of the sphere in the same way as it was done for wires by Plomp [27]. Then the same result is found.

The phase-object approximation holds for both Born approximation and refraction. This is due to the large correlation lengths of the objects resulting in scattering under very small angles, down to several micro-radians.

One can related the form factor to the polarization measured by a SESANS instrument. SESANS measures the polarization of the neutron beam as function of the spin echo length, l_{se} [15] (see also chapter 5):

$$l_{se} = c\lambda^2 BL\cot(\theta_1)/2\pi \quad , \tag{3.69}$$

where $c = 4.6368 \times 10^{14}$ T^{-1}m^{-2}, B the magnetic induction at the position of the $\pi/2$-flippers, L the distance between the magnets of one spin echo arm, θ_1 the angle of the interfaces of the precession regions to the neutron beam. The ratio of the measured polarization and the empty beam polarization, P_0 is proportional to the real part of the spatial coherence function:

$$\frac{P(l_{se})}{P_0(l_{se})} = \frac{\Re(G_r(l_{se}))}{\Re(G_r(0))} \quad , \tag{3.70}$$

so that the form factor is equal to the shape of the normalized polarization:

$$\frac{P(l_{se})}{P_0(l_{se})} - \frac{P(\infty)}{P_0(\infty)} = \left(1 - \frac{P(\infty)}{P_0(\infty)}\right) F(l_{se}) \quad . \tag{3.71}$$

The amplitude of the change in the normalized polarization is given by $1 - P(\infty)/P_0(\infty)$ equal to $\Re\{G_r(0) - G_r(\infty)\}/G_r(0)$, which for a sphere is :

$$1 - \frac{P(\infty)}{P_0(\infty)} = \frac{1}{2}\eta^2\zeta(\eta) \quad , \tag{3.72}$$

which in the kinematic and refraction limit reduces to:

$$\begin{aligned} 1 - \tfrac{P(\infty)}{P_0(\infty)} &= \tfrac{1}{2}\eta^2 \quad \eta \ll 1, \\ 1 - \tfrac{P(\infty)}{P_0(\infty)} &= 2 \qquad \eta \gg 1. \end{aligned} \tag{3.73}$$

Note that for the refraction limit this amplitude becomes larger than 1, effectively reversing the polarization of the incoming beam for very large value's of the spin echo length l_{se}.

Chapter 4

Propagation of polarization

To calculate instrumental effects on the measured count rate in case of polarized neutrons one should have a rigorous definition of polarization and measurement methods. For this the concept of *coherence matrix* is introduced. Although it is not a new concept in coherence theory [1], it has not been applied to propagation of neutrons. Matrix calculations are well known to determine the change in the polarization vector. These calculations are more or less based on the solution of Schrödinger equations for the spin-expectation values. The components of the polarization vector are 3 parts of the 4-parts Stokes parameters. The fourth part is the beam intensity. Together the Stokes parameters perfectly describe a quasi-monochromatic beam at a certain position. They however fail to indicate how the polarization or intensity of the beam is propagated. The coherence matrix facilitates this. A further advantage of the coherence matrix over the Stokes parameters is that the relation between non-magnetic scattering and the quantum nature of neutron scattering phenomena is not blurred and it can be incorporated in the coherence theory.

4.1 Definitions

For particle wave functions, where interaction with magnetic and electric forces can not be ignored, Dirac [28] was able to reduce the time-dependent Schrödinger equation using two linear dependent solutions. The same procedure is followed to find the equation for neutron wave functions, where in general electric and gravitational forces are ignored:

$$i\hbar\frac{\partial}{\partial t}\begin{pmatrix}\Psi^{+}(\vec{r},t)\\ \Psi^{-}(\vec{r},t)\end{pmatrix}=\left\{-\frac{\hbar^2}{2m}\nabla^2+V(\vec{r})-g_r\mu_N\widehat{\sigma}\cdot\vec{B}(\vec{r},t)\right\}\begin{pmatrix}\Psi^{+}(\vec{r},t)\\ \Psi^{-}(\vec{r},t)\end{pmatrix}, \quad (4.1)$$

where $\widehat{\sigma}$ is the Pauli spin matrix vector (components as shown in equation (4.5)), $V(\vec{r})$ is the complex nuclear optical potential, g_r the gyro magnetic ratio, μ_N the nuclear magneton and $\vec{B}(\vec{r},t)$ the magnetic flux density [5]. The linear dependent solutions $\Psi^{+}(\vec{r},t)$ and $\Psi^{-}(\vec{r},t)$ represent respectively the *up spin state* and *down spin state* part of the wave function. The quantity $g_r\mu_N B(\vec{r},t)$ is known as the Zeeman energy as it gives the energy gain or loss of a neutron experiencing a magnetic flux density ($g_r\mu_N \approx 60.3$ neV/T). The Zeeman energy

must be compared to the total kinetic energy of the neutron given by $\hbar^2\bar{k}^2/2m$ (≈ 20.5 meV for neutrons with a wavelength of 0.2 nm). For moderate values of the magnetic flux density of about 1/3 T, the Zeeman energy is 6 orders of magnitude smaller than the kinetic energy.

If, as in the previous chapter, a uniform quasi-monochromatic well-collimated and statistically stationary beam is considered one can define the 2×2 *coherence matrix*:

$$\widehat{\Gamma}(\vec{r}_1, \vec{r}_2, \tau) = \left\langle \begin{pmatrix} \Psi^+(\vec{r}_2, t+\tau) \\ \Psi^-(\vec{r}_2, t+\tau) \end{pmatrix} \begin{pmatrix} \Psi^+(\vec{r}_1, t)^* & \Psi^-(\vec{r}_1, t)^* \end{pmatrix} \right\rangle_t, \tag{4.2}$$

which can be reduced to:

$$\widehat{\Gamma}(\vec{r}_1, \vec{r}_2, \tau) = \begin{bmatrix} \Gamma^{++}(\vec{r}_1, \vec{r}_2, \tau) & \Gamma^{+-}(\vec{r}_1, \vec{r}_2, \tau) \\ \Gamma^{+-}(\vec{r}_2, \vec{r}_1, -\tau)^* & \Gamma^{--}(\vec{r}_1, \vec{r}_2, \tau) \end{bmatrix}, \tag{4.3}$$

where $\Gamma^{++}(\vec{r}_1, \vec{r}_2, \tau)$ is the mutual coherence function of the *up* state of the wave function, $\Gamma^{--}(\vec{r}_1, \vec{r}_2, \tau)$ the same of the *down* state and $\Gamma^{+-}(\vec{r}_1, \vec{r}_2, \tau)$ the *cross coherence function* of the two states. As was already noted by Mezei in 1980 [9] the polarization of a neutron beam can be interpreted as the degree of coherence between the wave functions representing the two spin states of neutron. Then, the *local* polarization is defined as:

$$P_j(\vec{r}) = \frac{\left\langle \begin{pmatrix} \Psi^+(\vec{r}, t)^* & \Psi^-(\vec{r}, t)^* \end{pmatrix} \widehat{\sigma}_j \begin{pmatrix} \Psi^+(\vec{r}, t) \\ \Psi^-(\vec{r}, t) \end{pmatrix} \right\rangle_t}{\langle \Psi^+(\vec{r}, t)\Psi^+(\vec{r}, t)^* \rangle_t + \langle \Psi^-(\vec{r}, t)\Psi^-(\vec{r}, t)^* \rangle_t}, \tag{4.4}$$

where the index j denotes the x, y or z component and $\widehat{\sigma}_j$ are the Pauli spin matrices:

$$\widehat{\sigma}_x = \begin{pmatrix} 0 & 1 \\ 1 & 0 \end{pmatrix}, \quad \widehat{\sigma}_y = \begin{pmatrix} 0 & -i \\ i & 0 \end{pmatrix} \text{ and } \widehat{\sigma}_z = \begin{pmatrix} 1 & 0 \\ 0 & -1 \end{pmatrix}. \tag{4.5}$$

The polarization vector at some position $\vec{r}$ can be described by the elements of the coherence matrix:

$$\vec{P}(\vec{r}) = \frac{1}{\Gamma^{++}(\vec{r}, \vec{r}, 0) + \Gamma^{--}(\vec{r}, \vec{r}, 0)} \begin{pmatrix} \Gamma^{+-}(\vec{r}, \vec{r}, 0) + \Gamma^{+-}(\vec{r}, \vec{r}, 0)^* \\ i\Gamma^{+-}(\vec{r}, \vec{r}, 0) - i\Gamma^{+-}(\vec{r}, \vec{r}, 0)^* \\ \Gamma^{++}(\vec{r}, \vec{r}, 0) - \Gamma^{--}(\vec{r}, \vec{r}, 0) \end{pmatrix}. \tag{4.6}$$

or in short notation:

$$P_j(\vec{r}) = \frac{\mathrm{Tr}(\widehat{\Gamma}(\vec{r}, \vec{r}, 0)\widehat{\sigma}_j)}{\mathrm{Tr}(\widehat{\Gamma}(\vec{r}, \vec{r}, 0))}, \tag{4.7}$$

where again the index j denotes the x, y or z component and $\mathrm{Tr}(\widehat{A})$ denotes the trace of matrix $\widehat{A}$. This can be reversed into:

$$\frac{\widehat{\Gamma}(\vec{r}, \vec{r}, 0)}{\mathrm{Tr}(\widehat{\Gamma}(\vec{r}, \vec{r}, 0))} = \frac{1}{2}\left(\widehat{I} + P_x(\vec{r})\widehat{\sigma}_x + P_y(\vec{r})\widehat{\sigma}_y + P_z(\vec{r})\widehat{\sigma}_z\right). \tag{4.8}$$

Note that the polarization is fully known if the coherence matrix is known, but not vise versa.

Although for insight in the design of an instrument or experiment it can be useful to examine changes in the polarization vector for a neutron passing along a certain path through

the instrument, this view is not sufficient to understand all possible effects. For instance, the neutron flux is given by:

$$\vec{J}(\vec{r}) = 2\vec{v}_p \mathrm{Tr}(\widehat{\Gamma}(\vec{r},\vec{r},0)). \tag{4.9}$$

As in equation (2.3), is was assumed that the beam has the same direction as $\vec{v}_p$ for both up and down spin states. In general this is not the case as in principle the up and down spin states can propagate through a magnetic flux density in different directions (see section 4.6). However in most practical cases the coherence length is too small or the spread in directions too large to observe the beam splitting and the above approximation is valid. This was already stressed by Mezei in [9] and [29].

4.2 Propagation of coherence matrix

If the magnetic flux density and complex optical potential is constant in time, the wave equations for the coherence matrix can be derived from their definition (4.2) and the above Schrödinger equation:

$$\nabla_1^2 \widehat{\Gamma}(\vec{r}_1,\vec{r}_2,\tau) = -\widehat{\Gamma}(\vec{r}_1,\vec{r}_2,\tau)\left\{k(\vec{r}_1)^2\widehat{I} + \kappa(\vec{r}_1)^2\left(\widehat{\sigma}\cdot\vec{n}_B(\vec{r}_1)\right)\right\}, \tag{4.10}$$

$$\nabla_2^2 \widehat{\Gamma}(\vec{r}_1,\vec{r}_2,\tau) = -\left\{k(\vec{r}_2)^2\widehat{I} + \kappa(\vec{r}_2)^2\left(\widehat{\sigma}\cdot\vec{n}_B(\vec{r}_2)\right)\right\}\widehat{\Gamma}(\vec{r}_1,\vec{r}_2,\tau), \tag{4.11}$$

where $k(\vec{r})^2 = \bar{k}^2 - 2mV(\vec{r})/\hbar^2$, $\kappa(\vec{r})^2 = 2mg_r\mu_N B(\vec{r})/\hbar^2$ and $\widehat{I}$ is the 2×2 identity matrix. $\vec{n}_B(\vec{r})$ is a unit vector in the direction of the magnetic flux density, $\vec{B}(\vec{r})$. These two equations describe the propagation of the coherence matrix and can be solved given a certain profile for the magnetic flux density and complex optical potential.

In most cases where the magnetic flux density is generated by macroscopic objects $\kappa(\vec{r}) \ll k(\vec{r})$ the propagation will be determined mainly by the first term of the above equations and the difference between the propagation of the elements of the coherence matrix is very small. To underline the difference the reduced coherence matrix $\widehat{\gamma}_B$ is defined as:

$$\widehat{\Gamma}(\vec{r}_1,\vec{r}_2,\tau) = \Gamma_0(\vec{r}_1,\vec{r}_2,\tau)\widehat{\gamma}_B(\vec{r}_1,\vec{r}_2,\tau), \tag{4.12}$$

where $\Gamma_0(\vec{r}_1,\vec{r}_2,\tau)$ would have been the mutual coherence function of the wave function when all magnetics flux densities were turned off and obeys the wave equations for the mutual coherence function for the non-magnetic wave function:

$$\nabla_j^2\Gamma_0(\vec{r}_1,\vec{r}_2,\tau) = -k(\vec{r}_j)^2\Gamma_0(\vec{r}_1,\vec{r}_2,\tau). \tag{4.13}$$

Note that the polarization vector can be calculated directly from the reduced coherence matrix. Let the vector $\vec{k}(\vec{r}_1)$ be defined as:

$$\vec{\nabla}_1\Gamma_0(\vec{r}_1,\vec{r}_2,\tau) = -i\vec{k}^*(\vec{r}_1)\Gamma_0(\vec{r}_1,\vec{r}_2,\tau). \tag{4.14}$$

The complex conjugate is used because of the definition of Γ_0 (equation (2.6)). Then also, because $\Gamma_0(\vec{r}_1,\vec{r}_2,\tau) = \Gamma_0(\vec{r}_2,\vec{r}_1,-\tau)^*$:

$$\vec{\nabla}_2\Gamma_0(\vec{r}_1,\vec{r}_2,\tau) = i\vec{k}(\vec{r}_2)\Gamma_0(\vec{r}_1,\vec{r}_2,\tau). \tag{4.15}$$

For a slowly varying complex optical potential $\left|\vec{\nabla}_j \cdot \vec{k}(\vec{r}_j)\right| \ll |k(\vec{r}_1)|^2 \approx |k(\vec{r}_2)|^2$ it can be shown that:

$$\vec{k}(\vec{r}_1)^* \cdot \vec{\nabla}_1 \widehat{\gamma}_B(\vec{r}_1, \vec{r}_2, \tau) = -\frac{i\kappa(\vec{r}_1)^2}{2} \widehat{\gamma}_B(\vec{r}_1, \vec{r}_2, \tau) \left(\widehat{\sigma} \cdot \vec{n}_B(\vec{r}_1)\right), \tag{4.16}$$

$$\vec{k}(\vec{r}_2) \cdot \vec{\nabla}_2 \widehat{\gamma}_B(\vec{r}_1, \vec{r}_2, \tau) = \frac{i\kappa(\vec{r}_2)^2}{2} \left(\widehat{\sigma} \cdot \vec{n}_B(\vec{r}_2)\right) \widehat{\gamma}_B(\vec{r}_1, \vec{r}_2, \tau). \tag{4.17}$$

Equations (4.13), (4.16) and (4.17) describe the propagation of the coherence matrix. The mutual coherence function of the unpolarized beam, without interaction with the magnetic flux density, Γ_0 propagates as discussed in chapter 2. Note that in the derivation of this conclusion it was assumed that the Zeeman energy was much smaller than the kinetic energy of the neutrons. This implies that the reflection of the neutrons at any transition in the magnetic flux density is neglected. Note that the differential equations (4.16) and (4.17) are not independent of Γ_0, because of the definition (4.14) of $\vec{k}(\vec{r})$. In the following section the propagation of $\widehat{\gamma}_B$ is discussed.

4.3 Constant magnetic flux density direction

For some region in space where the *direction* of the magnetic flux density is constant one can always make the spin-quantization direction equal to this direction by appropriate rotation of the reference frame [30]. Rotation of the reference frame from the z-direction ($\vec{e}_z$) to the direction of the magnetic flux density,

$$\vec{n}_B = \begin{pmatrix} \cos\vartheta \sin\theta \\ \sin\vartheta \sin\theta \\ \cos\theta \end{pmatrix} \tag{4.18}$$

transforms the coherence matrix through:

$$\widehat{\Gamma}_{rot}(\vec{r}_1, \vec{r}_2, \tau) = \widehat{R}_{\vec{n}_B(\vec{r}_2)} \widehat{\Gamma}(\vec{r}_1, \vec{r}_2, \tau) \widehat{R}^{\dagger}_{\vec{n}_B(\vec{r}_1)}, \tag{4.19}$$

where $\widehat{R}^{\dagger}$ represents the conjugate transpose of $\widehat{R}$ and $\widehat{R}_{\vec{n}_B} = \widehat{T}_y(\theta)\widehat{T}_z(\vartheta)$ and

$$\widehat{T}_y(\tau) = \begin{pmatrix} \cos\frac{\tau}{2} & \sin\frac{\tau}{2} \\ -\sin\frac{\tau}{2} & \cos\frac{\tau}{2} \end{pmatrix} \quad \text{and} \quad \widehat{T}_z(\tau) = \begin{pmatrix} e^{i\tau/2} & 0 \\ 0 & e^{-i\tau/2} \end{pmatrix}. \tag{4.20}$$

For the region of a magnetic flux density in the z- or quantization- direction the equations (4.16) and (4.17) reduce to ($\vec{n}_B = \vec{e}_z$):

$$\vec{k}(\vec{r}_1)^* \cdot \vec{\nabla}_1 \widehat{\gamma}_B(\vec{r}_1, \vec{r}_2, \tau) = -\frac{i\kappa(\vec{r}_1)^2}{2} \widehat{\gamma}_B(\vec{r}_1, \vec{r}_2, \tau) \widehat{\sigma}_z, \tag{4.21}$$

$$\vec{k}(\vec{r}_2) \cdot \vec{\nabla}_2 \widehat{\gamma}_B(\vec{r}_1, \vec{r}_2, \tau) = \frac{i\kappa(\vec{r}_2)^2}{2} \widehat{\sigma}_z \widehat{\gamma}_B(\vec{r}_1, \vec{r}_2, \tau). \tag{4.22}$$

For a completely coherent and homogeneous beam in vacuum $\vec{k}(\vec{r}) = \bar{k}\vec{n}_k$ is constant and the solution of these differential equations is given by:

$$\widehat{\gamma}_B(\vec{r}_1, \vec{r}_2, \tau) = \widehat{T}_z(\phi(\vec{r_2'}, \vec{r}_2)) \widehat{\gamma}_B(\vec{r_1'}, \vec{r_2'}, \tau) \widehat{T}_z(\phi(\vec{r_1'}, \vec{r}_1))^{\dagger}, \tag{4.23}$$

where $\vec{r}_j - \vec{r}'_j = \left|\vec{r}_j - \vec{r}'_j\right| \vec{n}_k$ and

$$\phi(\vec{r}', \vec{r}) = \bar{k}^{-1} \int_{\vec{r}'}^{\vec{r}} \kappa(\vec{r})^2 dr = \frac{2mg_r\mu_N}{\hbar^2 \bar{k}} \int_{\vec{r}'}^{\vec{r}} B(\vec{r}) dr \tag{4.24}$$

is a measure for the extra phase acquired by the neutron wave function due to the interaction with the magnetic flux density and closely related to S as defined in equation (3.25).

Equation (4.23) shows that the propagation of the coherence matrix from one position to another through a magnetic flux density with constant direction can be calculated by means of the line integral representing the extra phase acquired by a specific neutron (up or down spin state) when traveling from the first position to the last position along the classical neutron path. Combining equation (4.19) and (4.23) for a region with constant magnetic flux density direction $\vec{n}_B$ results in:

$$\widehat{\gamma}_B(\vec{r}_1, \vec{r}_2, \tau) = \widehat{M}(\vec{r}_2, \vec{r}'_2)\widehat{\gamma}_B(\vec{r}'_1, \vec{r}'_2, \tau)\widehat{M}(\vec{r}_1, \vec{r}'_1)^\dagger, \tag{4.25}$$

where $\widehat{M}(\vec{r}, \vec{r}') = \widehat{R}^{-1}_{\vec{n}_B(\vec{r})}\widehat{T}_z(\phi(\vec{r}', \vec{r}))\widehat{R}_{\vec{n}_B(\vec{r}')}$. The most general form of this matrix is a *rotation* matrix, $\widehat{H}$, some of which properties are discussed in appendix A. In the following sections these properties are exploited together with the fact that a trace of a matrix is invariable to cyclic permutations and that the trace of a sum of matrices is the same as the sum of the traces of these matrices.

4.4 Larmor precession

In a region of length L where both the direction, $\vec{n}$ and the magnitude of the magnetic flux density, B are constant, matrix $\widehat{M}$ as defined in the previous section is given by:

$$\widehat{M} = \widehat{R}^{-1}_{\vec{n}}\widehat{T}_z(c\bar{\lambda}BL)\widehat{R}_{\vec{n}}, \tag{4.26}$$

where $c = -4\pi m g_r \mu_N / h^2 = 4.63209 \times 10^{14}\ \mathrm{T^{-1}m^{-2}}$. This equation can be rewritten as:

$$\widehat{M} = \widehat{I}\cos\frac{\gamma_L B t_L}{2} - i\left(n_x\widehat{\sigma}_x + n_y\widehat{\sigma}_y + n_z\widehat{\sigma}_z\right)\sin\frac{\gamma_L B t_L}{2}, \tag{4.27}$$

where $t_L = 2L/v_p$ is the travel time of a neutron with wavelength, $\bar{\lambda}$ through the region of magnetic flux density, $\gamma_L = -2g_r\mu_N/\hbar = 1.832472 \times 10^8\ \mathrm{T^{-1}s^{-1}}$ and $\gamma_L B$ is known as the *Larmor* frequency, independent of the wavelength of the neutrons. As shown in appendix A this matrix can be interpreted as a rotation of the polarization vector of $\gamma_L B t_L$ radians around the direction of the magnetic flux density. This is why this type of propagation of the coherence matrix is know as *Larmor precession*.

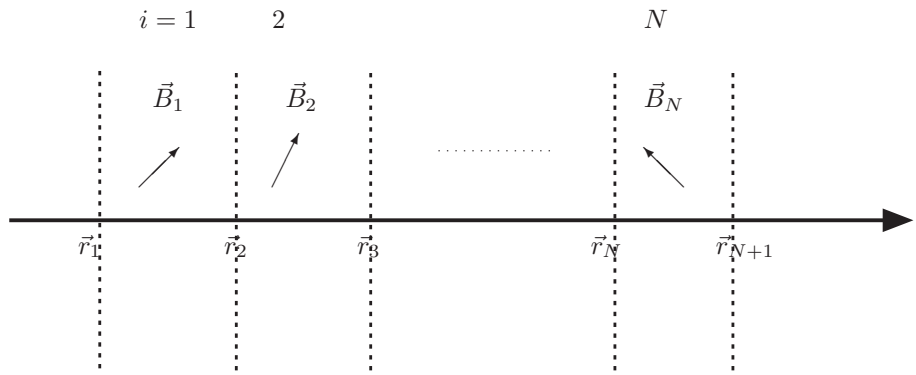

Figure 4.1: Sequence in space of magnetic flux densities representing a space dependent magnetic flux density $\vec{B}(\vec{r})$.

4.5 General magnetic flux density

If between $\vec{r}$ and $\vec{r'}$ the direction of the magnetic flux density changes too much (see figure 4.1) the region between $\vec{r'}$ and $\vec{r}$ can be divided into N regions where the direction does not change appreciable. The matrix $\widehat{M}(\vec{r}, \vec{r'})$ in equation (4.25) must be replaced by

$$\widehat{D}(\vec{r}, \vec{r'}) = \prod_{i=1}^{N} \widehat{M}_i(\vec{r}_{i+1}, \vec{r}_i), \tag{4.28}$$

where $\vec{r}_1 = \vec{r'}$, $\vec{r}_{N+1} = \vec{r}$, $\vec{r}_i$ indicates the border between region i and $i+1$ and the matrix $\widehat{M}_i(\vec{r}_{i+1}, \vec{r}_i)$ describes the propagation of the reduced coherence matrix in region i. Matrix $\widehat{D}$ is called a device matrix as it describes the influence of the neutron manipulation device on the propagation of the coherence matrix. Note that as in this case $\widehat{D}$ is a product of rotation (or streaming) matrices only, it can also be represented by a rotation matrix.

For a constant magnetic flux density and optical potential the propagation of the coherence matrix can also be derived in the way shown by Mandel [1] to obtain equation (2.26). The procedure applies twice Rayleigh's first diffraction formula and uses the definition of the mutual coherence function. Rayleigh's first diffraction formula describes the propagation of a wave function from a plane. Here one must take into account that the wavevector of the up and down neutron wave function is different, due to the magnetic interaction. This yields for the propagation of the coherence matrix when $R_i \gg \lambda$:

$$\widehat{\Gamma}(\vec{r}_1, \vec{r}_2, \tau) = \int\int_{x=0} \frac{\cos\theta_1 \cos\theta_2}{4\pi^2 R_1 R_2} \widehat{T}_k(R_2) \widehat{\Gamma}\left(\vec{r'_1}, \vec{r'_2}, \tau\right) \widehat{T}_k(R_1)^\dagger d^2 r'_1 d^2 r'_2, \tag{4.29}$$

where

$$\widehat{T}_k(R) = \begin{pmatrix} k^+ e^{ik^+ R} & 0 \\ 0 & k^- e^{ik^- R} \end{pmatrix} \tag{4.30}$$

and $k^{\pm} = (\bar{k}^2 \pm \kappa^2)^{1/2}$. k^+ represents the (average) wavevector of the up spin wave (parallel to the magnetic flux density) and k^- the same for the down spin wave. Because $\kappa \ll \bar{k}$ it is possible to expand $k^{\pm}$ as $\bar{k} \pm \delta\kappa$, where $\delta\kappa = \kappa^2/2\bar{k}$ and use the approximation:

$$\widehat{T}_k(R) \approx \bar{k} e^{i\bar{k}R} \widehat{T}_z(\delta\kappa R). \tag{4.31}$$

Then the above equation reduces to:

$$\widehat{\Gamma}(\vec{r}_1, \vec{r}_2, \tau) = \tag{4.32}$$

$$\int\int_{x=0} \frac{\cos\theta_1 \cos\theta_2 e^{i\bar{k}(R_2 - R_1)}}{R_1 R_2 \bar{\lambda}^2} \widehat{T}_z(\delta\kappa R_2) \widehat{\Gamma}\left(\vec{r'_1}, \vec{r'_2}, \tau\right) \widehat{T}_z(\delta\kappa R_1)^\dagger d^2 r'_1 d^2 r'_2.$$

If the transversal coherence length (see section 2.2) of the neutron beam, $r_c \ll \delta\kappa^{-1}$ and the far-zone of the field is considered (see section 2.5) the matrices just before and after the coherence matrix inside the integral do not depend on $\vec{r'}_1$ and $\vec{r'}_2$ and can be put outside the integral. The integral then gets the same form as the propagation integral equation (2.35) of the mutual coherence function. It can be repeated over subsequent regions in space where a (different strength) magnetic flux density exists, so that the arguments of the matrices before and after the integral are converted into a sum over all regions which is equal to the line integral as defined in equation (4.24). Hence, the above equation can be rewritten using the definition of the reduced coherence matrix into:

$$\widehat{\gamma}_B(\vec{r}_1, \vec{r}_2, \tau) =$$

$$\widehat{T}_z(\phi(\vec{r'_2}, \vec{r}_2) \frac{\int\int_{x=0} e^{-i\bar{k}r_{12}} \Gamma_0(\vec{r'_1}, \vec{r'_2}, \tau) \widehat{\gamma}_B(\vec{r'_1}, \vec{r'_2}, \tau) d^2 r'_1 d^2 r'_2}{\int\int_{x=0} e^{-i\bar{k}\vec{r}_{12}} \Gamma_0(\vec{r'_1}, \vec{r'_2}, \tau) d^2 r'_1 d^2 r'_2} \widehat{T}_z(\phi(\vec{r'_1}, \vec{r}_1)^\dagger, \tag{4.33}$$

where $r_{12} = \vec{r}_2 \cdot \vec{r'_2}/r_2 - \vec{r}_1 \cdot \vec{r'_1}/r_1$. If $\widehat{\gamma}_B(\vec{r'}_1, \vec{r'}_2, \tau)$ on the $x = 0$ plane does not depend on $\vec{r'}_1$ or $\vec{r'}_2$ it reduces to:

$$\widehat{\gamma}_B(\vec{r}_1, \vec{r}_2, \tau) = \widehat{T}_z(\phi(\vec{r'_2}, \vec{r}_2) \widehat{\gamma}_B(\vec{r'}_1, \vec{r'}_2, \tau) \widehat{T}_z(\phi(\vec{r'_1}, \vec{r}_1)^\dagger, \tag{4.34}$$

the same as equation (4.23).

One can extend the above reasoning to the general case where the magnetic flux density varies *slowly* in space. Slowly means that the changes in the magnetic flux density are on a scale much larger than $\delta\kappa^{-1}$. In this situation the matrices before and after the coherence matrix in equation (4.32) are converted into matrices according to equation (4.28) and equation (4.32) changes to:

$$\widehat{\Gamma}(\vec{r}_1, \vec{r}_2, \tau) = \tag{4.35}$$

$$\int\int_{x=0} \frac{\cos\theta_1 \cos\theta_2 e^{i\bar{k}(R_2 - R_1)}}{R_1 R_2 \bar{\lambda}^2} \widehat{D}(\vec{r}_2, \vec{r'_2}) \widehat{\Gamma}\left(\vec{r'_1}, \vec{r'_2}, \tau\right) \widehat{D}(\vec{r}_1, \vec{r'_1})^\dagger d^2 r'_1 d^2 r'_2,$$

reducing in the far-zone limit to:

$$\widehat{\Gamma}(\vec{r}_1, \vec{r}_2, \tau) = \tag{4.36}$$

$$\frac{\cos\theta_1 \cos\theta_2 e^{i\bar{k}(r_2 - r_1)}}{r_1 r_2 \bar{\lambda}^2} \int\int_{x=0} e^{-i\bar{k}r_{12}} \widehat{D}(\vec{r}_2, \vec{r'_2}) \widehat{\Gamma}\left(\vec{r'_1}, \vec{r'_2}, \tau\right) \widehat{D}(\vec{r}_1, \vec{r'_1})^\dagger d^2 r'_1 d^2 r'_2.$$

It is also possible to calculate the device matrix $\widehat{D}$ if the magnetic flux density changes in a specific way. This was done by Schwink and Schärpf [31] for helical magnetic structures.

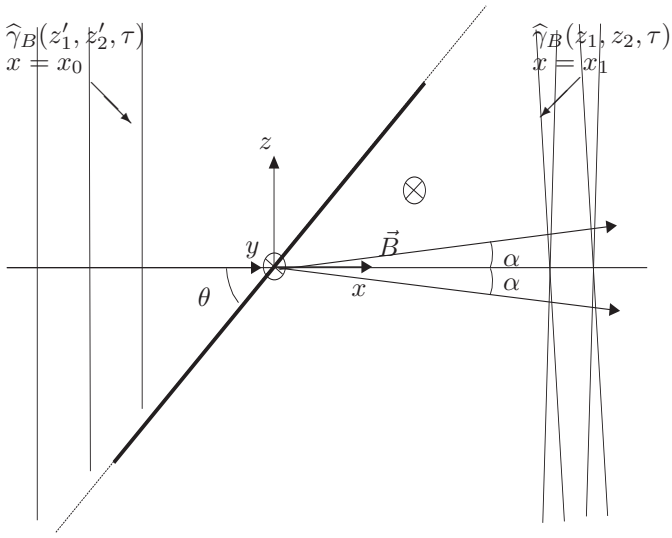

Figure 4.2: Polarized beam splitting by a region of constant magnetic flux density.

They found that in these cases the up and down spin states propagate *both* with the two wavevectors $\vec{k}^+$ and $\vec{k}^-$. The propagation reduced to a propagation with one wavevector if the quantization axis is continuously rotated and taken along the direction of the magnetic flux density.

4.6 Beam splitting

In case the direction of the magnetic flux density in some region is parallel to a fixed-axis the propagation of the coherence matrix can be calculated according to the previous section. If a neutron beam propagates along the x-axis and the boundary of the magnetic flux density is not perpendicular to the propagation direction, so-called beam splitting is observed as shown in figure 4.2. The propagation of the coherence matrix is given by equation (4.32). The propagation of the two diagonal elements of this matrix are comparable to the propagation of the mutual coherence function as given in section 3.4. The refraction index is now given by $n^{\pm} = 1 \pm \delta\kappa/\bar{k}$, where $+$ denotes the up-spin wave and $-$ the down-spin wave. The refraction angle (see figure 4.2) $\alpha = \delta\kappa/\bar{k}\cot\theta$. For a magnetic flux density of 1/3 T, $\theta = 45^o$ and a neutron wavelength of 0.2 nm $\alpha \approx 0.5$ μrad. The down-spin wave is refracted at the boundary with an angle exactly opposite to the one of the up-spin wave. The off-diagonal elements of the coherence matrix propagate in the same way, but have an extra phase shift of $\delta\kappa(R_2 + R_1)$. If $R_2 + R_1 \gg \delta\kappa^{-1}$ the value of the integral reduces very fast to 0. To observe beam splitting it is needed that equation (4.32) can not be reduced to equation (4.34). This is the case when the transversal coherence length is of the same order or larger than $\delta\kappa^{-1}$ as shown in the previous section. If the transversal coherence length is much smaller than $\delta\kappa^{-1}$ the splitting of the beam can be neglected and equation (4.34)

can be used to calculate the propagation of the coherence matrix. Note that the transversal coherence length is also a measure of the divergence of the beam (see section 2.8). The larger the coherence length the smaller the beam divergence. Hence the minimum coherence length required to observe beam splitting can be translated into the maximum allowed beam divergence to observe beam splitting. Clearly the beam divergence should be less or of the same order as α.

4.7 Polarization analysis

A typical layout of a neutron polarization manipulating instrument is shown in figure 4.3. The source can be a reactor or pulsed-source, producing unpolarized neutrons. The polarizer and analyser are devices which preferentially transmit one spin state over the other. The polarizer creates a polarized beam and the analyser is used to analyze the polarization of the beam at the exit of the instrument. Here, it is assumed that the device matrix of a polarizer can be characterized by two functions: the polarizing power P_P and the transmission T_P:

$$\widehat{D}_P(\vec{r'},\vec{r}) = \sqrt{\frac{T_P(\vec{r'},\vec{r})}{2}} \begin{pmatrix} \sqrt{1+P_P(\vec{r'},\vec{r})} & 0 \\ 0 & \sqrt{1-P_P(\vec{r'},\vec{r})} \end{pmatrix}, \tag{4.37}$$

and the same for the analyser with subscript P replaced by A. Note that the matrix in this equation is *not* a rotation matrix except if $P_P(\vec{r'},\vec{r}) = 0$.

For a directed quasi-monochromatic beam the neutron flux at the detector position is given by:

$$\vec{J}(\vec{r}_d) = 2\vec{v}_p \mathrm{Tr}(\widehat{\Gamma}(\vec{r}_d,\vec{r}_d,0)), \tag{4.38}$$

which with equations (4.12) and (4.36) can be reduced to ($\cos\theta_1 \approx \cos\theta_2 \approx 1$):

$$\vec{J}(\vec{r}_d) = \frac{2\vec{v}_p}{r_d^2\bar{\lambda}^2} \times \tag{4.39}$$

$$\int\int_{x=0} e^{-i\vec{p}\cdot(\vec{r_2'}-\vec{r_1'})} \Gamma_0(\vec{r_1'},\vec{r_2'},0) \mathrm{Tr}\left(\widehat{M}(\vec{r}_d,\vec{r_2'})\widehat{\gamma}_B(\vec{r_1'},\vec{r_2'},0)\widehat{M}(\vec{r}_d,\vec{r_1'})^\dagger\right) d^2r_1' d^2r_2'.$$

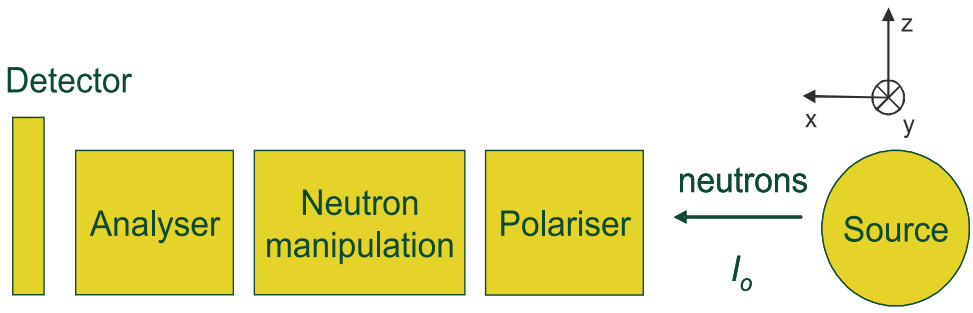

Figure 4.3: Scheme of neutron polarization manipulation instrument.

where $\vec{p} = \bar{k}\vec{r}_d/r_d$ and $\widehat{M}$ is the matrix describing the whole instrument:

$$\widehat{M}(\vec{r}_d, \vec{r'}) = \widehat{D}_A(\vec{r}_d, \vec{r'})\widehat{D}(\vec{r}_d, \vec{r'})\widehat{D}_P(\vec{r}_d, \vec{r'}), \tag{4.40}$$

and $\widehat{D}$ the overall matrix of the neutron manipulation devices between the analyser and polarizer. Remember that the matrix $\widehat{M}(\vec{r}_1, \vec{r}_0)$ can be calculated as a product of matrices corresponding to regions with a constant magnetic flux density encountered by the neutron traveling in a straight line form $\vec{r}_0$ to $\vec{r}_1$. Further, if the neutron source is unpolarized: $\widehat{\gamma}_B(\vec{r'}_1, \vec{r'}_2, 0) = \widehat{I}/2$ yielding:

$$\vec{J}(\vec{r}_d) = \frac{\vec{v}_p}{r_d^2\bar{\lambda}^2}\int\int_{x=0} e^{-i\vec{p}\cdot(\vec{r_2'}-\vec{r_1'})}\Gamma_0(\vec{r_1'}, \vec{r_2'}, 0)\mathrm{Tr}\left(\widehat{M}(\vec{r}_d, \vec{r_2'})\widehat{M}(\vec{r}_d, \vec{r_1'})^\dagger\right) d^2r_1' d^2r_2'. \tag{4.41}$$

The neutron flux at the detector position can be calculated from the elements of matrix $\widehat{M}$ describing the spin-manipulations in the instrument. The matrix describing the action of the analyser on the neutron spin, $\widehat{D}_A(\vec{r}_d, \vec{r'})$ will in general only depend slightly on $\vec{r'}$. Over ranges within the coherence length it will be constant. Hence

$$\widehat{D}_A(\vec{r}_d, \vec{r_2'})\widehat{D}_A(\vec{r}_d, \vec{r_1'})^\dagger \approx \widehat{D}_A(\vec{r}_d, \vec{r_1'})\widehat{D}_A(\vec{r}_d, \vec{r_1'})^\dagger = T_A(\vec{r_1'}, \vec{r}_d)\frac{\widehat{I} + P_A(\vec{r}_d, \vec{r_1'})\widehat{\sigma}_z}{2} \tag{4.42}$$

and the same holds for the polarizer. Now equation (4.41) this can be rewritten as:

$$\vec{J}(\vec{r}_d) = \frac{2\vec{v}_p}{r_d^2\bar{\lambda}^2}\times \tag{4.43}$$

$$\int\int_{x=0} e^{-i\vec{p}\cdot(\vec{r_2'}-\vec{r_1'})}\Gamma_0(\vec{r_1'}, \vec{r_2'}, 0)T_A(\vec{r_1'}, \vec{r}_d)T_P(\vec{r_1'}, \vec{r}_d)\Omega(\vec{r}_d, \vec{r_1'}, \vec{r_2'})d^2r_1' d^2r_2',$$

where

$$\Omega(\vec{r}_d, \vec{r_1'}, \vec{r_2'}) = \mathrm{Tr}\left(\frac{\widehat{I} + P_A(\vec{r}_d, \vec{r_1'})\widehat{\sigma}_z}{2}\widehat{D}(\vec{r}_d, \vec{r_2'})\frac{\widehat{I} + P_P(\vec{r}_d, \vec{r_1'})\widehat{\sigma}_z}{2}\widehat{D}(\vec{r}_d, \vec{r_1'})^\dagger\right). \tag{4.44}$$

One can insert flippers just before the analyser and directly after the polarizer. The manipulation of a flipper on the polarization can be represented by a rotation matrix $\widehat{F}(\vec{r}_d, \vec{r'})$ for which holds $\widehat{F}(\vec{r}_d, \vec{r'})\widehat{F}(\vec{r}_d, \vec{r'})^\dagger = 1$. Such a matrix will in general only depend slightly on $\vec{r'}$. Over ranges within the coherence length it will be constant and $\widehat{F}(\vec{r}_d, \vec{r_2'})\widehat{F}(\vec{r}_d, \vec{r_1'})^\dagger = 1$. The matrices $\widehat{D}$ transform to:

$$\widehat{D}^f(\vec{r}_d, \vec{r'}) = \widehat{F}_A(\vec{r}_d, \vec{r'})\widehat{D}(\vec{r}_d, \vec{r'})\widehat{F}_P(\vec{r}_d, \vec{r'}) \tag{4.45}$$

and

$$\Omega_f(\vec{r}_d, \vec{r_1'}, \vec{r_2'}) = \mathrm{Tr}(\frac{\widehat{I} + P_A(\vec{r}_d, \vec{r_1'})\widehat{F}_A(\vec{r}_d, \vec{r_1'})^\dagger\widehat{\sigma}_z\widehat{F}_A(\vec{r}_d, \vec{r_1'})}{2}\widehat{D}(\vec{r}_d, \vec{r_2'})\times$$

$$\frac{\widehat{I} + P_P(\vec{r}_d, \vec{r_1'})\widehat{F}_P(\vec{r}_d, \vec{r_1'})\widehat{\sigma}_z\widehat{F}_P(\vec{r}_d, \vec{r_1'})^\dagger}{2}\widehat{D}(\vec{r}_d, \vec{r_1'})^\dagger). \tag{4.46}$$

This enables the definition of the *4-shim neutron flux* $\vec{J}_s^{(4)}(\vec{r}_d)$, *4-flip neutron flux* $\vec{J}_f^{(4)}(\vec{r}_d)$ and *4-measured polarization* $P_m^{(4)}(\vec{r}_d)$:

$$J_s^{(4)}(\vec{r}_d) = \frac{\left|\vec{J}_{nn}(\vec{r}_d) + \vec{J}_{nf}(\vec{r}_d) + \vec{J}_{fn}(\vec{r}_d) + \vec{J}_{ff}(\vec{r}_d)\right|}{4}, \tag{4.47}$$

$$J_f^{(4)}(\vec{r}_d) = \frac{\left|\vec{J}_{nn}(\vec{r}_d) - \vec{J}_{nf}(\vec{r}_d) - \vec{J}_{fn}(\vec{r}_d) + \vec{J}_{ff}(\vec{r}_d)\right|}{4} \tag{4.48}$$

and

$$P_m^{(4)}(\vec{r}_d) = \frac{J_f^{(4)}(\vec{r}_d)}{J_s^{(4)}(\vec{r}_d)}, \tag{4.49}$$

where the indexes f and n indicate when the flipper is *on* or *off*. For *perfect* flippers $\widehat{F}_A\widehat{\sigma}_z\widehat{F}_A^\dagger = -\widehat{\sigma}_z$ and the same for $\widehat{F}_P$ so that $J_s^{(4)}(\vec{r}_d)$ is given by equation (4.43) with Ω replaced by

$$\Omega_s^{(4)}(\vec{r}_d, \vec{r_1'}, \vec{r_2'}) = \frac{1}{4}\mathrm{Tr}\left(\widehat{D}(\vec{r}_d, \vec{r_2'})\widehat{D}(\vec{r}_d, \vec{r_1'})^\dagger\right), \tag{4.50}$$

independent of the polarizer or analyser properties. Under the same conditions $J_f^{(4)}(\vec{r}_d)$ becomes:

$$J_f^{(4)}(\vec{r}_d) = \tag{4.51}$$

$$\int\int_{x=0} e^{-i\vec{p}\cdot(\vec{r_2'}-\vec{r_1'})}\Gamma_0(\vec{r_1'}, \vec{r_2'}, 0)T_A(\vec{r}_d, \vec{r_1'})T_P(\vec{r}_d, \vec{r_1'})\Omega_m^{(4)}(\vec{r}_d, \vec{r_1'}, \vec{r_2'})d^2r_1'd^2r_2',$$

where

$$\Omega_m^{(4)}(\vec{r}_d, \vec{r_1'}, \vec{r_2'}) = \frac{1}{4}P_A(\vec{r}_d, \vec{r_1'})P_P(\vec{r}_d, \vec{r_1'})\mathrm{Tr}\left(\widehat{\sigma}_z\widehat{D}(\vec{r}_d, \vec{r_2'})\widehat{\sigma}_z\widehat{D}(\vec{r}_d, \vec{r_1'})^\dagger\right). \tag{4.52}$$

Sometimes instead of using 4 quantities the shim and polarization are determined by 2 quantities. The *2-shim neutron flux, 2-flip neutron flux* and *2-measured polarization* are defined as:

$$J_s^{(2)}(\vec{r}_d) = \frac{\left|\vec{J}_n(\vec{r}_d) + \vec{J}_f(\vec{r}_d)\right|}{2}, \tag{4.53}$$

$$J_f^{(2)}(\vec{r}_d) = \frac{\left|\vec{J}_n(\vec{r}_d) - \vec{J}_f(\vec{r}_d)\right|}{2} \tag{4.54}$$

and

$$P_m^{(2)}(\vec{r}_d) = \frac{J_f^{(2)}(\vec{r}_d)}{J_s^{(2)}(\vec{r}_d)}, \tag{4.55}$$

where the indexes f or n indicates when a flipper is *on* or *off*. The flipper can be either the one just before the analyser or the one after the polarizer. It the flipper at the analyser is used and assumed perfect $\vec{J}_s^{(2)}(\vec{r}_d)$ is given by equation (4.43) with Ω replaced by

$$\Omega_s^{(2)}(\vec{r}_d, \vec{r_1'}, \vec{r_2'}) = \frac{1}{2}\mathrm{Tr}\left(\widehat{D}(\vec{r}_d, \vec{r_1'})^\dagger\widehat{D}(\vec{r}_d, \vec{r_2'})\frac{\widehat{I} + P_P(\vec{r}_d, \vec{r_1'})\widehat{\sigma}_z}{2}\right). \tag{4.56}$$

Under the same conditions $J_f^{(2)}(\vec{r}_d)$ is given by equation (4.51) with $\Omega_m^{(4)}(\vec{r}_d, \vec{r_1'}, \vec{r_2'})$ replaced by:

$$\Omega_m^{(2)}(\vec{r}_d, \vec{r_1'}, \vec{r_2'}) = \frac{P_A(\vec{r}_d, \vec{r_1'})}{2} \mathrm{Tr}\left(\widehat{D}(\vec{r}_d, \vec{r_1'})^\dagger \widehat{\sigma}_z \widehat{D}(\vec{r}_d, \vec{r_2'}) \frac{\widehat{I} + P_P(\vec{r}_d, \vec{r_1'})\widehat{\sigma}_z}{2} \right). \quad (4.57)$$

Equations when the flipper is at the polarizer side can be derived in a similar manner.

Note that in general the different definitions of shim neutron flux and measured polarization give different results. In a special case however they are the same. If matrix $\widehat{D}$ only slightly depends on $\vec{r'}$, then within the coherence length it will be constant: $\widehat{D}(\vec{r}_d, \vec{r_2'}) \approx \widehat{D}(\vec{r}_d, \vec{r_1'})$. If also $\widehat{D}(\vec{r}_d, \vec{r'})$ can be represented by a rotation matrix:

$$\frac{1}{\sqrt{2}} \begin{pmatrix} \sqrt{1 + P_D(\vec{r}_d, \vec{r'})} e^{i\alpha_D(\vec{r}_d, \vec{r'})} & i\sqrt{1 - P_D(\vec{r}_d, \vec{r'})} e^{i\beta_D(\vec{r}_d, \vec{r'})} \\ i\sqrt{1 - P_D(\vec{r}_d, \vec{r'})} e^{-i\beta_D(\vec{r}_d, \vec{r'})} & \sqrt{1 + P_D(\vec{r}_d, \vec{r'})} e^{-i\alpha_D(\vec{r}_d, \vec{r'})} \end{pmatrix}, \quad (4.58)$$

then $\Omega_s^{(4)}(\vec{r}_d, \vec{r_1'}, \vec{r_2'}) = \Omega_s^{(2)}(\vec{r}_d, \vec{r_1'}, \vec{r_2'}) = \frac{1}{2}$ and the shim neutron flux is independent of all neutron manipulation devices. Also $\Omega_m^{(4)}$ and $\Omega_m^{(2)}$ are reduced to:

$$\Omega_m^{(4)}(\vec{r}_d, \vec{r_1'}, \vec{r_2'}) = \Omega_m^{(2)}(\vec{r}_d, \vec{r_1'}, \vec{r_2'}) = \frac{1}{2} P_A(\vec{r}_d, \vec{r_1'}) P_P(\vec{r}_d, \vec{r_1'}) P_D(\vec{r}_d, \vec{r_1'}), \quad (4.59)$$

describing the loss of polarization due to the neutron manipulating devices. In this case beam splitting is ignored and the polarization and neutron flux of the beam between analyser and polarizer are completely independent. Then, the influence of the magnetic flux density can also be described by means of its influence on the wave function, represented by two plane waves (up and down spins state) directed along the classical neutron path through the instrument. In the semi-classical approximation this comes down to determining the precession of the neutron spin along its travel through the instrument [30].

4.8 Scattering

The propagation of the coherence matrix through the sample can be determined by coupling the scattered coherence matrix to the incident coherence matrix. In general one can state that:

$$\widehat{\Gamma}_{sc}(\vec{r}_1, \vec{r}_2, \tau) = \widehat{M}_{sc}(\vec{r}_2) \widehat{\Gamma}_{in}(\vec{r}_1, \vec{r}_2, \tau) \widehat{M}_{sc}(\vec{r}_1)^\dagger, \quad (4.60)$$

where $\widehat{M}_{sc}$ is called the *scattering matrix*. Following the reasoning of section 4.2 one can split the scattering matrix in a non-magnetic part and a magnetic part. Using the phase-object approximation (section 3.3) one can write:

$$\widehat{M}_{sc}(\vec{r}) = e^{iS(\vec{r})} \widehat{H}_m(\vec{r}), \quad (4.61)$$

where $\widehat{H}_m$ is a rotation matrix describing the magnetic part of the scattering matrix. In case of only non-magnetic scattering this is just the unit matrix. In case where the magnetic flux density in the sample is everywhere in the direction of the quantization axis this is just a matrix $\widehat{T}_z$. Then the argument of this matrix is the extra phase difference between the up and down spin state acquired by the wave after traveling through the sample.

Equations (4.7) and (4.8) can be used to relate the polarization directly before and after the sample:

$$\mathrm{Tr}(\widehat{\Gamma}_{sc}(\vec{r},\vec{r},0)) = e^{iS(\vec{r})-iS^*(\vec{r})}\mathrm{Tr}(\widehat{\Gamma}_{in}(\vec{r},\vec{r},0)) \tag{4.62}$$

and

$$\begin{pmatrix} P_{x,sc}(\vec{r}) \\ P_{y,sc}(\vec{r}) \\ P_{z,sc}(\vec{r}) \end{pmatrix} = \widehat{D} \begin{pmatrix} P_{x,in}(\vec{r}) \\ P_{y,in}(\vec{r}) \\ P_{z,in}(\vec{r}) \end{pmatrix}, \tag{4.63}$$

where $\widehat{D}$ is called the *depolarization* matrix and given by its elements:

$$D_{jk} = \frac{1}{2}\mathrm{Tr}(\widehat{H}_m(\vec{r})\widehat{\sigma}_k\widehat{H}_m(\vec{r})^\dagger\widehat{\sigma}_j). \tag{4.64}$$

If the scattering matrix is presented as:

$$\widehat{H}_m = \widehat{I}\cos\theta + i\left(n_x\widehat{\sigma}_x + n_y\widehat{\sigma}_y + n_z\widehat{\sigma}_z\right)\sin\theta, \tag{4.65}$$

the depolarization matrix becomes:

$$\widehat{D} = \begin{pmatrix} 1 & 0 & 0 \\ 0 & 1 & 0 \\ 0 & 0 & 1 \end{pmatrix} + \tag{4.66}$$

$$-2\sin^2\theta \begin{pmatrix} n_y^2+n_z^2 & -n_xn_y & -n_xn_z \\ -n_yn_x & n_x^2+n_z^2 & -n_yn_z \\ -n_zn_x & -n_zn_y & n_x^2+n_y^2 \end{pmatrix} + 2\sin\theta\cos\theta \begin{pmatrix} 0 & -n_z & n_y \\ n_z & 0 & -n_x \\ -n_y & n_x & 0 \end{pmatrix}.$$

Chapter 5

Spin echo small angle neutron scattering

5.1 Introduction

A neutron spin echo instrument consists of two regions where the neutron spin precesses depending on some property of the neutron and its path through these regions. For conventional spin echo the important property that is coded is the neutron wavelength enabling inelastic measurements with a high time resolution. It is also possible to code the angle of the path a neutron has taken through the precession regions. The total precession is proportional to the difference in angles of the path through the first region and the second region. This is called Spin Echo Small Angle Neutron Scattering or *SESANS*. Detailed information can be found in for example [15] or [16].

The basis for this technique was first discussed by Mezei in 1972 [32] and Pynn in 1978 [33]. Keller [34] showed in 1995 it could be used for small angle neutrons scattering and Rekveldt [15] was first to consider the mathematical background of the technique in 1996 and introduced the SESANS correlation function as will be discussed later.

An example of the coding part of a SESANS instrument is shown in figure 5.1. Regions I and II are parallelogram shaped regions with approximately the same lengths L_1 and L_2. The dependence in the z direction is ignored. In region I the magnetic flux density

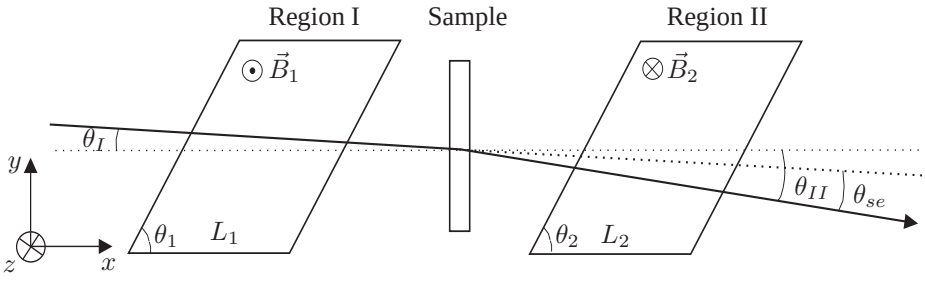

Figure 5.1: Principle of SESANS precession coding.

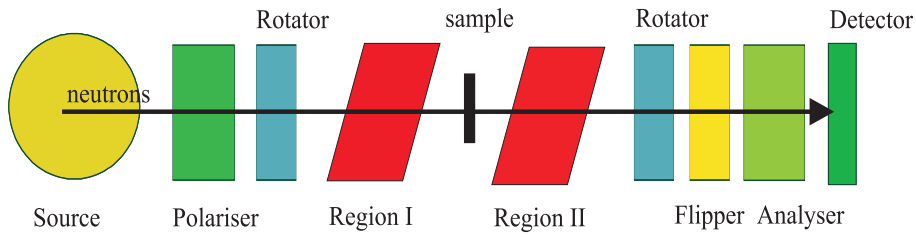

Figure 5.2: Principle of complete SESANS instrument.

(B_1) is constant and parallel to the z-axis. In region II the magnetic flux density (B_2) is approximately the same except in the opposite direction. Outside these regions the magnetic flux density is supposed to be 0. The inclination angle between region I and the x-axis is θ_1 and for Region II, θ_2. After interaction with the sample the angle the neutron path makes with region II is changed by θ_{se}. The influences on the propagation of the coherence matrix in regions I and II are given by equation (4.23) where terms of second and larger order in θ_I and θ_{II} are ignored:

$$\phi_I(\vec{r'},\vec{r}) = -c\bar{\lambda}B_1L_1(1-\theta_I\tan\theta_1) \tag{5.1}$$

and

$$\phi_{II}(\vec{r'},\vec{r}) = c\bar{\lambda}B_2L_2(1-\theta_{II}\tan\theta_2), \tag{5.2}$$

where $c = 4.63209\times10^{14}\,\mathrm{T^{-1}m^{-2}}$ as defined in section 4.4. Hence, the device matrices for the regions I and II are given by $\widehat{T}_z(\phi_I(\vec{r'},\vec{r}))$ and $\widehat{T}_z(\phi_{II}(\vec{r'},\vec{r}))$. If the sample scatters non-magnetic, $\theta_1 = \theta_2$ and $B_1L_1 = B_2L_2$ the device matrix for the combination of region I, the sample and region II is just $\widehat{T}_z(\vec{l}_{se}\cdot\vec{q}_{se})$, where $\vec{q}_{se}$ is the wavevector transfer at the sample position, the direction of $\vec{l}_{se}$ is the coding direction (here $\vec{e}_y$) and $l_{se} = c\bar{\lambda}^2B_1L_1\tan\theta_1/2\pi$ is called the *spin echo length*.

For a complete SESANS instrument the coding section is part of the whole instrument (see also figure 4.3). This is shown schematically in figure 5.2. The neutrons from the source are transmitted through the polarizer and the rotator rotates the polarization vector to the y-axis. This corresponds to a device matrix which consist of a rotation matrix, $\widehat{R}(\vec{r'},\vec{r})$. Then the neutron propagates through regions I and II and a second rotator which reverses the previous rotation, so its device matrix is the inverse (or hermitian adjunct) of the previous one, $\widehat{R}(\vec{r'},\vec{r})^\dagger$. Then the neutrons move through a flipper and analyser to enable polarization analysis. Now, the device matrix between polarizer and flipper is given by:

$$\widehat{E}(\vec{r},\vec{r'}) = \widehat{R}(\vec{r'},\vec{r})^\dagger\widehat{T}_z(\phi_{II}(\vec{r'},\vec{r}))\widehat{M}_{sc}(\vec{r},\vec{r'})\widehat{T}_z(\phi_I(\vec{r'},\vec{r}))\widehat{R}(\vec{r'},\vec{r}). \tag{5.3}$$

Note that without a scattering sample this matrix reduces to the identity matrix. If the scattering is non-magnetic this matrix reduces to:

$$\widehat{E}(\vec{r},\vec{r'}) = e^{iS(\vec{r})}\widehat{R}(\vec{r'},\vec{r})^\dagger\widehat{T}_z(\vec{l}_{se}\cdot\vec{q}_{se})\widehat{R}(\vec{r'},\vec{r}). \tag{5.4}$$

The polarizing factor of $\widehat{E}(\vec{r},\vec{r'})$ is:

$$P_E(\vec{r},\vec{r'}) = (1-P_R^2(\vec{r'},\vec{r}))\cos\left\{\vec{l}_{se}\cdot\vec{q}_{se}\right\} + P_R^2(\vec{r'},\vec{r}), \tag{5.5}$$

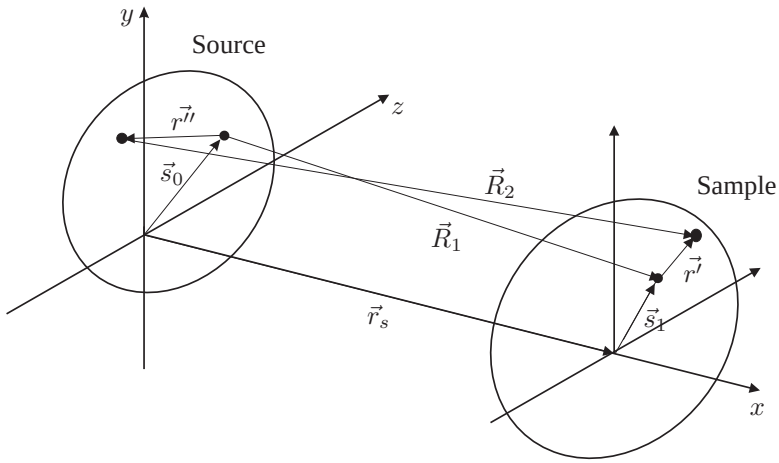

Figure 5.3: Illustrating the notation relating to the source far-zone showing the definition of the used symbols.

where P_R is the polarizing factor of $\widehat{R}(\vec{r'}, \vec{r})$. For a perfect spin echo instrument the factor before the cosine must be maximal and the other term minimal, hence $P_R = 0$.

5.2 Non-magnetic scattering

Assume the neutron beam is homogeneous and unpolarized before the polarizer and can be represented by a coherence matrix:

$$\widehat{\Gamma}_0\left(\vec{r''_1}, \vec{r''_2}, \tau\right) = \Gamma_0\left(0, \vec{r''}, \tau\right)\widehat{I}/2, \tag{5.6}$$

where $\Gamma_0\left(0, \vec{r''}, \tau\right)$ is the mutual coherence function at the source position. Then the difference in distance between 2 points in the source plane and two points at the sample plane is:

$$R_2 - R_1 \approx \frac{(\vec{r''} - \vec{r'}) \cdot (\vec{s}_0 - \vec{s}_1)}{r_s}, \tag{5.7}$$

where $\vec{s}_0$ is the component in the (y, z) plane at the source position of the first point at the source, $\vec{s}_0 + \vec{r''}$ the same of the second point at the source, $\vec{s}_1$ is the component in the (y, z) plane at the sample position of the first point at the sample and $\vec{s}_1 + \vec{r'}$ the same for the second point at the sample and r_s the distance along the x-axis between source and sample (see figure 5.3). The approximation holds as long as $\bar{k}\left|\vec{r''} - \vec{r'}\right|^2 \ll r_s$.

Using equation (4.35) in the far-zone limit and $\cos\theta_1 \approx \cos\theta_2 \approx 1$ the coherence matrix at the sample position becomes:

$$\widehat{\Gamma}_{in}(\vec{s}_1, \vec{s}_1 + \vec{r'}, \tau) = \frac{1}{2r_s^2}\int_{A_0} R_{in}(\vec{q}_0 - \vec{q}_1, \vec{r'}, \tau)\widehat{W}_P(\vec{r'_1}, \vec{r''_1})\widehat{W}_P(\vec{r'_1}, \vec{r''_1})^\dagger d^2 s_0, \tag{5.8}$$

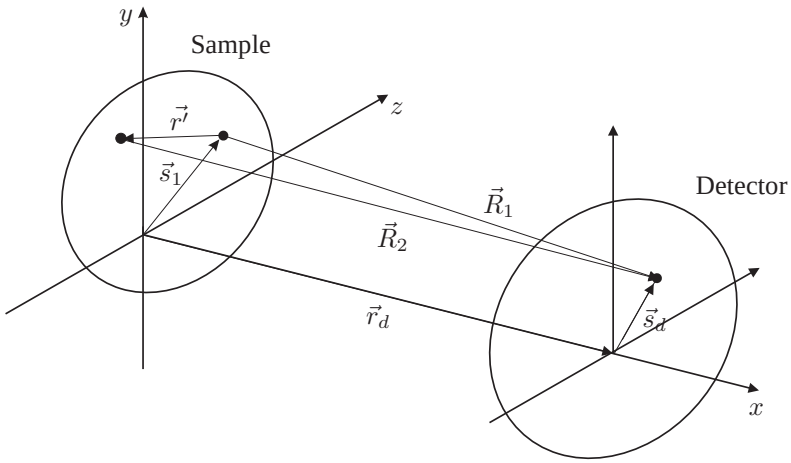

Figure 5.4: Illustrating the notation relating to the sample far-zone showing the definition of the used symbols.

where

$$R_{in}(\vec{q},\vec{r'},\tau) = \frac{e^{-i\vec{q}\cdot\vec{r'}}}{\bar{\lambda}^2}\int_{A_0} e^{i\vec{q}\cdot\vec{r''}}\Gamma_0\left(0,\vec{r''},\tau\right)d^2r'' \tag{5.9}$$

and $\vec{q_0} = \bar{k}\vec{s_0}/r_s$, $\vec{q_1} = \bar{k}\vec{s_1}/r_s$ and $\widehat{W}_P(\vec{r}_1,\vec{r}_2) = \widehat{M}_P(\vec{r}_1,\vec{r}_2)\widehat{D}_P(\vec{r}_1,\vec{r}_2)$. For a complete incoherent source (see section 2.6):

$$R_{in}(\vec{q},\vec{r'},\tau) = \frac{J_0 e^{-i\bar{k}v_p\tau}e^{-i\vec{q}\cdot\vec{r'}}}{8v_p\pi}. \tag{5.10}$$

The difference in distance between 2 points in the sample plane and one point at the detector plane is:

$$R_2 - R_1 \approx \frac{\vec{r'}\cdot(\vec{s}_1-\vec{s}_d)}{r_d}, \tag{5.11}$$

where $\vec{s}_d$ is the component in the (y,z) plane at the detector position of the point at the detector and r_d the distance along the x-axis between sample and detector (see figure 5.4). The approximation holds as long as $\bar{k}\left|\vec{r'}\right|^2 \ll r_d$.

Using equation (4.35) in the far-zone limit and $\cos\theta_1 \approx \cos\theta_2 \approx 1$ the coherence matrix at the detector position becomes:

$$\widehat{\Gamma}_d(\vec{r}_d,\vec{r}_d,\tau) = \frac{1}{r_d^2\bar{\lambda}^2}\times \tag{5.12}$$

$$\int_{A_s}\int_{A_s} e^{i\left(\frac{r_s}{r_d}\vec{q}_1-\vec{q}_d\right)\cdot\vec{r'}}\widehat{W}_A(\vec{r}_d,\vec{r_1'})\widehat{\Gamma}_{sc}\left(\vec{s}_1,\vec{s}_1+\vec{r'},\tau\right)\widehat{W}_A(\vec{r}_d,\vec{r_1'})^\dagger d^2s_1 d^2r',$$

where $\widehat{\Gamma}_{sc}\left(\vec{s}_1,\vec{s}_1+\vec{r'},\tau\right)$ is the coherence matrix just after scattering and $\vec{q}_d = \bar{k}\vec{s}_d/r_d$.

For non-magnetic scattering the scattering matrix (see equation (4.61)) reduces to the identity matrix and the scattered coherence matrix is:

$$\widehat{\Gamma}_{sc}(\vec{s}_1, \vec{s}_1 + \vec{r'}, \tau) = e^{iS(\vec{s}_1+\vec{r'})-iS^*(\vec{s}_1)}\widehat{\Gamma}_{in}\left(\vec{s}_1, \vec{s}_1 + \vec{r'}, \tau\right) \tag{5.13}$$

The same as in section 2.7, the detector count rate is determined as an integral of the neutron flux over the detector area. Using equation (4.9) this reduces to:

$$I_d = 2v_p \int_{A_d} \mathrm{Tr}(\widehat{\Gamma}(\vec{r}_d, \vec{r}_d, 0))d^2r_d, \tag{5.14}$$

The neutron count rate in the detector according to this equation becomes, after changing the integration order:

$$I_d = \frac{v_p}{r_s^2 r_d^2 \bar{\lambda}^2} \times \tag{5.15}$$

$$\int_{A_0}\int_{A_s}\int_{A_s} e^{i\frac{r_s}{r_d}\vec{q}_1\cdot\vec{r'}} e^{iS(\vec{s}_1+\vec{r'})-iS^*(\vec{s}_1)} R_{in}(\vec{q}_0 - \vec{q}_1, \vec{r'}, 0) X(\vec{r'}, \vec{r'_1}, \vec{r''_1}) d^2r' d^2s_1 d^2s_0,$$

where

$$X(\vec{r'}, \vec{r'_1}, \vec{r''_1}) = \int_{A_d} e^{-i\vec{q}_d\cdot\vec{r'}} \Omega_d(\vec{r}_d, \vec{r'_1}, \vec{r''_1}) d^2r_d \tag{5.16}$$

and

$$\Omega_d(\vec{r}_d, \vec{r'_1}, \vec{r''_1}) = T_A(\vec{r}_d, \vec{r'_1}) T_P(\vec{r'_1}, \vec{r''_1}) \times \tag{5.17}$$

$$\mathrm{Tr}\left(\frac{\widehat{I} + P_A(\vec{r}_d, \vec{r'_1})\sigma_z}{2}\widehat{E}(\vec{r}_d, \vec{r'_1}, \vec{r''_1})\frac{\widehat{I} + P_P(\vec{r'_1}, \vec{r''_1})\sigma_z}{2}\widehat{E}(\vec{r}_d, \vec{r'_1}, \vec{r''_1})^\dagger\right)$$

and $\widehat{E}(\vec{r}_d, \vec{r'_1}, \vec{r''_1}) = \widehat{M_A}(\vec{r}_d, \vec{r'_1})\widehat{M_P}(\vec{r'_1}, \vec{r''_1})$. In the following the transmission of the analyser and polarizer is assumed to be constant. The shim count rate can be calculated by taking $\Omega_d = \frac{1}{2}T_A T_P$ so that X can be replaced by:

$$X_s(\vec{r'}, \vec{r'_1}, \vec{r''_1}) = \frac{T_A T_P}{2}\frac{r_d^2}{\bar{k}^2}\int_{A_d} e^{-i\vec{q}_d\cdot\vec{r'}} d^2q_d \tag{5.18}$$

where the integral of s_d over A_d is replaced by an integral of $\vec{q}_d$. Now, if the detector area is large enough the integral over A_d is just a two-dimensional Dirac-delta function $4\pi^2\delta^{(2)}(\vec{r'})$. This reduces the shim count rate to:

$$I_s = \frac{v_p}{r_s^2}\frac{T_A T_P}{2}\int_{A_0}\int_{A_s} e^{iS(\vec{s}_1)-iS^*(\vec{s}_1)} R_{in}(\vec{q}_0 - \vec{q}_1, 0, 0) d^2s_1 d^2s_0, \tag{5.19}$$

which for a complete incoherent source can be reduced to:

$$I_s = \frac{T_A T_P}{4}\frac{J_0 A_0}{4\pi r_s^2} G_r(0), \tag{5.20}$$

where

$$G_r(0) = \int_{A_s} e^{iS(\vec{s}_1)-iS^*(\vec{s}_1)} d^2s_1, \tag{5.21}$$

is the sample correlation function for $\vec{r} = 0$ as defined in equation (3.29). If also the polarizing powers of analyser and polarizer are constant and the matrix $\widehat{E}$ only depends on the angle of the paths before and after the sample, the flip count rate can be calculated by taking Ω_d equal to

$$\Omega_f(\vec{q}_{se}) = \frac{1}{2} T_A T_P P_A P_P P_E(\vec{q}_{se}), \tag{5.22}$$

where $P_E(\vec{q}_{se})$ is the polarizing factor of the instrument between the flippers as given by equation (5.5), for a perfect spin echo instrument $P_E(\vec{q}_{se}) = \cos\left\{\vec{l}_{se} \cdot \vec{q}_{se}\right\}$ and $\vec{q}_{se} = \vec{q}_d + \vec{q}_0 - \vec{q}_1(r_s/r_d + 1)$. Now the flip count rate can be found by replacing X by:

$$X_f(\vec{r'}, \vec{r'_1}, \vec{r''_1}) = \frac{T_A T_P P_A P_P r_d^2}{2\bar{k}^2} \Re\left\{ e^{i\vec{l}_{se}\cdot(\vec{q}_0 - \vec{q}_1(r_s/r_d+1))} \int_{A_d} e^{-i\vec{q}_d\cdot(\vec{r'}-\vec{l}_{se})} d^2 q_d \right\}, \tag{5.23}$$

where the integral of s_d over A_d is replaced by an integral of $\vec{q}_d$. Now again, if the detector area is large enough the integral over A_d is just a two-dimensional Dirac-delta function $4\pi^2\delta^{(2)}(\vec{r'} - \vec{l}_{se})$. This reduces the flip count rate to:

$$I_f = \frac{v_p}{r_s^2} \frac{T_A T_P P_A P_P}{2} \times \tag{5.24}$$

$$\Re\left\{ \int_{A_0} \int_{A_s} e^{iS(\vec{s}_1 + \vec{l}_{se}) - iS^*(\vec{s}_1)} R_{in}(\vec{q}_0 - \vec{q}_1, \vec{l}_{se}, 0) e^{i\vec{l}_{se}\cdot(\vec{q}_0 - \vec{q}_1)} d^2 s_1 d^2 s_0 \right\},$$

the same as

$$I_f = \frac{v_p}{r_s^2} \frac{T_A T_P P_A P_P}{2} \Re\left\{ \int_{A_0} \int_{A_s} e^{iS(\vec{s}_1 + \vec{l}_{se}) - iS^*(\vec{s}_1)} R_{in}(\vec{q}_0 - \vec{q}_1, 0, 0) d^2 s_1 d^2 s_0 \right\}. \tag{5.25}$$

Assume a complete incoherent source, then this can be reduced further to:

$$I_f = P_A P_P \frac{T_A T_P}{4} \frac{J_0 A_0}{4\pi r_s^2} \Re\left\{ G_r(\vec{l}_{se}) \right\}. \tag{5.26}$$

The measured polarization becomes:

$$P_m = P_A P_P \frac{\Re\left\{ G_r(\vec{l}_{se}) \right\}}{G_r(0)}, \tag{5.27}$$

so that the measured polarization is proportional to the real part of the SESANS correlation function. The correlation is measured in the coding direction $\vec{l}_{se}$.

One should realize that the above equation only holds for scattering in the phase-object approximation. A further limitation is that it holds for an *ideal* spin echo instrument, where the polarizing powers and transmissions of the polarizer and analyser are constant and the polarizing factor of the instrument between the polarizer and analyser is proportional to $\cos\{\vec{l}_{se} \cdot \vec{q}_{se}\}$. If this is not the case one can try to solve equation (5.15) differently or by means of numerical calculations.

5.3 Magnetic scattering

Recently Grigoriev et al. [35], [36] have shown the possibility of spin echo small angle neutron scattering measurements for *magnetic* samples. For magnetic scattering the scattering matrix should be incorporated. Here, it is assumed that the source is completely incoherent and the polarizing powers and transmissions of polarizer and analyser are constant. Further the rotation matrices before and after the precession regions I and II are ideal and given by:

$$\widehat{R} = \frac{1}{\sqrt{2}} \begin{pmatrix} e^{i\alpha} & ie^{i\beta} \\ ie^{-i\beta} & e^{-i\alpha} \end{pmatrix}, \tag{5.28}$$

so that $\widehat{R}\sigma_z\widehat{R}^\dagger = T_z(2\alpha + 2\beta)\sigma_y$. The detector count rate can be calculated according to equation (5.15) where Ω_d is replaced by:

$$\begin{aligned}\Omega_d(\vec{r}_d, \vec{r_1'}, \vec{r'}, \vec{r_1''}) = \frac{T_A T_P}{4}\mathrm{Tr}(\widehat{H}_m(\vec{s}_1 + \vec{r'})\widehat{H}_m(\vec{s}_1)^\dagger) + \\ \frac{T_A T_P P_A}{4}\mathrm{Tr}(\widehat{\sigma}_y\widehat{T}_z(\phi_2)\widehat{H}_m(\vec{s}_1 + \vec{r'})\widehat{H}_m(\vec{s}_1)^\dagger\widehat{T}_z(\phi_2)^\dagger) + \\ \frac{T_A T_P P_P}{4}\mathrm{Tr}(\widehat{\sigma}_y\widehat{T}_z(\phi_1)^\dagger\widehat{H}_m(\vec{s}_1)^\dagger\widehat{H}_m(\vec{s}_1 + \vec{r'})\widehat{T}_z(\phi_1)) + \\ \frac{T_A T_P P_P P_A}{4}\mathrm{Tr}(\widehat{T}_z(-2\phi_2)\widehat{\sigma}_y\widehat{H}_m(\vec{s}_1 + \vec{r'})\widehat{T}_z(2\phi_1)\widehat{\sigma}_y\widehat{H}_m(\vec{s}_1)^\dagger),\end{aligned} \tag{5.29}$$

where $\phi_2 = \phi_{II} - \alpha - \beta$ and $\phi_1 = \phi_I + \alpha + \beta$. Note that the second and third term contain either ϕ_1 or ϕ_2. As ϕ_1 and ϕ_2 vary fast with the position and angle, these terms will not contribute to the detector count rate. The integrals in equation (5.15) of these terms yield 0. This also collapses the difference between the *2-shim neutron flux* and *4-shim neutron flux* and the same for the flip neutron fluxes and measured polarizations. If the values of ϕ_1 or ϕ_2 are large enough the shim count rate is represented by the first term and the flip count rate by the fourth term. Filling in equation (5.15) for the shim count rate and assuming the detector area is large enough, gives:

$$I_s = \frac{v_p}{r_s^2}\frac{T_A T_P}{2}\int_{A_0}\int_{A_s} e^{iS(\vec{s}_1) - iS^*(\vec{s}_1)} R_{in}(\vec{q}_0 - \vec{q}_1, 0, 0) d^2 s_1 d^2 s_0, \tag{5.30}$$

not dependent on the magnetic scattering, the same result as for a non-magnetic sample. To calculate the flip count rate remember that any rotation matrix can be written as a matrix sum of a matrix representing a rotation along the z-axis and a flipping matrix. In this case spin dependent reflection and absorption phenomena are ignored as follows from the phase-object approximation. If these phenomena are to be taken into account the following derivation should be adjusted. For now, the scattering matrix $\widehat{H}_m$ can be written as a sum of $\widehat{T}_z$ and $\widehat{F}_z$:

$$\widehat{H}_m = \sqrt{\frac{1 + P_m}{2}}\widehat{T}_z(2\gamma_m) + \sqrt{\frac{1 - P_m}{2}}\widehat{F}_z(2\delta_m) \tag{5.31}$$

so that

$$\begin{aligned}\mathrm{Tr}(\widehat{T}_z(-2\phi_2)\widehat{\sigma}_y\widehat{H}_m(\vec{s}_1 + \vec{r'})\widehat{T}_z(2\phi_1)\widehat{\sigma}_y\widehat{H}_m(\vec{s}_1)^\dagger) = \\ \sqrt{1 + P_m(\vec{s}_1 + \vec{r'})}\sqrt{1 + P_m(\vec{s}_1)}\cos(\phi_1 + \phi_2 + \gamma_m(\vec{s}_1 + \vec{r'}) + \gamma_m(\vec{s}_1)) -\end{aligned} \tag{5.32}$$

$$\sqrt{1-P_m(\vec{s}_1+\vec{r'})}\sqrt{1-P_m(\vec{s}_1)}\cos(\phi_2-\phi_1+\delta_m(\vec{s}_1)+\delta_m(\vec{s}_1+\vec{r'})),$$

The second term of equation (5.32) depends on the difference $\phi_2-\phi_1$, which according to equations (5.1) and (5.2) also varies fast with angle and position. This term also averages to zero. Hence, again by filling in equation (5.15) the flip count rate is given by:

$$I_f = \frac{v_p}{r_s^2 r_d^2 \bar{\lambda}^2}\times \tag{5.33}$$

$$\int_{A_0}\int_{A_s}\int_{A_s} e^{i\frac{r_s}{r_d}\vec{q}_1\cdot\vec{r'}} e^{iS(\vec{s}_1+\vec{r'})-iS^*(\vec{s}_1)} R_{in}(\vec{q}_0-\vec{q}_1,\vec{r'},0) X_f(\vec{r'},\vec{r'_1},\vec{r''_1}) d^2r' d^2s_1 d^2s_0,$$

where

$$X_f(\vec{r'},\vec{r'_1},\vec{r''_1}) = \frac{T_A T_P P_A P_P}{4}\sqrt{1+P_m(\vec{s}_1+\vec{r'})}\sqrt{1+P_m(\vec{s}_1)}\times \tag{5.34}$$

$$\int_{A_d}\cos(\phi_I+\phi_{II}+\gamma_m(\vec{s}_1+\vec{r'})+\gamma_m(\vec{s}_1)) e^{-i\vec{q}_d\cdot\vec{r'}} d^2r_d,$$

which after filling in $\phi_I+\phi_{II}=\vec{l}_{se}\cdot\vec{q}_{se}$, $\vec{q}_{se}=\vec{q}_d+\vec{q}_0-\vec{q}_1(r_s/r_d+1)$ and if the detector area is large enough can be replaced by:

$$X_f(\vec{r'},\vec{r'_1},\vec{r''_1}) = \frac{T_A T_P P_A P_P}{4}\frac{4\pi^2 r_d^2}{\bar{k}^2}\sqrt{1+P_m(\vec{s}_1+\vec{r'})}\sqrt{1+P_m(\vec{s}_1)}\times \tag{5.35}$$

$$\Re\left\{e^{i\vec{l}_{se}\cdot(\vec{q}_0-\vec{q}_1(r_s/r_d+1))+i\gamma_m(\vec{s}_1+\vec{r'})+i\gamma_m(\vec{s}_1)}\delta^{(2)}(\vec{r'}-\vec{l}_{se})\right\},$$

giving for the flip count rate for a completely incoherent source:

$$I_f = P_A P_P \frac{T_A T_P}{4}\frac{J_0 A_0}{4\pi r_s^2}\Re\left\{\int_{A_s} e^{2i\gamma_m(\vec{s}_1)} H_r(\vec{s}_1+\vec{l}_{se}) H_r(\vec{s}_1)^* d^2s_1\right\}, \tag{5.36}$$

where

$$H_r(\vec{r}) = \sqrt{\frac{1+P_m(\vec{r})}{2}} e^{iS(\vec{r})+i\gamma_m(\vec{r})}. \tag{5.37}$$

The measured polarization is determined by the z-rotation part, $\widehat{T}_z$ of the scattering matrix. The flip part $\widehat{F}_z$ is completely depolarized. If a flipper (represented by a flipping matrix $\widehat{F}_z(2\tau)$) is inserted between region I and the sample, the scattering matrix is replaced by $\widehat{H}_f=\widehat{H}_m\widehat{F}_z(2\tau)$ which can be accounted for by replacement of the following variables:

$$P_{f,p}(\vec{r}) = -P_m(\vec{r}), \tag{5.38}$$

$$\gamma_{f,p}(\vec{r}) = \delta_m(\vec{r})-\tau-\pi, \tag{5.39}$$

$$\delta_{f,p}(\vec{r}) = \gamma_m(\vec{r})+\tau. \tag{5.40}$$

This means that by flipping the neutron spin just before the sample the correlation function that is measured changes from the $\widehat{T}_z$ part of the scattering matrix to the $\widehat{F}_z$ part. The same holds for a flipper between the sample and region II:

$$P_{f,a}(\vec{r}) = -P_m(\vec{r}), \tag{5.41}$$

$$\gamma_{f,a}(\vec{r}) = -\delta_m(\vec{r})+\tau+\pi, \tag{5.42}$$

$$\delta_{f,a}(\vec{r}) = -\gamma_m(\vec{r})+\tau. \tag{5.43}$$

5.4 Magnetic scattering in domains

For a sample consisting of domains of some size and shape the scattering matrix must be calculated using the procedure shown in figure 4.1 of section 4.5, where now each region represents a single domain. Using equation (4.28) and the definition of the angles θ_i and ϑ_i according to equation (4.18):

$$\widehat{H}_m(\vec{r}) = \prod_{j=1}^{N} \widehat{T}_z(\vartheta_j)^\dagger \widehat{T}_y(\theta_j)^\dagger \widehat{T}_z(\phi_j) \widehat{T}_y(\theta_j) \widehat{T}_z(\vartheta_j), \tag{5.44}$$

where

$$\phi_j = -cB'(\vec{r}_j + x_j\vec{e}_x)\bar{\lambda}(x_{j+1} - x_j), \tag{5.45}$$

$c = -4\pi m g_r \mu_N / h^2$, the same as before and $B'(\vec{r}_j)$ is the *pseudomagnetic flux density* [5] in domain j:

$$B'(\vec{r}) = -\frac{\rho_m(\vec{r})h^2}{2\pi g_r \mu_N m} = \frac{2\rho_m(\vec{r})}{c}, \tag{5.46}$$

where $\rho_m(\vec{r})$ is the *magnetic scattering length density* so that:

$$\phi_j = -2\bar{\lambda}\rho_m(\vec{r}_j + x_j\vec{e}_x)(x_{j+1} - x_j), \tag{5.47}$$

Equation (5.44) can be reduced to:

$$\widehat{H}_m(\vec{r}) = \prod_{j=1}^{N} \left\{ \widehat{I}\cos(\phi_j/2) + i\frac{\sin(\phi_j/2)}{B'(x_j)} \left(B'_x(x_j)\widehat{\sigma}_x + B'_y(x_j)\widehat{\sigma}_y + B'_z(x_j)\widehat{\sigma}_z \right) \right\}, \tag{5.48}$$

where the dependence of B' on $\vec{r}_j + x_j\vec{e}_x$ is written as $B'(x_j)$.

Using the fact that $(n_x\widehat{\sigma}_x + n_y\widehat{\sigma}_y + n_z\widehat{\sigma}_z)^2 = \widehat{I}$, this can be rewritten as:

$$\widehat{H}_m(\vec{r}) = \prod_{j=1}^{N} e^{i\frac{c\bar{\lambda}}{2}(x_{j+1}-x_j)\left(B'_x(x_j)\widehat{\sigma}_x + B'_y(x_j)\widehat{\sigma}_y + B'_z(x_j)\widehat{\sigma}_z\right)}, \tag{5.49}$$

which can be approximated when $\phi_j \ll 1$ or $\vec{n}_j \approx \vec{n}_{j+1}$ by:

$$\widehat{H}_m(\vec{r}) = e^{i\left(\zeta_x(\vec{r})\widehat{\sigma}_x + \zeta_y(\vec{r})\widehat{\sigma}_y + \zeta_z(\vec{r})\widehat{\sigma}_z\right)}, \tag{5.50}$$

where ζ_k is a measure for the average pseudomagnetic flux density in the k-direction along the neutron beam:

$$\zeta_k(\vec{r}) = \frac{c\bar{\lambda}}{2}\sum_{j=1}^{N} B'_k(\vec{r} + x_j\vec{e}_x)(x_{j+1} - x_j) = \frac{c\bar{\lambda}d_x}{2}\left\langle B'_k(\vec{r})\right\rangle, \tag{5.51}$$

where k represents the indexes x, y or z. Equation (5.50) can be expanded to:

$$\widehat{H}_m(\vec{r}) = \widehat{I}\cos\zeta(\vec{r}) + i\left(\zeta_x(\vec{r})\widehat{\sigma}_x + \zeta_y(\vec{r})\widehat{\sigma}_y + \zeta_z(\vec{r})\widehat{\sigma}_z\right)\frac{\sin\zeta(\vec{r})}{\zeta(\vec{r})}, \tag{5.52}$$

where $\zeta(\vec{r}) = \sqrt{\zeta_x(\vec{r})^2 + \zeta_y(\vec{r})^2 + \zeta_z(\vec{r})^2}$. Note that any rotation matrix can be put in this form. The exact interpretation of ζ_x, ζ_y and ζ_z depends on the properties of the sample and

the validity of the above or other approximations. The relation between ζ_x, ζ_y, ζ_z and P_m, γ_m, δ_m using the notation of equation (5.31) is:

$$e^{i\gamma_m} = \frac{\zeta\cos\zeta + i\zeta_z\sin\zeta}{\sqrt{\zeta^2\cos^2\zeta + \zeta_z^2\sin^2\zeta}} \tag{5.53}$$

$$e^{i\delta_m} = \frac{\zeta_x - i\zeta_y}{\sqrt{\zeta_x^2 + \zeta_y^2}} \tag{5.54}$$

$$P_m = 1 - 2(\zeta_y^2 + \zeta_x^2)\frac{\sin^2\zeta}{\zeta^2}. \tag{5.55}$$

Now equation (5.36) becomes:

$$I_f = P_A P_P \frac{T_A T_P}{4}\frac{J_0 A_0}{4\pi r_s^2}\Re\left\{\int_{A_s} P_r(\vec{s}_1)H_r(\vec{s}_1 + \vec{l}_{se})H_r(\vec{s}_1)^* d^2 s_1\right\}, \tag{5.56}$$

where

$$P_r(\vec{r}) = \frac{(\zeta(\vec{r})\cos\zeta(\vec{r}) + i\zeta_z(\vec{r})\sin\zeta(\vec{r}))^2}{\zeta(\vec{r})^2\cos^2\zeta(\vec{r}) + \zeta_z(\vec{r})^2\sin^2\zeta(\vec{r})}, \tag{5.57}$$

and

$$H_r(\vec{r}) = \left(\cos\zeta(\vec{r}) + i\zeta_z(\vec{r})\frac{\sin\zeta(\vec{r})}{\zeta(\vec{r})}\right)e^{iS(\vec{r})}. \tag{5.58}$$

Note that P_r does not depend on the spin echo length. If a flipper is inserted ($\tau = n\pi$) between region I and the sample the flip count rate can be found by using equations (5.38)-(5.40):

$$I_{f,f} = P_A P_P \frac{T_A T_P}{4}\frac{J_0 A_0}{4\pi r_s^2}\Re\left\{\int_{A_s} P_{r,f}(\vec{s}_1)H_{r,f}(\vec{s}_1 + \vec{l}_{se})H_r(\vec{s}_1)^* d^2 s_1\right\}, \tag{5.59}$$

where

$$P_{r,f}(\vec{r}) = \frac{(\zeta_x(\vec{r}) - i\zeta_y(\vec{r}))^2}{\zeta_x(\vec{r})^2 + \zeta_y(\vec{r})^2}, \tag{5.60}$$

and

$$H_{r,f}(\vec{r}) = (\zeta_x(\vec{r}) - i\zeta_y(\vec{r}))\frac{\sin\zeta(\vec{s}_1)}{\zeta(\vec{s}_1)}e^{iS(\vec{r})}. \tag{5.61}$$

For spin echo lengths where $H_r(\vec{s}_1 + \vec{l}_{se}) \approx H_r(\vec{s}_1)$ and the same for $H_{r,f}$ this equation can be reduced further. If also the nuclear scattering is neglected the measured polarizations are given by:

$$\frac{P_m}{P_A P_P} = \left\langle \cos^2\zeta(\vec{s}_1) - \zeta_z(\vec{s}_1)^2\frac{\sin^2\zeta(\vec{s}_1)}{\zeta(\vec{s}_1)^2}\right\rangle_{A_s}, \tag{5.62}$$

$$\frac{P_{m,f}}{P_A P_P} = \left\langle (\zeta_x(\vec{s_1})^2 - \zeta_y(\vec{s_1})^2)\frac{\sin^2\zeta(\vec{s}_1)}{\zeta(\vec{s}_1)^2}\right\rangle_{A_s}. \tag{5.63}$$

One should realize however that as soon as the value of ϕ_I or ϕ_{II} reduces to almost 0 (hence for small spin echo lengths) the above approximation (ignoring the terms which contain $\phi_1 - \phi_2$, is not valid any more. An example of such a measurement is the so-called

neutron depolarization technique [37]. In this case the flip count rate should be evaluated different from the one represented before. The term containing $\phi_2 - \phi_1$ in equation (5.32) should also be taken into account so that the 4-flip count rate becomes:

$$I_f = P_A P_P \frac{T_A T_P}{4} \frac{J_0 A_0}{4\pi r_s^2} \times \tag{5.64}$$

$$\int_{A_s} e^{iS(\vec{s}_1) - iS^*(\vec{s}_1)} \left(\frac{1 + P_m(\vec{s}_1)}{2} \cos(2\gamma_m(\vec{s}_1)) - \frac{1 - P_m(\vec{s}_1)}{2} \cos(2\delta_m(\vec{s}_1)) \right) d^2 s_1.$$

From this equation the 4-measured polarization can be evaluated using the results of the previous section (equation (5.53)-(5.55)) and neglecting the nuclear scattering:

$$\frac{P_m}{P_A P_P} = \left\langle 1 - 2(\zeta_x(\vec{s}_1)^2 + \zeta_z(\vec{s}_1)^2) \frac{\sin^2 \zeta(\vec{s}_1)}{\zeta(\vec{s}_1)^2} \right\rangle_{A_s}, \tag{5.65}$$

different from the one derived in the previous section. This corresponds to the zz-element of the depolarization matrix as found in section 4.8. In this case, introducing an extra π-flipper between region I and the sample just reverses the sign of the measured polarization.

Chapter 6

Reflectometry

In this chapter a derivation is given of the measured count rate in the detector of a reflectometer. Firstly, the propagation of the mutual coherence function through the reflectometer is discussed. The properties of the incident mutual coherence function at the sample surface are determined from the geometry of the reflectometer. Secondly, it will be shown that the detector count rate can be calculated from the scattered mutual coherence function at the sample position. Finally, for specific cases a method is described coupling the scattered mutual coherence function to the incident mutual coherence function, coupling the measurements to the sample properties.

6.1 Geometry

For reflectometers a typical instrument geometry is shown in figure 6.1. A neutron wave function created by a source at $x = x_0$, represented by a mutual coherence function, Γ_0 propagates through space toward the sample position at $x = x_s$. At the sample the mutual coherence function Γ_{in} interacts with a sample. After the interaction the mutual coherence function is transformed into Γ_{sc}. This scattered mutual coherence function propagates through space until it reaches the detector at $x = x_d$. In the following sections examples of properties of a reflectometer are given. In these instances the parameters as shown in table 6.1 are used.

6.1.1 Propagation from source to sample

The mutual coherence function between points P_1 and P_2 on the sample surface can be found by assuming $R_i >> 2\pi/\bar{k}$, where R_i is the distance between the source point S_i at location $\vec{r_i'}$ and sample surface point P_i at location $\vec{r}_i$. Hence, $R_i = \left|\vec{r}_i - \vec{r_i'}\right| = \sqrt{{r_i'}^2 + r_i^2 - 2(\vec{r_i'} \cdot \vec{r}_i)^2}$. It must be realized that the vectors $\vec{r}_1$ and $\vec{r}_2$ are vectors in the xz-plane and the vectors $\vec{r_1'}$ and $\vec{r_2'}$ are vectors in the yz-plane, so that the vector product only contains the z-components. $\bar{k}$ is the average wavevector of the quasi-monochromatic

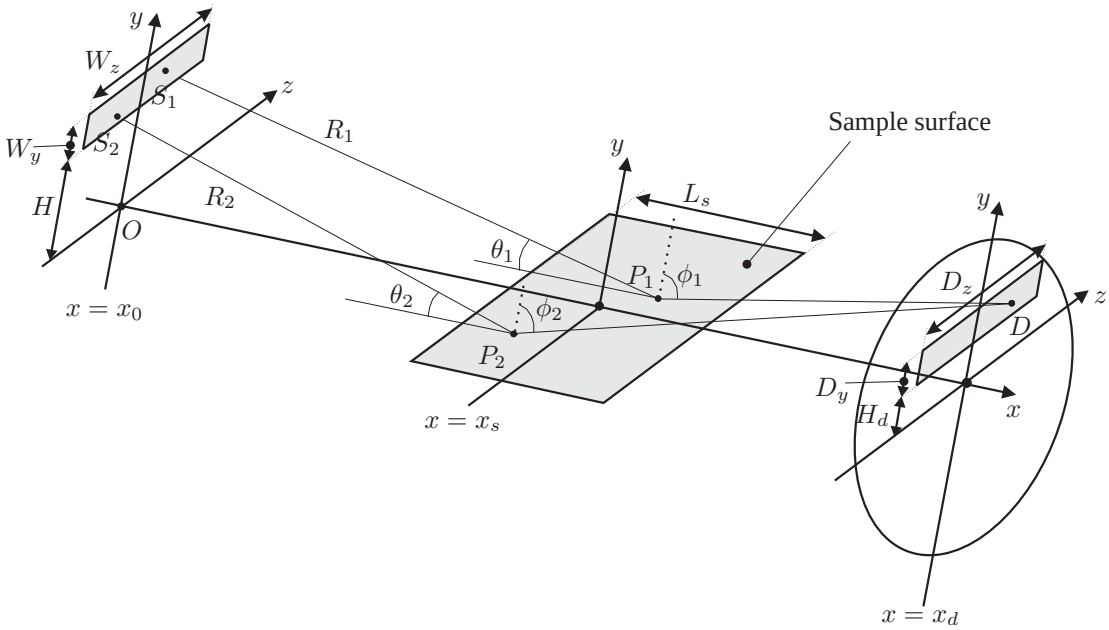

Figure 6.1: Notation relating to the propagation of the mutual coherence function through a reflectometer.

symbol	description	quantity	unit
H	Height diaphragm above sample surface	4	cm
W_y	Width diaphragm in y-direction	1	mm
W_z	Width diaphragm in z-direction	10	cm
r_1	Distance between diaphragm and sample	4	m
H_d	Height detector diaphragm above sample surface	4	cm
D_y	Width detector diaphragm in y-direction	1	mm
D_z	Width detector diaphragm in z-direction	10	cm
r_{ds}	Distance between sample and detector	1	m
λ	Wavelength used in calculations	0.2	nm

Table 6.1: Parameters for calculation of examples of properties of a reflectometer.

beam. Applying equation (2.31) yields:

$$\Gamma_{in}(\vec{r}_1,\vec{r}_2,\tau)=\int\int_{x=x_0}\frac{\cos\theta_1\cos\theta_2 e^{i\bar{k}(R_2-R_1)}}{R_1R_2\bar{\lambda}^2}\Gamma_0(\vec{r_1'},\vec{r_2'},\tau)d^2r_1'd^2r_2'. \tag{6.1}$$

For a completely homogeneous incoherent source with area A_0 (see section 2.6) the mutual coherence function at the sample surface reduces to:

$$\Gamma_{in}(\vec{r}_1,\vec{r}_2,\tau)=\frac{J_0}{2v_p}\frac{e^{-i\bar{k}v_p\tau}}{4\pi}\int_{A_0}\frac{\cos\theta_1\cos\theta_2 e^{i\bar{k}(R_2-R_1)}}{R_2R_1}d^2r_1', \tag{6.2}$$

where J_0 is the isotropic neutron source flux in neutrons per second per squared meter. For reflectometry in the far-zone $\cos\theta_i\approx 1$. If $\vec{r}_2=\vec{r}_1+\vec{r}$, $\vec{r}=(\Delta x,\Delta y,\Delta z)^{\mathrm{T}}$ and $r\ll r_1$ than R_2-R_1 can be approximated by:

$$R_2-R_1\approx-\Delta x\left(1-\frac{(y-y_1)^2+(z-z_1)^2}{2r_1^2}\right)-\Delta y\frac{y-y_1}{r_1}-\Delta z\frac{z-z_1}{r_1}, \tag{6.3}$$

where $z_1=\vec{r}_1\cdot\vec{e}_z$ and $y_1=\vec{r}_1\cdot\vec{e}_y$. The denominator in the integral of equation (6.2) can be reduced to r_1^2 without introducing a large error. If the source aperture is rectangular with a height W_y and a width W_z and the middle of the aperture is situated at $y=H$ and $z=0$ the integral can be evaluated as:

$$\Gamma_{in}(\vec{r}_1,\vec{r}_1+\vec{r},\tau)\approx\frac{J_0}{2v_p}\frac{e^{-i\bar{k}(\Delta x+v_p\tau)}}{4\pi r_1^2}\times \tag{6.4}$$

$$\int_{H-\frac{W_y}{2}-y_1}^{H+\frac{W_y}{2}-y_1}e^{i\frac{\pi}{2}\left(\kappa_x^2y^2+2\kappa_y y\right)}dy\int_{-\frac{W_z}{2}-z_1}^{\frac{W_z}{2}-z_1}e^{i\frac{\pi}{2}\left(\kappa_x^2z^2+2\kappa_z z\right)}dz,$$

where $\kappa_x^2=\bar{k}\frac{\Delta x}{\pi r_1^2}$, $\kappa_y=\frac{\bar{k}\Delta y}{\pi r_1}$ and $\kappa_z=\frac{\bar{k}\Delta z}{\pi r_1}$. This integral can be reduced further to:

$$\Gamma_{in}(\vec{r}_1,\vec{r}_1+\vec{r},\tau)\approx\frac{J_0}{2v_p}\frac{e^{i\bar{k}(\Delta x-v_p\tau)}}{4\pi r_1^2}\times \tag{6.5}$$

$$e^{i\frac{\pi}{2}(\kappa_y/\kappa_x)^2}\frac{E(\kappa_x(\kappa_y/\kappa_x^2+H-y_1+W_y/2))-E(\kappa_x(\kappa_y/\kappa_x^2+H-y_1-W_y/2))}{\kappa_x}\times$$

$$e^{i\frac{\pi}{2}(\kappa_z/\kappa_x)^2}\frac{E(\kappa_x(\kappa_z/\kappa_x^2-z_1+W_z/2))-E(\kappa_x(\kappa_z/\kappa_x^2-z_1-W_z/2))}{\kappa_x},$$

with

$$E(x)=C(x)+iS(x), \tag{6.6}$$

where $C(x)$ and $S(x)$ are the cosine and sine Fresnel integrals [26].

Note that $\lim_{x\to\infty}E(x)=(1+i)/2-i\,exp(-i\pi x^2/2)/\pi x+O(x^{-3})$. This limit can be used to find the mutual coherence function for $|\Delta x|\ll\Delta y^2\bar{k},\Delta z^2\bar{k}$:

$$\Gamma_{in}(\vec{r}_1,\vec{r}_1+\vec{r},\tau)\approx\frac{J_0}{2v_p}\frac{W_yW_ze^{i\bar{k}(\Delta x-v_p\tau)}}{4\pi r_1^2}\frac{\sin(\frac{\pi}{2}\kappa_yW_y)}{\frac{\pi}{2}\kappa_yW_y}\frac{\sin(\frac{\pi}{2}\kappa_zW_z)}{\frac{\pi}{2}\kappa_zW_z}. \tag{6.7}$$

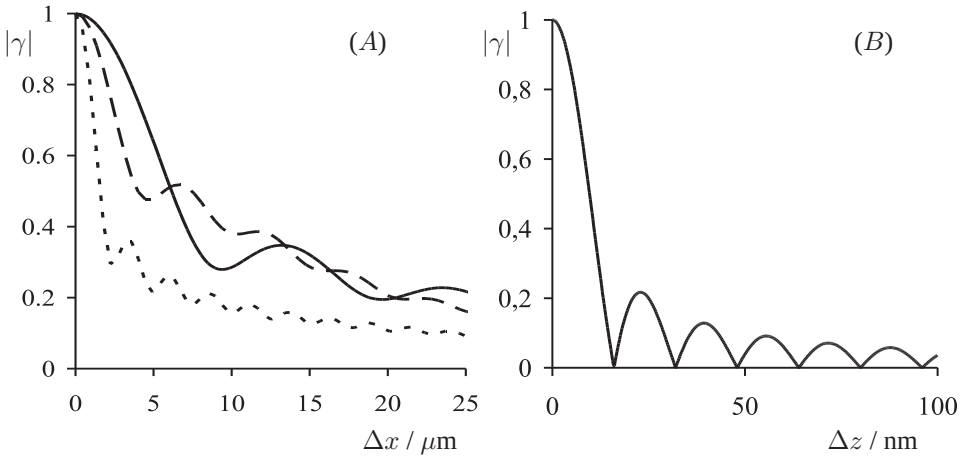

Figure 6.2: (A) Amplitude of the normalized mutual coherence function or complex degree of coherence γ along x-axis at the sample surface for $z_1 = 0$ (full line), $z_1 = 1$ cm (long-dashed line) and $z_1 = 2.5$ cm (short-dashed line). (B) Amplitude of complex degree of coherence γ along the z-axis at the sample surface for $z_1 = 0$ (black line). The parameters used are given in table 6.1.

Note that for $\lim_{x\to 0} E(x) = x(1 + O(x^4)) - ix^3(\pi/6 + O(x^4))$. This limit can be used to find the neutron density at the sample surface:

$$\Gamma_{in}(\vec{r}, \vec{r}, 0) = \frac{J_0}{2v_p} \frac{W_z W_y}{4\pi r_1^2}. \tag{6.8}$$

Examples of the amplitude of the normalized mutual coherence function or complex degree of coherence, γ are shown in figure 6.2. Figure 6.2A shows the function along the x-direction ($\Delta z = 0$) at the sample surface $y_1 = 0$ and $\Delta y = 0$. Figure 6.2B shows the same along the z-direction ($\Delta x = 0$). The parameters used in the calculations are given in table 6.1. Note the difference in scale for the x- and z-direction. This is due to the difference in diaphragm width and due to the small glancing angles θ_i[1]. In figure 6.2A the mutual coherence function for $z_1 = 1$ cm and $z_1 = 2.5$ cm are also shown. The width of the mutual coherence function reduces when the distance to the center of the sample changes. This can be explained as due to an increase in the (effective) width of the diaphragm in the z-direction. A two-dimensional plot of the mutual coherence function along the sample surface is shown in figure 6.3. Note the difference in scales in the x- and z-direction. Interesting fact is that the mutual coherence function has an extended tail in the direction $\Delta z \approx \Delta x(W_z + 4z_1)/4r_1$. This shows that if the coherence properties of the beam are split in two separate contributions for the x- and z-direction the coherence of the beam might be

[1]The coherence length in the x-direction holds for a quasi-monochromatic beam. Sometimes it is argued that for a real beam with a finite wavelength spread one should also take into account the longitudinal or time coherence (section 2.2). For a relative wavelength spread of 0.01 this is of the order of several nanometer. From off-specular neutron reflectometry measurements it is known that structures can be determined which have dimensions of several *hundreds* of nanometers. This indicates scattering is not determined by interactions of the mutual coherence function but by the interactions of the neutron wave function with the (time-averaged) scattering potential.

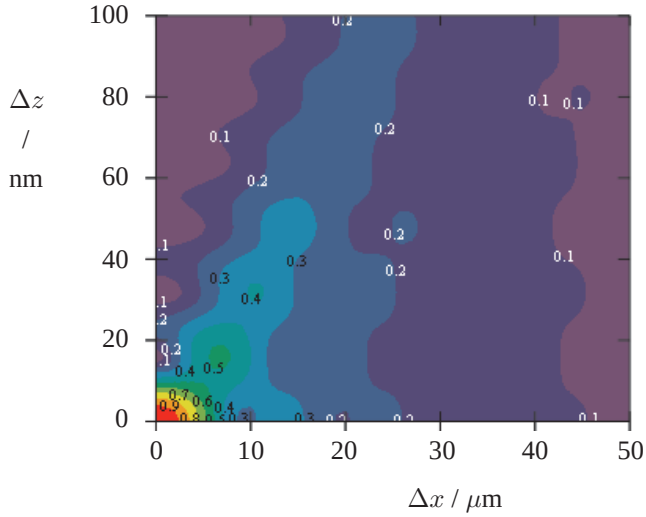

Figure 6.3: Amplitude of normalize mutual coherence function or complex degree of coherence at the center of the sample. The parameters used are given in table 6.1.

under or over estimated.

6.1.2 Propagation from sample to detector

The count rate in the detector is due to the scattered mutual coherence function propagated from the sample position to the detector (see section 2.5 and 2.7). Here equation (2.31) can be used to calculate the propagation to the detector:

$$\Gamma(\vec{r}_d, \vec{r}_d, 0) = \int\int_{y=0} \frac{\cos\phi_1 \cos\phi_2 e^{i\bar{k}(R_2-R_1)}}{R_1 R_2 \bar{\lambda}^2} \Gamma_{sc}(\vec{r_1}, \vec{r_2}, 0) d^2 r_2 d^2 r_1, \qquad (6.9)$$

where $R_i = |\vec{r}_d - \vec{r}_i|$. Now for the integration area the sample plane must be taken ($y = 0$) and $\cos\phi_i = y_d/R_i$, where $(x_d, y_d, z_d)^{\mathrm{T}} = \vec{r}_d$. If, again, $\vec{r}_2 = \vec{r}_1 + \vec{r}$, $\vec{r} = (\Delta x, 0, \Delta z)^{\mathrm{T}}$ and $r \ll R_1$ this can be reduced to:

$$\Gamma(\vec{r}_d, \vec{r}_d, 0) = \int_{y=0} \frac{\cos^2\phi_1}{R_1^2 \bar{\lambda}^2} \int_{y=0} e^{-i\vec{p}\cdot\vec{r}} \Gamma_{sc}(\vec{r}_1, \vec{r}_1 + \vec{r}, 0) d^2 r d^2 r_1, \qquad (6.10)$$

where $\vec{p} = \bar{k}(\vec{r}_d - \vec{r}_1)/R_1$. The inner-integral of this formula can be interpreted as a Fourier transform of the mutual coherence function at position $\vec{r}_1$ on the sample plane. The outer-integral is an average of that Fourier transform over the whole sample. In the far-zone approximation the angles ϕ_i are almost $\pi/2$ radians (see figure 6.1) and R_i in the cosine factors and the denominator inside the integral can be taken constant: $R_i \approx r_{ds}$ Hence, the above equation becomes:

$$\Gamma(\vec{r}_d, \vec{r}_d, 0) = \frac{y_d^2}{r_{ds}^4 \bar{\lambda}^2} \int\int_{y=0} e^{-i\vec{p}\cdot\vec{r}} \Gamma_{sc}(\vec{r}_1, \vec{r}_1 + \vec{r}, 0) d^2 r d^2 r_1. \qquad (6.11)$$

If the detector is located at the sample's horizon (i.e. $y_d = 0$) the neutron density due to the scattered beam becomes 0. The explanation is that the sample area as seen by a detector at this position is zero. If the detector area is large and the scattering is in the specular direction so that y_d/r_{ds} can be taken equal to y_1/r_1, the total count rate in the detector is given by (comparable to equation (2.50)):

$$I_d = 2v_p \int_{x=0} \frac{y_1^2}{r_1^2} \Gamma_{sc}(\vec{r_1}, \vec{r_1}, 0) d^2 r_1. \tag{6.12}$$

If the scattered mutual coherence function is sufficiently narrow $\vec{p} \cdot \vec{r}$ can be approximated by:

$$\vec{p} \cdot \vec{r} \approx \bar{k}\Delta x - \bar{k}\Delta x \frac{y_d^2 + (z_d - z_1)^2}{2(x_d - x_1)^2} - \bar{k}\Delta z \frac{z_d - z_1}{x_d - x_1}. \tag{6.13}$$

If further, the second and third term can be neglected ($\ll 1$), the above integral equation (6.11) reduces to equation (2.46). The maximum value of the second or third term is given by the maximum of $k\Delta x$ or $k\Delta z$ and the maximum of either $y_d/(x_d - x_1)$ or $(z_d - z_1)/(x_d - x_1)$. The position of the detector should be approximately in the position of the reflected beam. This limits the maximum values of $y_d/(x_d - x_1)$ and $(z_d - z_1)/(x_d - x_1)$. The maxima for Δx and Δz are determined by the spatial resolution of the reflectometer under consideration. If for the maximum of Δx the first maximum in figure 6.2A is taken and for Δz the first 0 of equation (6.7) is taken, the maximum of the second and third term is of the order of 1. Hence, if the sample correlations extend over much smaller distances than the resolution of the reflectometer as determined by the entrance slit and the sample size, one can safely apply equation (2.46). However, for sample correlations extending toward and over the resolution of the reflectometer the above integral equation should be used to calculate the detector count rate.

6.2 Specular reflection

For smooth interfaces a method is described coupling the scattered mutual coherence function to the incident mutual coherence function. The procedure is the same as in chapter 3. The scattered-wave function is coupled to the incident-wave function and then the definition of the mutual coherence function is applied.

6.2.1 Scattering

If the scattering potential $V(\vec{r})$ of the sample is statistically stationary and only a function of the direction perpendicular to the sample surface (here the y-direction) the three-dimensional time-dependent Schrödinger equation can be reduced to a one-dimensional time independent equation. The procedure is to suppose the wave function can be factorized:

$$\Psi(\vec{r}, t) = e^{-i\omega_k t} \int \int \psi_{k_x}(x)\psi_{k_z}(z)\psi_{k_y}(y) dk_x dk_z, \tag{6.14}$$

where $\vec{k}$ is the wavevector, $\omega_k = \hbar k^2/2m$ and m the neutron mass. The time-dependent Schrödinger equation [5],

$$i\hbar \frac{\partial \Psi(\vec{r}, t)}{\partial t} = -\frac{\hbar^2}{2m} \nabla^2 \Psi(\vec{r}, t) + V(\vec{r}) \Psi(\vec{r}, t), \tag{6.15}$$

then reduces to three independent differential equations:

$$\frac{d^2\psi_{k_x}(x)}{dx^2} + k_x^2\psi_{k_x}(x) = 0, \tag{6.16}$$

$$\frac{d^2\psi_{k_z}(z)}{dz^2} + k_z^2\psi_{k_z}(z) = 0 \tag{6.17}$$

and

$$\frac{d^2\psi_{k_y}(y)}{dy^2} + \left\{k_y^2 - k_c^2(y)\right\}\psi_{k_y}(y) = 0, \tag{6.18}$$

where $k_x^2 + k_y^2 + k_z^2 = k^2$ and $k_c^2(y) = 2mV(y)/\hbar^2$, is called the *critical wavevector* equal to $4\pi\rho_b$. ρ_b is the *scattering-length density*. k_c^2 can be interpreted as the potential in 'wave-vector squared units' and is closely related to the refraction index (see section 3.22). The scattering-length density can be calculated by

$$\rho_b = \langle Nb_n\rangle - \frac{i}{2}\left\langle N(\sigma_{abs}(\lambda) + \sigma_{inc})/\lambda\right\rangle. \tag{6.19}$$

Here b_n is the nuclear-scattering length, N the atomic-number density, $\sigma_{abs}(\lambda)$ is the neutron absorption cross section and proportional to λ for a $1/v$-absorber, σ_{inc} the incoherent-neutron cross section and constant for most practical cases. Note that the imaginary part of ρ_b is independent of the wavelength for a $1/v$-absorber, when the incoherent scattering is negligible. For some homogeneous materials the real and imaginary parts of k_c^2 are given in table 6.2. The first two differential equations are linear second order differential equations and can easily be solved:

$$\psi_{k_x}(x) = \alpha_x(k_x)e^{ik_x x} + \beta_x(k_x)e^{-ik_x x} \tag{6.20}$$

and

$$\psi_{k_z}(z) = \alpha_z(k_z)e^{ik_z z} + \beta_z(k_z)e^{-ik_z z}. \tag{6.21}$$

The last differential equation depends on the potential $V(y)$. In the region $y > 0$ above the sample the potential is 0 and this equation also reduces to a linear second order differential equation, with a general solution [38]:

$$\psi_{k_y}(y) = e^{-ik_y y} + \rho e^{ik_y y}. \tag{6.22}$$

The first term at the right hand side corresponds to the incident beam $\psi_{k_y,in} = e^{-ik_y y}$ and the second term to the (specular) reflected beam $\psi_{k_y,sc} = \rho e^{ik_y y}$, where ρ is the reflectance. The reflectance only depends on $V(y)$ and k_y and can be determined by dividing the potential $V(y)$ into a finite number of slices with some (varying) thickness and a constant potential for each slice (see figure 6.4) [38]. In every slice, j the solution of the Schrödinger equation has the form of equation (6.21):

$$y_j < y < y_{j+1}: \quad \psi_{k_y}(y) = \alpha_j e^{iq_j(y-y_j)} + \beta_j e^{-iq_j(y-y_j)}, \tag{6.23}$$

where $q_j = +\sqrt{k_y^2 - (k_c^{(j)})^2}$ and $k_c^{(j)}$ is the critical wavevector in slice j. The factors α_j and β_j in each slice can be determined by imposing the boundary conditions (continuity of

Material	$\Re(k_c^2)$ 10^{-3} nm^{-2}	$\Im(k_c^2)$ 10^{-6} nm^{-2}
Al	2.614(5)	< 0.1
Ar[1]	0.512(3)	< 0.1
^{36}Ar[1]	6.67(4)	0.39(4)
Au	5.54(5)	20.00(3)
B	8.68(8)	350(4)
^{10}B	-0.16(50)	1890(20)
C, graphite	9.42(4)	< 0.1
C, diamond	14.70(6)	< 0.1
Cd	2.83(3)	408(8)
Co	2.84(4)	13.3(2)
Fe	10.07(3)	0.88(4)
Gd	2.5(2)[2]	5258(13)[2]
Ni	11.8(2)	3.1(2)
^{58}Ni	16.5(2)	1.5(1)
N_2 [3]	4.087(8)	< 0.1
Si[4]	2.6037(6)	< 0.1
Ti	-2.45(1)	1.8(1)
SiO_2, cristobalite	4.60(2)	< 0.1
SiO_2, lechatelierite	4.34(2)	< 0.1
SiO_2, tridymite	4.48(2)	< 0.1
SiO_2, quartz	5.25(7)	< 0.1
H_2O	-0.7024(26)	9.40(1)
D_2O	7.993(6)	0.26(1)

[1] Liquid Ar at triple point (83.78 K; 0.687 bar).
[2] Strongly wavelength dependent.
[3] Liquid N_2 at 77.35 K; 1 bar.
[4] Single crystal at 295.7 K; 1 bar.

Table 6.2: Real nuclear ($\Re(k_c^2)$) and (negative) imaginary ($\Im(k_c^2)$) part of the critical wavevector for some materials at 293 K and 1 bar for a neutron wavelength of 0.18 nm.

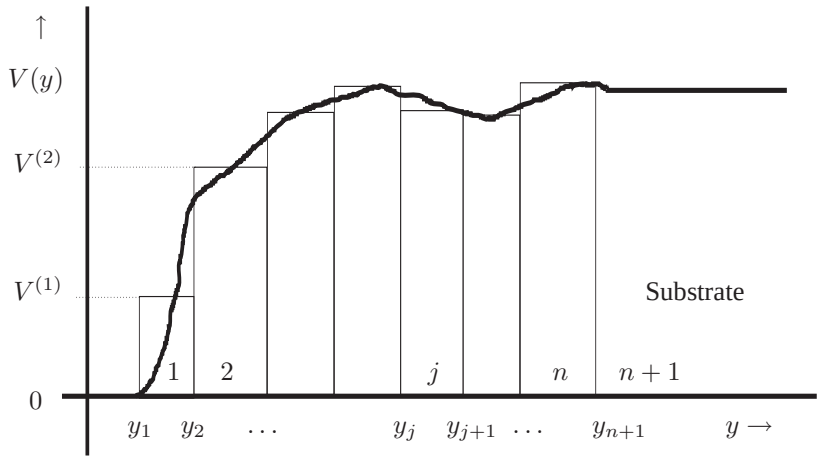

Figure 6.4: An arbitrary potential $V(y)$, divided in n layers of constant potential $V^{(j)}$.

the wave function and its derivative) at each interface:

$$\begin{pmatrix} \alpha_{j+1} \\ \beta_{j+1} \end{pmatrix} = M_j \begin{pmatrix} \alpha_i \\ \beta_j \end{pmatrix} \ , \qquad M_j = \tfrac{1}{2} \begin{pmatrix} 1+\epsilon_j & 1-\epsilon_j \\ 1-\epsilon_j & 1+\epsilon_j \end{pmatrix} \begin{pmatrix} \mathrm{e}^{iq_j d_j} & 0 \\ 0 & \mathrm{e}^{-iq_j d_j} \end{pmatrix} \ , \tag{6.24}$$

where $\epsilon_j = q_j/q_{j+1}$. The second matrix at the right-hand side of the equation shifts the y position over d_j, the thickness of layer j. d_0 is zero and if j is greater than 0, d_j is given by $y_{j+1} - y_j$. For the total multilayer with n layers is found

$$\begin{pmatrix} \alpha_{n+1} \\ \beta_{n+1} \end{pmatrix} = M_n M_{n-1} \cdots M_1 M_0 \begin{pmatrix} \alpha_0 \\ \beta_0 \end{pmatrix} = M \begin{pmatrix} \alpha_0 \\ \beta_0 \end{pmatrix} \ . \tag{6.25}$$

As in equation (6.22) the reflection and transmission amplitudes are defined by:

$$\alpha_0 = 1 \qquad \beta_0 = \rho(q_0) \ , \qquad \alpha_{n+1} = \tau(q_0) \quad \beta_{n+1} = 0 \ , \tag{6.26}$$

so

$$\begin{pmatrix} \tau(q_0) \\ 0 \end{pmatrix} = M \begin{pmatrix} 1 \\ \rho(q_0) \end{pmatrix} = \begin{pmatrix} m_{11} & m_{12} \\ m_{21} & m_{22} \end{pmatrix} \begin{pmatrix} 1 \\ \rho(q_0) \end{pmatrix} \ . \tag{6.27}$$

Hence, for the reflectance and the reflectivity is found

$$r(q_0) = -\frac{m_{21}}{m_{22}} \quad \text{and} \quad R(q_0) = |r(q_0)|^2 \ . \tag{6.28}$$

From equation (6.24) it can easily be shown that it is possible to calculate the reflectance from recursion relations of the reflectance, $r_j = \beta_j/\alpha_j$ in each layer j:

$$r_j = \mathrm{e}^{2iq_j d_j} \frac{r_j^F + r_{j+1}}{1 + r_j^F r_{j+1}} \ , \tag{6.29}$$

where $r_j^F = (\epsilon_j - 1)(\epsilon_j + 1)^{-1}$, the Fresnel reflectance from material j to $j+1$ and $r_{n+1} = 0$. This relation is similar to the recursion relations derived by Parrat [39] for X-ray reflection. The advantage of recursion relations is that per layer fewer calculations are needed than for the matrix method. However, for extended repetitions of the same structure in a multilayer it is faster to use the matrix calculations.

6.2.2 Propagation from sample to detector

A quasi-monochromatic beam at the sample surface can be thought of as an ensemble average of plane waves. The scattered mutual coherence function can be calculated by realizing that the propagation formula for the mutual coherence function (2.31) consists of two integrals. One integrating the incident-wave function reaching point $\vec{r}_1$ from $\vec{r'}_1$ and the other integrating the incident-wave function reaching point $\vec{r}_2$ from $\vec{r'}_2$. To find the scattered mutual coherence function one has to multiply (before integrating) the incident-wave functions by the appropriate reflectance according to the above equation:

$$\Gamma_{sc}(\vec{r}_1, \vec{r}_2, \tau) = \int\int_{y=0} \rho^*(q_1)\rho(q_2) \frac{\cos\theta_1 \cos\theta_2 e^{i\bar{k}(R_2 - R_1)}}{R_1 R_2 \bar{\lambda}^2} \Gamma_0(\vec{r'_1}, \vec{r'_2}, \tau) d^2 r'_1 d^2 r'_2, \tag{6.30}$$

where $q_i = \bar{k}(\vec{r'_i} \cdot \vec{e}_y)/R_i$. This equation can also be derived using the results of section C.1.

Now the same procedure as in section 6.1.1 is followed, with the same symbols used. For a completely homogeneous incoherent source the mutual coherence function at the sample surface reduces to:

$$\Gamma_{sc}(\vec{r}_1, \vec{r}_2, \tau) = \frac{J_0}{2v_p} \frac{e^{-i\bar{k}v_p\tau}}{4\pi} \int_{A_0} \rho(q_1)^* \rho(q_2) \frac{\cos\theta_1 \cos\theta_2 e^{i\bar{k}(R_2 - R_1)}}{R_2 R_1} d^2 r'_1, \tag{6.31}$$

If the mutual coherence function is sufficiently narrow $q_i \approx q_1$ so that the above equation reduces further to:

$$\Gamma_{sc}(\vec{r}_1, \vec{r}_2, \tau) = \frac{J_0}{2v_p} \frac{e^{-i\bar{k}v_p\tau}}{4\pi} \int_{A_0} R(q_1) \frac{\cos\theta_1 \cos\theta_2 e^{i\bar{k}(R_2 - R_1)}}{R_2 R_1} d^2 r'_1, \tag{6.32}$$

where $R(q)$ is the reflectivity defined as $R(q) = \rho(q)\rho^*(q)$. If the source aperture is rectangular the integral can be evaluated as:

$$\Gamma_{sc}(\vec{r}_1, \vec{r}_1 + \vec{r}, \tau) = \tilde{R}(q, \Delta q, \alpha) \Gamma_{in}(\vec{r}_1, \vec{r}_1 + \vec{r}, \tau), \tag{6.33}$$

where $q = \bar{k}H/r_1$, $\Delta q = \bar{k}W_y/2r_1$, $\alpha = \sqrt{\Delta x/\pi\bar{k}}$ and

$$\tilde{R}(q, \Delta q, \alpha) = \frac{\int_{q-\Delta q}^{q+\Delta q} R(\eta) e^{-i\frac{\pi}{2}\alpha^2\eta^2} d\eta}{\int_{q-\Delta q}^{q+\Delta q} e^{-i\frac{\pi}{2}\alpha^2\eta^2} d\eta}, \tag{6.34}$$

is a folded reflectivity. Note that for $\Delta x = 0$ this reduces to:

$$\tilde{R}(q, \Delta q, 0) = \frac{\int_{q-\Delta q}^{q+\Delta q} R(\eta) d\eta}{2\Delta q}. \tag{6.35}$$

If the scattering (or reflection) is mainly in the specular direction and the detector area is large enough, the total count rate in the detector is given by equation (6.12):

$$I_d = 2v_p \int_{A_s} \frac{q^2}{\bar{k}^2} \tilde{R}(q, \Delta q, 0) \Gamma_{in}(\vec{r}_1, \vec{r}_1, 0) d^2 r_1, \tag{6.36}$$

which using equation (6.8) reduces for an incoherent source to:

$$I_d = J_0 W_z W_y \int_{A_s} \frac{q^2}{\bar{k}^2} \frac{\tilde{R}(q, \Delta q, 0)}{4\pi r_1^2} d^2 r_1 \tag{6.37}$$

and for the slit geometry assumed here:

$$I_d = \frac{J_0 A_s W_z W_y}{4\pi r_1^2} \frac{\int_{q-\Delta q}^{q+\Delta q} \eta^2 R(\eta) d\eta}{\bar{k}^2 2\Delta q}. \tag{6.38}$$

Note that the total reflected beam is detected by the detector and it is assumed that the sample is small so that the resolution is due to the entrance diaphragm and the distance to the sample only.

6.3 Born approximation

To find the scattered neutron count rate due to a rough surface (described in appendix B) the first Born approximation can be used. It is based on equation (3.18), where G_s is found using equation (3.21):

$$S_k(\vec{q}) = \int e^{-i\vec{q}\cdot\vec{r}} \int_{V_s} \rho_b(\vec{r}_s) \rho_b(\vec{r}_s + \vec{r}) d^3 r_s d^3 r, \tag{6.39}$$

Using equation (3.19) for the scattering length density and equation (B.6) for the potential this becomes:

$$S_k(\vec{q}) = \rho_b^2 \int_{V_s} \int_{V_s} e^{-i\vec{q}\cdot(\vec{r}-\vec{r}_s)} d^3 r_s d^3 r, \tag{6.40}$$

where $\rho_b = -2\pi m V_0/h^2$, the scattering length density of the homogeneous sample and the integration extends over the sample volume. Transforming to Cartesian coordinates and ignoring effects due to the finite beam cross section this becomes:

$$S_k(\vec{q}) = \frac{\rho_b^2 A_s}{q_y^2} \int_{A_s} e^{-i(q_x x + q_z z)} \left\{ e^{-\frac{q_y^2 g(x,z)}{2}} - 2\cos(q_y d) e^{-\frac{q_y^2 \sigma^2}{2}} + 1 \right\} dx dz, \tag{6.41}$$

where $\vec{r} = (x, y, z)^{\mathrm{T}}$ and $\vec{q} = (q_x, q_y, q_z)^{\mathrm{T}}$. The first term inside the integral represents the beam scattered from the top (rough) surface, the second term the interference between the top and bottom and the third term the beam scattered from the bottom (flat) surface. In general the second and third term are ignored, yielding [40]:

$$S_k(\vec{q}) = \rho_b^2 A_s \left(S_s(\vec{q}) + S_d(\vec{q}) \right), \tag{6.42}$$

where

$$S_s(\vec{q}) = \frac{4\pi^2 e^{-q_y^2 \sigma^2}}{q_y^2} \delta(q_x) \delta(q_z) \tag{6.43}$$

is the *specular* component and

$$S_d(\vec{q}) = \frac{e^{-q_y^2\sigma^2}}{q_y^2}\int_{A_s} e^{-i(q_x x+q_z z)}\left(e^{q_y^2 C(x,z)}-1\right)dxdz \tag{6.44}$$

the *diffuse* component of the scattering. Hence, the sample correlation function can also be split in two components: $G_s(\vec{r}) = G_{s,s}(\vec{r}) + G_{s,d}(\vec{r})$:

$$G_{s,s}(\vec{r}) = \frac{1}{(2\pi)^3}\int e^{i\vec{q}\cdot\vec{r}} S_s(\vec{q})d\vec{q} = \sigma f\left(\frac{y}{2\sigma}\right), \tag{6.45}$$

where $f(x) = x\,\mathrm{erf}(x) + e^{-x^2}/\sqrt{\pi}$ and

$$G_{s,d}(\vec{r}) = \frac{1}{(2\pi)^3}\int e^{i\vec{q}\cdot\vec{r}} S_d(\vec{q})d\vec{q}. \tag{6.46}$$

The incident mutual coherence function is given by equation (6.4):

$$\Gamma_{in}(\vec{r}_1,\vec{r}_1+\vec{r},\tau) \approx \frac{J_0}{2v_p}\frac{e^{-i\bar{k}(x+v_p\tau)}}{4\pi r_1^2}\times \tag{6.47}$$

$$\int_{H-\frac{W_y}{2}-y_1}^{H+\frac{W_y}{2}-y_1} e^{i\frac{\pi}{2}\left(\kappa_x^2 y'^2+2\kappa_y y'\right)}dy' \int_{-\frac{W_z}{2}-z_1}^{\frac{W_z}{2}-z_1} e^{i\frac{\pi}{2}\left(\kappa_x^2 z'^2+2\kappa_z z'\right)}dz',$$

where $\kappa_x^2 = \bar{k}\frac{x}{\pi r_1^2}$, $\kappa_y = \frac{\bar{k}y}{\pi r_1}$ and $\kappa_z = \frac{\bar{k}z}{\pi r_1}$. The detector count rate can be determined by applying equation (3.10):

$$I_d = 2v_p\int R_{out}(\vec{r}_1,\vec{r}_1+\vec{r})G_s(\vec{r})\Gamma_{in}(\vec{r}_1,\vec{r}_1+\vec{r},0)d^3r, \tag{6.48}$$

where

$$R_{out}(\vec{r}_1,\vec{r}_1+\vec{r}) = \int_{A_d}\frac{e^{-i\vec{p}\cdot\vec{r}}}{\left|\vec{r}_d-\vec{r}_1\right|^2}d^2r_d \tag{6.49}$$

and $\vec{p} = \bar{k}(\vec{r}_d-\vec{r}_1)/\left|\vec{r}_d-\vec{r}_1\right|$ and it was assumed that $\cos\theta_d \approx 1$. Conform equation (6.13) it follows that:

$$\vec{p}\cdot\vec{r} \approx \bar{k}\left(-x + \frac{(y_d-y_1)^2}{2r_{ds}^2}x + \frac{(z_d-z_1)^2}{2r_{ds}^2}x - \frac{y_d-y_1}{r_{ds}}y + \frac{z_d-z_1}{r_{ds}}z\right) \tag{6.50}$$

and $R_{out}(\vec{r}_1,\vec{r}_1+\vec{r})$ can be evaluated as:

$$R_{out}(\vec{r}_1,\vec{r}_1+\vec{r}) = \frac{e^{i\bar{k}x}}{r_{ds}^2}\int_{H_d-y_1-\frac{D_y}{2}}^{H_d-y_1+\frac{D_y}{2}} e^{i\frac{\pi}{2}\left(2k_y y_d-k_x^2 y_d^2\right)}dy_d \int_{-\frac{D_z}{2}-z_1}^{\frac{D_z}{2}-z_1} e^{i\frac{\pi}{2}\left(-2k_z z_d-k_x^2 z_d^2\right)}dz_d, \tag{6.51}$$

where $k_x^2 = \bar{k}\frac{x}{\pi r_{ds}^2}$, $k_y = \frac{\bar{k}y}{\pi r_{ds}}$ and $k_z = \frac{\bar{k}z}{\pi r_{ds}}$. D_y and D_z are the width and height of the detector and H_d the y-position of the detector. In general equation (6.48) can only be evaluated numerically. In special cases one can try to reduce the above integral.

6.3.1 Specular count rate

For the specular scattered neutrons this can be done by realizing that $G_{s,s}(\vec{r})$ does not depend on x or z and hence the integral reduces to ($y_1 = 0$):

$$I_d = \frac{J_0\pi}{\bar{k}^2 r_1^2 r_{ds}^2} \int G_{s,s}(\vec{r}) \int_{-\frac{D_z}{2}-z_1}^{\frac{D_z}{2}-z_1} \int_{-\frac{W_z}{2}-z_1}^{\frac{W_z}{2}-z_1} \times \tag{6.52}$$

$$\int_{H_d-\frac{D_y}{2}}^{H_d+\frac{D_y}{2}} \int_{H-\frac{W_y}{2}}^{H+\frac{W_y}{2}} e^{i\bar{k}y\left(\frac{y_d}{r_{ds}}+\frac{y'}{r_1}\right)} \delta\left(\frac{z'}{r_1} - \frac{z_d}{r_{ds}}\right) \delta\left(\frac{y'^2+z'^2}{2r_1^2} - \frac{y_d^2+z_d^2}{2r_{ds}^2}\right) dy' dy_d dz' dz_d dy,$$

where it was used that:

$$\int e^{-iq_x x} dx \int e^{-iq_z z} dz = 4\pi^2 \delta(q_x)\delta(q_z). \tag{6.53}$$

Further integrating over z_d, y_d and assuming the detector width and height are large enough to catch all specular reflected neutrons, yields:

$$I_d = \frac{J_0 W_z \pi}{\bar{k}^2 r_1} \int G_{s,s}(\vec{r}) \int_{H-\frac{W_y}{2}}^{H+\frac{W_y}{2}} \frac{e^{2i\bar{k}yy'/r_1}}{y'} dy' dy. \tag{6.54}$$

The inner integral over y' can be evaluated assuming that y' in the nominator is constant, which is a good approximation when $W_y \ll H$. Then

$$I_d = \frac{2\pi J_0 W_z W_y}{\bar{k} r_1^2 q_y} \int G_{s,s}(\vec{r}) e^{iq_y y} \frac{\sin(\bar{k}yW_y/r_1)}{\bar{k}yW_y/r_1} dy. \tag{6.55}$$

where $q_y = 2\bar{k}H/r_1$.

If the height of the entrance diaphragms is sufficiently small $y\bar{k}W_y/r_1 \ll 1$ then the sinc function ≈ 1. The integral then reduces to a one-dimensional Fourier transform comparable to equation (6.41) with the transform over x and y omitted, resulting in equation (6.43) where the factor $4\pi^2\delta(q_x)\delta(q_z)$ is omitted:

$$\int G_{s,s}(\vec{r}) e^{iq_y y} dy = \frac{\rho_b^2 A_s}{q_y^2} e^{-q_y^2\sigma^2}. \tag{6.56}$$

Finally the detector count rate becomes:

$$I_d = \frac{2\pi J_0 W_z W_y \rho_b^2 A_s}{\bar{k} r_1^2} \frac{e^{-q_y^2\sigma^2}}{q_y^3}. \tag{6.57}$$

For the empty beam the detector count rate is given by equation (2.50):

$$I_{d,empty} = 2v_p A_b \Gamma_{in}(\vec{r}_1, \vec{r}_1, 0) = \frac{J_0 A_b W_z W_y}{4\pi r_1^2}, \tag{6.58}$$

where A_b is the beam cross section at the sample position. If it is assumed the sample area covers the whole incident beam, then $A_s = A_b/\sin\theta_s$ where $\theta_s \approx q_y/2\bar{k}$ is the angle between beam and the sample surface. The specular component of the reflectivity, defined

as the count rate in the detector due to the specular component of the sample correlation function divided by the count rate of the whole beam at the sample position becomes [40]:

$$R_s = \frac{16\pi^2\rho_b^2 e^{-q_y^2\sigma^2}}{q_y^4}. \tag{6.59}$$

For $\sigma = 0$ this reduces to the large q limit of the Fresnel theory, equivalent to Porods law [41]. If the height of the entrance diaphragm is not sufficiently small equation (6.54) can be rewritten as:

$$I_d = \frac{J_0 W_z W_y 4\pi\rho_b^2 A_b}{r_1^2 q_y^4}\frac{1}{\eta}\int_{-\eta/2}^{\eta/2}\frac{e^{-(x+1)^2 q_y^2\sigma^2}}{(x+1)^3}dx \tag{6.60}$$

where $\eta = W_y/H$ and the specular component of the reflectivity becomes:

$$R_s = \frac{16\pi^2\rho_b^2 e^{-q_y^2\sigma_y^2}}{q_y^4}\frac{1}{\eta}\int_{-\eta/2}^{\eta/2}\frac{e^{-(x+1)^2 q_y^2\sigma^2}}{(x+1)^3}dx, \tag{6.61}$$

which can be approximated by:

$$R_s = \frac{16\pi^2\rho_b^2 e^{-q_y^2\sigma_y^2}}{q_y^4}\frac{\sinh\eta q_y^2\sigma_y^2}{\eta q_y^2\sigma_y^2}. \tag{6.62}$$

The function $\sinh x/x \geq 1$ so that the reflectivity measured with a finite resolution is always larger than the one calculated using the above method. The result is that a fit of the reflectivity of measured data with equation (6.59) always yields a roughness which is too small. This was already mentioned by Braslau at al. [42].

6.3.2 Diffuse count rate

The diffuse component of the scattering can be evaluated analytical if it is assumed that all instrumental resolution effects can be ignored. This can be achieved by reducing the width and height of the source and detector to infinitely small values. Then equation (6.48) can be reduced to:

$$I_d = \frac{J_0 D_y D_z W_y W_z}{4\pi r_1^2 r_{ds}^2}\rho_b^2 A_s S_d((q_x, q_y, q_z)^{\mathrm{T}}), \tag{6.63}$$

where $q_x = \bar{k}\left(\frac{H^2+z_1^2}{2r_1^2} - \frac{H_d^2+(z_d-z_1)^2}{2r_{ds}^2}\right)$, $q_y = \bar{k}\left(\frac{H}{r_1} + \frac{H_d}{r_{ds}}\right)$ and $q_z = \bar{k}\left(\frac{z_1-z_d}{r_{ds}} - \frac{z_1}{r_1}\right)$.

6.4 Distorted-wave Born approximation

The first Born approximation is only valid for weak scattering. If the intensity of the refracted beam becomes of the same order as the incident beam (near the critical angle for total reflection) this condition is no longer valid and the results of the previous section can no longer be applied. In that case one can try to calculate the intensity of the refracted or reflected beam by using the distorted-wave Born approximation [40], [43], [44], [45]. In short it comes down to making an accurate enough estimate of the neutron wave function in and near the sample and use this estimate to calculate the scattered intensity (see also section 3.1). In most treatments the estimate of the neutron wave function in the sample is based on the solution of the one-dimensional Schrödinger equation for a smooth surface with a sharp or graded interface. First the incident-wave function must be determined, then the scattering of the incident-wave function into the scattered-wave function and then the scattered mutual coherence function must be established.

6.4.1 Scattering of incident-wave function

Let $\Psi(\vec{r},t)$ denote a neutron wave function characterizing the field at point $\vec{r}$ at time t. The neutron wave function $\Psi(\vec{r},t)$ is constructed by its constituting monochromatic plane-wave components (see also section 2.1):

$$\Psi(\vec{r},t) = e^{-i\omega_k t}\int \psi(\vec{k},\vec{r})d^2k, \tag{6.64}$$

where $\vec{k}$ is the wavevector, $\omega_k = \hbar k^2/2m$ and m the neutron mass. The integral is over two dimensions only as for a monochromatic wave the length of the wavevector is constant. If further it is assumed that the incident neutron beam is directed to positive value's of x and z only, the wavevector $\vec{k} = \vec{k}_{\parallel} + k_y\vec{e}_y$, where $k_y = \vec{k}\cdot\vec{e}_y$ so that $k_y = -\sqrt{\bar{k}^2 - k_{\parallel}^2}$. The negative sign denotes that the plane wave is traveling in the $-y$ direction. The plane-wave components of the incident beam can be described by:

$$\psi_{in}(\vec{k},\vec{r}) = \psi_0(\vec{k}_{\parallel})e^{i\vec{k}\cdot\vec{r}}. \tag{6.65}$$

Hence, the incident-wave function can be described by:

$$\Psi_{in}(\vec{r},t) = e^{-i\omega_k t}\int e^{i\vec{k}\cdot\vec{r}}\psi_0(\vec{k}_{\parallel})d^2k_{\parallel}. \tag{6.66}$$

For a surface with some roughness or structure the scattering potential $V(\vec{r})$ can be split in two parts:

$$V(\vec{r}) = V^{(0)}(y) + V^{(1)}(\vec{r}), \tag{6.67}$$

where $V^{(0)}(y)$ represents the potential of the smooth surface and $V^{(1)}(\vec{r})$ is the disturbance of the potential due to the interface roughness or structure. Using the previous defined height of the surface the above potentials are given by (assuming the sample thickness is much larger than the surface roughness):

$$V^{(0)}(y) = \frac{\hbar^2 k_c^2}{2m}u(-y) \tag{6.68}$$

and

$$V^{(1)}(\vec{r}) = \frac{\hbar^2 k_c^2}{2m}(u(y) - u(y - H(x,z))), \tag{6.69}$$

where $k_c^2 = 2mV_0/\hbar^2 = 4\pi\rho_b$. Assume the distortion of the scattered wave can be described by:

$$\psi_{sc}(\vec{k},\vec{r}) = \psi_{sc}^{(0)}(\vec{k},\vec{r}) + \psi_{sc}^{(1)}(\vec{k},\vec{r}), \tag{6.70}$$

where $\psi_{sc}^{(0)}(\vec{k},\vec{r})$ is the undisturbed scattered-wave function from the perfectly flat sample surface. Using equation (3.1) it can be shown that

$$\psi_{sc}^{(0)}(\vec{k},\vec{r}) = \psi_{in}(\vec{k},\vec{r}) - \frac{2m}{\hbar^2}\int G_0(\vec{r},\vec{r}_s)V^{(0)}(y_s)\psi_{sc}^{(0)}(\vec{k},\vec{r}_s)d^3r_s \tag{6.71}$$

and

$$\psi_{sc}^{(1)}(\vec{k},\vec{r}) = -\frac{2m}{\hbar^2}\int G_0(\vec{r},\vec{r}_s)\left(V^{(0)}(y_s)\psi_{sc}^{(1)}(\vec{k},\vec{r}_s) + V^{(1)}(\vec{r}_s)\psi_{sc}(\vec{k},\vec{r}_s)\right)d^3r_s, \tag{6.72}$$

where $G_0(\vec{r},\vec{r}_s)$ is the free particle Green function for scattered waves. For the solution of this last equation the first term inside the integral is neglected, which is allowed if the first integral is much smaller than the second. This is the case if $\psi_{sc}^{(1)}(\vec{k},\vec{r}_s) \ll \psi_{sc}^{(0)}(\vec{k},\vec{r}_s)$ or when $V^{(1)}(\vec{r}_s)$ has only Fourier components much smaller than $\bar{k}$. This is why this approximation is called distorted-wave *Born approximation*. In the second term the equality of equations (3.1) and (3.4) can be used, so that up to first order the scattered-wave function becomes:

$$\psi_{sc}^{(1)}(\vec{k},\vec{r}) = -\frac{2m}{\hbar^2}\int G^{(+)}(\vec{r},\vec{r}_s)V^{(1)}(\vec{r}_s)\psi_{sc}^{(0)}(\vec{k},\vec{r}_s)d^3r_s. \tag{6.73}$$

To solve this equation a precise estimate of the Green function and the undisturbed scattered-wave function is needed. The Green function can be estimated by means of the Green function for a smooth surface, which is a further approximation. Note that ψ_{sc} contains both the scattering due to the smooth potential $V^{(0)}(y)$ and due to the potential of the surface roughness or structure $V^{(1)}(\vec{r})$. This is split in a part due to the smooth surface only ($\psi_{sc}^{(0)}$) and due to the surface roughness or structure ($\psi_{sc}^{(1)}$). However, for evaluating the total scattering one should not neglect the interference between the two parts when determining the scattered mutual coherence function. In general the interference term reduces the specular reflected part of the mutual coherence function as will be discussed in section 6.4.5.

6.4.2 Undisturbed scattered-wave function

The plane waves which are reflected or refracted at the perfectly flat sample surface are given by (assuming a very thick sample):

$$\psi_{sc}^{(0)}(\vec{k},\vec{r}) = \psi_0(\vec{k}_\parallel)e^{i\vec{k}_\parallel\cdot\vec{r}}\Psi_k(y), \tag{6.74}$$

where

$$\begin{aligned} \Psi_k(y) &= e^{ik_y y} + \rho(k_y)e^{-ik_y y} \quad y \geq 0, \\ \Psi_k(y) &= \tau(k_y)e^{ik'_y y} \qquad\qquad\quad y < 0, \end{aligned} \tag{6.75}$$

and $k'_y = -\sqrt{k_y^2 - k_c^2}$, the negative sign is used as k_y is also negative due to the reflection geometry. $k_c^2 = 2mV_0/\hbar^2 = 4\pi\rho_b$, $\rho(k_y) = (k_y - k'_y)/(k_y + k'_y)$ and $\tau(k_y) = 2k_y/(k_y + k'_y)$ (see also section 6.2). It can also be derived by transforming equation (6.71) (see section 3.1) to:

$$\psi_{sc}^{(0)}(\vec{k},\vec{r}) = \psi_{in}(\vec{k},\vec{r}) - \frac{2m}{\hbar^2}\int G^{(+)}(\vec{r},\vec{r}_s)V^{(0)}(y_s)\psi_{in}(\vec{k},\vec{r}_s)d^3r_s. \tag{6.76}$$

Inserting the incident-wave function (6.65), the appropriate Green function (see appendix D) and the undisturbed potential (6.68):

$$\psi_{sc}^{(0)}(\vec{k},\vec{r}) = \psi_0(\vec{k}_\parallel)e^{i\vec{k}_\parallel\cdot\vec{r}}\left(e^{ik_y y} + e^{-ik_y y}\frac{k_c^2\tau(k_y)}{2ik_y}\int_{-\infty}^{0} e^{-i(k_y+k'_y)y_s}dy_s\right), \tag{6.77}$$

for $y \geq 0$. The integral over y_s can be performed assuming a little absorption so that the lower limit vanishes, yielding

$$\psi_{sc}^{(0)}(\vec{k},\vec{r}) = \psi_0(\vec{k}_\parallel)e^{i\vec{k}_\parallel\cdot\vec{r}}\left(e^{ik_y y} + \rho(k_y)e^{-ik_y y}\right). \tag{6.78}$$

The same can be done for $y < 0$, yielding equation (6.74). This solution for the undisturbed scattered-wave function is used by Steyerl [43], Sinha et al. [40], Pynn [44] and De Boer [45]. Weber et al. [46] were not able to fit their data with this approximation and found a good fit with the following approximation for the undisturbed scattered-wave function:

$$\begin{aligned} \Psi_k(y) &= e^{ik_y y} + \rho_r(k_y)e^{-ik_y y} \quad y \geq 0, \\ \Psi_k(y) &= \tau_r(k_y)e^{ik'_y y} \qquad\qquad\quad y < 0, \end{aligned} \tag{6.79}$$

where ρ_r and τ_r are the transmission and reflection coefficients for the *rough* surface determined by an appropriate graded interface.

6.4.3 Green function

The Green function for scattered waves can be approximated by taking the Green function for scattered waves for the undisturbed potential [43], [47], [48] defined by:

$$\left(\nabla^2 + \bar{k}^2 - \frac{2mV^{(0)}(\vec{r}_s)}{\hbar^2}\right)G^{(+)}(\vec{r},\vec{r}_s) = \delta(\vec{r} - \vec{r}_s), \tag{6.80}$$

which for large distances ($|\vec{r} - \vec{r}_s| > \bar{\lambda}$) and small scattering angle reduces to (see also appendix D):

$$G^{(+)}(\vec{r},\vec{r}_s) = G_0(\vec{r} - \vec{r}_s)e^{ip_y y_s}\Psi_p(y_s), \tag{6.81}$$

where $y_s = \vec{r}_s \cdot \vec{e}_y$, $\vec{p} = \bar{k}(\vec{r} - \vec{r}_s)/|\vec{r} - \vec{r}_s|$, $G_0(\vec{r})$ is the free particle Green function as defined in equation (2.33), which can be expressed in terms of $\vec{p}$:

$$G_0(\vec{r}) = \frac{e^{i\vec{p}\cdot\vec{r}}}{4\pi r} \tag{6.82}$$

and $\Psi_p(y)$ is the part of the Green function determined by the sample details:

$$\begin{aligned} \Psi_p(y) &= e^{-ip_y y} + \rho(p_y)e^{ip_y y} \quad y \geq 0, \\ \Psi_p(y) &= \tau(p_y)e^{-ip'_y y} \qquad\quad y < 0, \end{aligned} \tag{6.83}$$

where $\rho(p_y) = (p_y - p'_y)/(p_y + p'_y)$, the reflection coefficient of the wave reflecting at the sample surface (see also section 6.2). $p'_y = +\sqrt{p_y^2 - k_c^2}$, the accent denotes the value of the variable in the sample material and the positive sign is taken as p_y is also positive and $\tau(p_y) = 2p_y/(p_y + p'_y)$, the transmission of the wave function traversing the sample surface from outside to inside. Sinha et al. [40] use for $\Psi_p(y)$ the so-called *time reversed solution*:

$$\begin{aligned} \Psi_p(y) &= e^{-ip_y y} + \rho(p_y)^* e^{ip_y y} \quad y \geq 0, \\ \Psi_p(y) &= \tau(p_y)^* e^{-ip'_y y} \qquad\quad y < 0, \end{aligned} \tag{6.84}$$

which only deviates by the complex conjugated values of ρ and τ, which do not influence the final results. Pynn [44] decided to use:

$$\begin{aligned} \Psi_p(y) &= e^{-ip_y y} + \rho_r(p_y)^* e^{ip_y y} \quad y \geq 0, \\ \Psi_p(y) &= \tau_r(p_y)^* e^{-ip'_y y} \qquad\quad y < 0, \end{aligned} \tag{6.85}$$

where ρ_r and τ_r are the reflection and transmission coefficients for the rough surface. De Boer [45] mentioned the *irregular* solution of the one-dimensional Scrödinger equation:

$$\begin{aligned} \Psi_p(y) &= \tilde{\tau}(p_y)e^{-ip_y y} \qquad\quad y \geq 0, \\ \Psi_p(y) &= e^{-ip'_y y} - \rho(p_y)e^{ip'_y y} \quad y < 0, \end{aligned} \tag{6.86}$$

which gives the transmission and reflection amplitude of the wave starting inside the sample traveling outside. He uses this to find the one-dimensional Green function and gives the same formula as Sinha et al.

6.4.4 Scattered-wave function

Finally, to conclude, equation (6.70) can be inserted in equation (6.64) to find the scattered-wave function in the far-zone:

$$\Psi_{sc}(\vec{r}, t) = e^{-i\omega_k t} \int \left\{ \psi_{sc}^{(0)}(\vec{k}, \vec{r}) + \psi_{sc}^{(1)}(\vec{k}, \vec{r}) \right\} d^2k_{\parallel}, \tag{6.87}$$

where

$$\psi_{sc}^{(0)}(\vec{k}, \vec{r}) = \rho(k_y)e^{-2ik_y}\psi_{in}(\vec{k}, \vec{r}) = \rho(p_y)\psi_0(\vec{p}_{\parallel})e^{i\vec{p}\cdot\vec{r}}, \tag{6.88}$$

where $\vec{p}_{\parallel} = \vec{k}_{\parallel}$ and $p_y = -k_y$. The first term of equation (6.74) ($y \geq 0$) is ignored as it does not contribute to the mutual coherence function at the detector position.

Using the Green function derived in the previous section and the undisturbed scattered-wave function (in the sample), equation (6.73) in the far zone reduces to:

$$\psi_{sc}^{(1)}(\vec{k}, \vec{r}) = -\frac{2m}{\hbar^2} \int \psi_0(\vec{k}_{\parallel}) \frac{e^{i\vec{p}\cdot\vec{r}} e^{-i\vec{Q}_{\parallel}\cdot\vec{r}_s}}{4\pi \left|\vec{r} - \vec{r}_s\right|} \Psi_k(y_s)\Psi_p(y_s)V^{(1)}(\vec{r}_s)d^3r_s, \tag{6.89}$$

where $\vec{Q}_{\parallel}$ is the wavevector transfer parallel to the surface defined as $\vec{Q}_{\parallel} = \vec{p}_{\parallel} - \vec{k}_{\parallel}$.

6.4.5 Scattered mutual coherence function

The scattered-wave function (equation (6.87)) can be inserted in the definition of the mutual coherence function (equation (2.6)) to find the scattered mutual coherence function, which splits up into four parts:

$$\Gamma_{sc}(\vec{r}_1,\vec{r}_2,\tau)=\Gamma_{sc}^{(0,0)}(\vec{r}_1,\vec{r}_2,\tau)+\Gamma_{sc}^{(1,0)}(\vec{r}_1,\vec{r}_2,\tau)+\Gamma_{sc}^{(0,1)}(\vec{r}_1,\vec{r}_2,\tau)+\Gamma_{sc}^{(1,1)}(\vec{r}_1,\vec{r}_2,\tau), \tag{6.90}$$

where

$$\Gamma_{sc}^{(a,b)}(\vec{r}_1,\vec{r}_2,\tau)=e^{-i\omega_k\tau}\int\int\left\langle\psi_{sc}^{(a)}(\vec{k}_1,\vec{r}_1)^*\psi_{sc}^{(b)}(\vec{k}_2,\vec{r}_2)\right\rangle d^2k_{1,\parallel}d^2k_{2,\parallel} \tag{6.91}$$

and indexes a and b have values 1 or 0.

The part with index $(0,0)$ represents the mutual coherence function due to scattering from the undisturbed potential, $V^{(0)}$. The derivation of this part is given in section 6.2.2 or appendix C. The parts with indexes $(1,0)$ and $(0,1)$ represent the interference terms between both wave functions. The part with index $(1,1)$ represents the mutual coherence function of the scattering due to the rough or structured potential $V^{(1)}(\vec{r})$.

If $\psi_{sc}^{(a)}$ and $\psi_{sc}^{(b)}$ are inserted in the above equation the ensemble average can be put inside the integrals resulting in a factor $\left\langle\psi_0(\vec{k}_\parallel)^*\psi_0(\vec{k}_\parallel)\right\rangle$. As shown in appendix C this factor can be calculated by means of the incident mutual coherence function. If the incident mutual coherence function is homogeneous, the wavevector distribution $W_{in}(\vec{r}_s,\vec{k}_\parallel)$ as defined in equation (C.7) can be used for $\left\langle\psi_0(\vec{k}_\parallel)^*\psi_0(\vec{k}_\parallel)\right\rangle$.

Another term that occurs when evaluating the $(1,1)$ term is the product of two Green functions, each depending on its own vector $\vec{p}$. According to its definition $\vec{p}$ is dependent on $\vec{r}_s$, which is different for both wave functions in equation (C.4). However, vector $\vec{p}$ of one wave function can be approximated by vector $\vec{p}$ of the other as long as the sample correlation length is much smaller than $\sqrt{r_{ds}/k}$ (≈ 6 μm for a detector distance of 1 m and a wavelength of 0.2 nm). This is just the same effect as discussed in section 6.1.2.

Using these approximations it can be shown that (neglecting the far-zone interference between incident and scattered beam):

$$\Gamma_{sc}^{(1,1)}(\vec{r}_d,\vec{r}_d+\vec{r},\tau)=\int\int\int\frac{e^{i(\vec{p}\cdot\vec{r}-\vec{Q}_\parallel\cdot\vec{s}-\omega_k\tau)}W_{in}(\vec{r}_s,\vec{k}_\parallel)}{4\pi^2r_{ds}^2}\Xi(\vec{s},\vec{r}_s)d^3sd^3r_sd^2k_\parallel, \tag{6.92}$$

where

$$\Xi(\vec{s},\vec{r}_s)=\Psi_k(y_s+s_y)\Psi_k(y_s)^*\Psi_p(y_s+s_y)\Psi_p(y_s)^*\left(\frac{m}{2\pi\hbar^2}\right)^2V^{(1)}(\vec{r}_s)^*V^{(1)}(\vec{r}_s+\vec{s}). \tag{6.93}$$

If the sample size is much smaller than the distance between sample and detector r_{ds} and $W_{in}(\vec{r}_s,\vec{k}_\parallel)$ can be taken constant over the sample volume and the scattered mutual coherence function reduces to:

$$\Gamma_{sc}(\vec{r}_d,\vec{r}_d+\vec{r},\tau)=\frac{e^{i(\vec{p}\cdot\vec{r}-\omega_k\tau)}}{4\pi^2r_{ds}^2}\int W_{in}(\vec{r}_s,\vec{k}_\parallel)S_k(\vec{p},\vec{k})d^2k_\parallel, \tag{6.94}$$

where the *sample surface structure factor* is defined as:

$$S_k(\vec{p},\vec{k}) = \int e^{-i\vec{Q}_\parallel\cdot\vec{r}_\parallel} G_s(\vec{p},\vec{k},\vec{r}) d^2 r_\parallel \tag{6.95}$$

and the *sample correlation function* consists of 4 parts (see also appendix D):

$$G_s^{(0,0)}(\vec{p},\vec{k},\vec{r}) = \frac{R(k_y)p_y^2 A_s}{4\pi^2}, \tag{6.96}$$

$$G_s^{(1,0)}(\vec{p},\vec{k},\vec{r}) = \left(\frac{m}{2\pi\hbar^2}\right)^2 V_0 \frac{\tau(p_y)^2}{2ip_y} \int \Psi_p(y_s)^* \Psi_k(y_s)^* V^{(1)}(\vec{r}_s)^* d^3 r_s, \tag{6.97}$$

$$G_s^{(0,1)}(\vec{p},\vec{k},\vec{r}) = G_s^{(1,0)}(\vec{p},\vec{k},\vec{r})^* \tag{6.98}$$

and

$$G_s^{(1,1)}(\vec{p},\vec{k},\vec{r}_\parallel) = \left(\frac{m}{2\pi\hbar^2}\right)^2 \times \tag{6.99}$$

$$\int\int \Psi_p(y_s)^* \Psi_k(y_s)^* \Psi_p(y_s+y) \Psi_k(y_s+y) V^{(1)}(\vec{r}_s)^* V^{(1)}(\vec{r}_s+\vec{r}_\parallel) d^3 r_s dy.$$

If the sample size can not be neglected but the extension of the sample correlation function is much smaller than the distance between sample and detector, the integral over the sample volume can be split up in parts. For each part the above approximation holds and all the parts are added resulting in:

$$\Gamma_{sc}(\vec{r}_d,\vec{r}_d+\vec{r},\tau) = \frac{1}{A_s}\int_{A_s} \frac{e^{i(\vec{p}\cdot\vec{r}-\omega_k\tau)}}{4\pi^2 r_{ds}^2} \int W_{in}(\vec{r}_s,\vec{k}_\parallel) S_k(\vec{p},\vec{k}) d^2 k_\parallel d^2 r_s, \tag{6.100}$$

where the summation over the parts is transformed back into an integral.

All information about the sample is contained in the sample correlation functions $G_s^{(a,b)}$. $G_s^{(0,0)}$ represents the sample correlation function of the flat surface. $G_s^{(1,0)}$ and $G_s^{(0,1)}$ represent the correlation between the flat surface and the surface structure. $G_s^{(1,1)}$ represents the correlations in the surface structure. Note that $G_s^{(1,1)}$ is determined by three factors: the incident-wave function (represented by Ψ_k), the undisturbed scattered-wave function (Ψ_p) and the sample structure potential ($V^{(1)}$).

To determine this function Steyerl [43] assumed that both Green function and undisturbed scattered-wave function could be approximated for all y_s by their expressions for $y_s = 0$, which is only reasonable if $p_y\sigma \ll 1$ and $k_y\sigma \ll 1$, where σ is the standard deviation of the height distribution. Sinha et al. [40], Pynn [44] and others assumed that for diffuse scattering both Green function and undisturbed scattered-wave function could be approximated for all y_s by their analytic expressions for either $y_s < 0$ or $y_s \geq 0$. Since both functions and their derivatives are continuous at $y_s = 0$ this is a reasonable approximation as long as $k_c\sigma < 3$ [44]. Pynn and others assumed that this approximation would also hold for the specular component, while Sinha et al. used the full expression dividing the specular contribution up into four components.

Using the above approximation the sample correlation function becomes:

$$G_s^{(1,0)}(\vec{p},\vec{k},\vec{r}) = \left(\frac{m}{2\pi\hbar^2}\right)^2 \frac{T(k_y)T(p_y)}{2ip_y} V_0 \int e^{2i(p'_y)^* y_s} V^{(1)}(\vec{r}_s)^* d^3 r_s \tag{6.101}$$

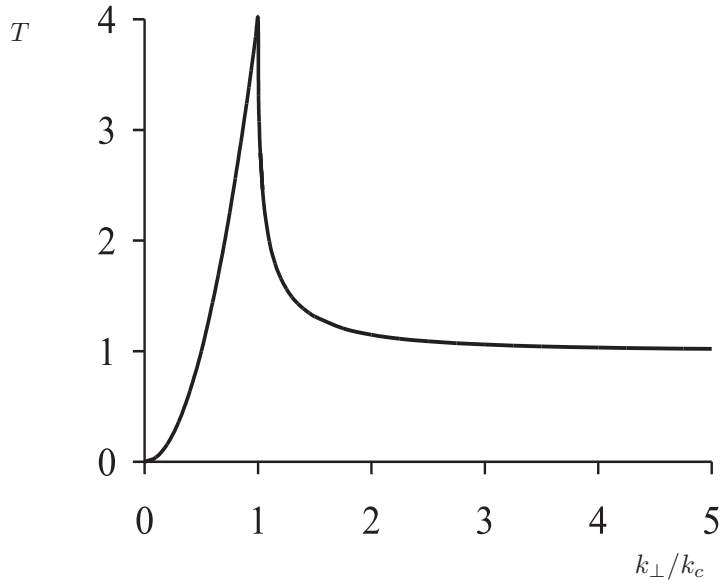

Figure 6.5: Transmission factor, T as function of the component of the wavevector perpendicular to the sample surface. k_c is the critical wavevector depending on the sample scattering length density, ρ_b ($k_c^2 = 4\pi\rho_b$).

and

$$G_s^{(1,1)}(\vec{p},\vec{k},\vec{r}_\parallel) = \left(\frac{m}{2\pi\hbar^2}\right)^2 T(k_y)T(p_y)\times \tag{6.102}$$
$$\int e^{i\kappa_y^* y}\int e^{i(\kappa_y^*-\kappa_y)y_s}V^{(1)}(\vec{r}_s)^* V^{(1)}(\vec{r}_s+\vec{r}_\parallel)d^3r_s dy,$$

where $\kappa_y = p'_y - k'_y$ equals the wavevector transfer inside the sample (remember that $\Re(k'_y) < 0$ and $\Re(p'_y) > 0$) and $T(k_y)$ and $T(p_y)$ are the transmission factors for the incident and reflected beam respectively, given in table 6.3. If κ_y is real the sample surface structure factor reduces to the product of $T(k_y)T(p_y)$ times the Fourier transform of the sample correlation function as given in equation (6.39), where $\vec{q} = \vec{Q}_\parallel - \kappa_y\vec{e}_y$. The factors $T(k_y)$ and $T(p_y)$ are shown in figure 6.5. The maxima are due to standing waves that build up at the surface at the critical angle. These result in so-called *Yoneda* peaks [49] in the diffuse scattering pattern.

6.4.6 Sample surface structure factor

The sample surface structure factor can be split up in a specular part and diffuse part in a similar way as introduced for the Fourier transform of the sample correlation function in section 6.3. It consists of four terms:

$$S_k(\vec{p},\vec{k}) = S_k^{(0,0)}(\vec{p},\vec{k}) + S_k^{(1,0)}(\vec{p},\vec{k}) + S_k^{(0,1)}(\vec{p},\vec{k}) + S_k^{(1,1)}(\vec{p},\vec{k}), \tag{6.103}$$

where the first term is the contribution due to the flat surface ($V^{(0)}(y_s)$):

$$S_k^{(0,0)}(\vec{p},\vec{k}) = R(p_y)p_y^2 A_s \delta^{(2)}(\vec{q}_\parallel) = \frac{A_s\pi^2\rho_b^2 T(k_y)^2}{p_y^2}\delta^{(2)}(\vec{q}_\parallel). \tag{6.104}$$

The two-dimensional Dirac-delta function indicates that this part of the sample surface structure factor only contributes to the specular reflection: $\vec{q}_\parallel = 0$, so $\vec{p}_\parallel = \vec{k}_\parallel$ and $p_y = -k_y$. The second and third terms are interference effects between the flat surface and surface structure and can be evaluated in the same way as before:

$$S_k^{(1,0)}(\vec{p},\vec{k}) = \frac{A_s\pi^2\rho_b^2 T(k_y)^2}{p_y(p_y')^*}\delta^{(2)}(\vec{q}_\parallel)\left(E[e^{2i(p_y')^* H(x,z)}] - 1\right), \tag{6.105}$$

where $E[x]$ is the expectation value of x. If p_y' is real and the surface structure is a Gaussian distributed roughness, the expectation value is given by equation (B.2): $e^{-2(p_y')^2\sigma^2}$. Further

$$S_k^{(0,1)}(\vec{p},\vec{k}) = S_k^{(1,0)}(\vec{p},\vec{k})^*. \tag{6.106}$$

Note that in the total reflection region (as long as $p_y \leq k_c$) p_y' is purely imaginary and the sum of $S_k^{(1,0)}$ and $S_k^{(0,1)}$ is 0. The last term is due to the structure of the surface:

$$S_k^{(1,1)}(\vec{p},\vec{k}) = -\frac{p_y^2}{|\kappa_y|^2}S_k^{(0,0)} - \frac{p_y}{p_y'}S_k^{(1,0)}(\vec{p},\vec{k}) - \frac{p_y}{(p_y')^*}S_k^{(0,1)}(\vec{p},\vec{k}) + \tag{6.107}$$

$$\rho_b^2 A_s \frac{T(k_y)T(p_y)}{|\kappa_y|^2}\int\int e^{-i(q_x x + q_z z)}E[e^{i\kappa_y^* H(x_s,z_s) - i\kappa_y H(x_s+x,z_s+z)}]dxdz.$$

If κ_y is real and the surface structure is a Gaussian distributed roughness, the expectation values are given by equation (B.3): $e^{-\kappa_y^2 g(x,z)/2}$ and if κ_y is complex the expectation value is given by [40], [50]:

$$E[e^{i\kappa_y^* H(x_s,z_s) - i\kappa_y H(x_s+x,z_s+z)}] = e^{-(\kappa_y-\kappa_y^*)^2\sigma^2/2}e^{-|\kappa_y|^2 g(x,z)/2} + O(\kappa_y^2\sigma^2). \tag{6.108}$$

Using equations (6.100) and (C.28) the neutron flux at the detector position becomes:

$$\vec{J}(\vec{r}_d,\vec{r}_d,0) = \frac{J_0}{2v_p 4\pi r_{ds}^2 r_{s0}^2}\int_{A_0} S_k(\vec{p},\vec{k})d^2r', \tag{6.109}$$

	Sinha et al. [40] De Boer [45]	Pynn [44]	Weber [46]
$\Psi_k(y)$	$\tau(k_y)e^{ik_y' y}$	$\tau(k_y)e^{ik_y' y}$	$\tau_r(k_y)e^{ik_y' y}$
$\Psi_p(y)$	$\tau(p_y)^* e^{ip_y' y}$	$\tau_r(p_y)^* e^{ip_y' y}$	$\tau_r(p_y)^* e^{ip_y' y}$
$T(k_y)$	$\tau(k_y)\tau(k_y)^*$	$\tau(k_y)\tau(k_y)^*$	$\tau_r(k_y)\tau_r(k_y)^*$
$T(p_y)$	$\tau(p_y)\tau(p_y)^*$	$\tau_r(p_y)\tau_r(p_y)^*$	$\tau_r(p_y)\tau_r(p_y)^*$

Table 6.3: Undisturbed scattering function, $\Psi_k(y)$, Green function $\Psi_p(y)$ and transmission factors, $T(p_y)$ and $T(p_y)$ for calculation of the diffuse sample surface structure factor from different references.

where $\vec{k} = \bar{k}(\vec{r}_{s0} - \vec{r'})/r_{s0}$. By using equation (2.44) the count rate in the detector becomes:

$$I_d = \frac{J_0}{4\pi r_{ds}^2 r_{s0}^2} \int_{A_d} \int_{A_0} S_k(\vec{p}, \vec{k}) d^2r' d^2r_d. \tag{6.110}$$

Assume, as before (equation (6.42)), the sample surface structure factor can be split in a specular and diffuse component:

$$S_k(\vec{p}, \vec{k}) = \rho_b^2 A_s \left(S_s(\vec{p}, \vec{k}) + S_d(\vec{p}, \vec{k}) \right), \tag{6.111}$$

then, the specular component is given by $p_y > k_c$:

$$S_s(\vec{p}, \vec{k}) = \frac{\pi^2 T(k_y)^2}{p_y^2} \left(1 + \frac{p_y}{p'_y} \left(e^{-2\Re(p'_y)^2\sigma^2} - 1 \right) \right)^2 \delta^{(2)}(\vec{q}_{\parallel}), \tag{6.112}$$

which reduces to the first factor only in case $p_y \leq k_c$ and the diffuse component by:

$$S_d(\vec{p}, \vec{k}) = \frac{T(k_y)T(p_y)e^{-\Re\left(\kappa_y^2\right)\sigma^2}}{|\kappa_y|^2} \int\int e^{-i(q_x x + q_z z)} \left(e^{|\kappa_y|^2 C(x,z)} - 1 \right) dxdz. \tag{6.113}$$

Note that these structure factors have essential the same form as the expressions derived using the Born approximation (section 6.3). They only differentiate via the factor $T(k_y)T(p_y)$ and the different wavevectors p'_y and κ_y used in the exponentials. For values $p_y \gg k_c$ the expressions become the same.

6.4.7 Specular count rate

The count rate due to the specular structure factor can be calculated by inserting it in equation (6.110):

$$I_d^s = \frac{J_0 A_s}{4\pi r_{s0}^2 \bar{k}^2} \int_{A_0} k_y^2 R_{DWBA}(k_y) d^2r', \tag{6.114}$$

where $\vec{k} = \bar{k}(\vec{r}_{s0} - \vec{r'})/r_{s0}$. For the specific geometry as discussed in section 6.1 this can be reduced to:

$$I_d^s = \frac{J_0 A_s W_z W_y}{4\pi r_{s0}^2} \frac{\int_{q-\Delta q}^{q+\Delta q} q^2 R_{DWBA}(q) dq}{\bar{k}^2 2\Delta q}, \tag{6.115}$$

where $q = \bar{k}H/r_1$ and $\Delta q = \bar{k}W_y/2r_1$, equal to equation (6.38). The specular reflectivity is given for the present case by:

$$R_{DWBA}(k_y) = R(k_y) \left(1 + \frac{p_y}{p'_y} \left(e^{-2\Re(p'_y)^2\sigma^2} - 1 \right) \right)^2. \tag{6.116}$$

This specular reflectivity was obtained by Sinha et al. [40] within the same accuracy as in the present case and can be reduced to ($k_y > k_c$):

$$R_{DWBA}(k_y) = R(k_y) \left(e^{-4k_y k'_y \sigma^2} + O(k_y (k'_y)^3 \sigma^4) \right), \tag{6.117}$$

equal to that given by Névot and Croce [51]. Approximately the same result can be obtained

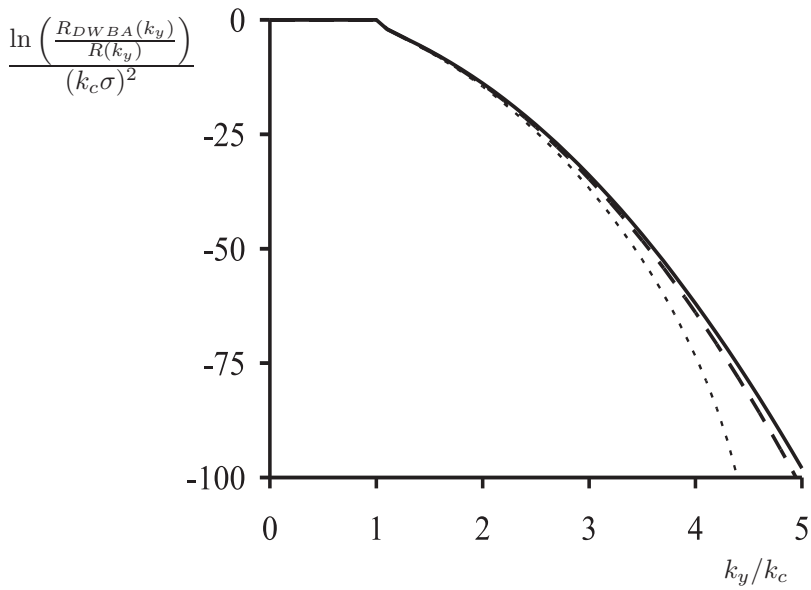

Figure 6.6: Ratio of reflectivity for several approximations. Full line: according to Sinha, Pynn and present text for $k_c\sigma \ll 1$; long-dashed line: present text $k_c\sigma = 0.2$; short-dashed line: present text $k_c\sigma = 0.3$.

with a graded interface where the profile of the index of reflection is the average over the xz-plane [38], [44], [2].

The difference between the above approximations for the specular reflectivity of a rough surface is shown in figure 6.6. In this figure $\ln(R_{DWBA}(k_y)/R(k_y))/(k_c\sigma)^2$ is plotted as function of k_y/k_c. In the same figure the specular reflectivity obtained by Sinha and Pynn is shown. Clearly there is some difference, however when $k_c\sigma < 0.3$ the difference between the two approximations can be neglected, more so for the region close to the critical edge at $k_y \approx k_c$. De Boer [45] introduces an approximation for R_{DWBA} that depends on the correlation length of the roughness. This correction however, is small and only of some importance at $k_y \approx> k_c$. For more accurate results, also the coherence length of the neutron beam should be incorporated in the above picture, viz by using equation (C.6) instead of (C.7) and equation (6.92) instead of (6.94). In general, this can only be done numerically. However, in view of the accuracy of the distorted wave born approximation (the difference between several versions of the distorted wave born approximation can not be neglected) in general this will not yield a more reliable interpretation of the experimental data.

6.4.8 Diffuse count rate

The count rate due to the diffuse structure factor can be calculated by inserting it in equation (6.110). If both the detector area and the source area are very small this reduces to:

$$I_d^d = \frac{J_0 A_0 A_d A_s \rho_b^2}{4\pi r_{ds}^2 r_{s0}^2} S_d(\vec{p}, \vec{k}), \tag{6.118}$$

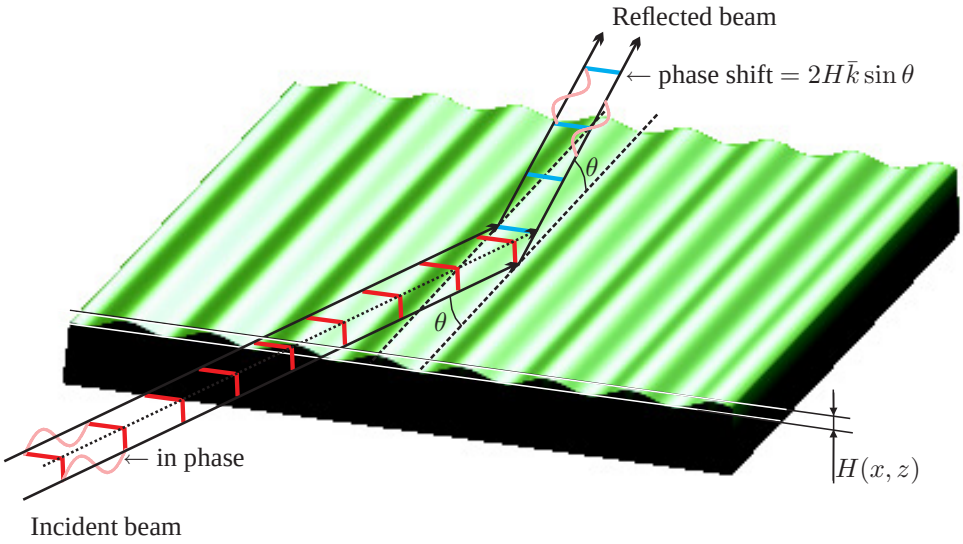

Figure 6.7: Model of grating with neutron beam parallel to grove direction of grating. The extra phase-shift acquired by the neutron wave function for a height difference of $H(x,z)$ is indicated in the figure.

comparable to equation (6.63) except for the enhancement factors $T(k_y)$ and $T(p_y)$.

This is the same as given by Sinha et al. [40], Pynn [44], De Boer [45] and others (see also table 6.3). Weber et al. [46] finds that this solution is not able to fit their data and argues that for the Green function the time reversed version of the solution of the rough surface should be taken, and for the undisturbed wave the solution itself. If this is done, their data can be fitted by the above theory. De Boer [45], [52] argues that it depends on the correlation length of the sample surface structure factor which solution one should actually take.

6.5 Phase-object approximation

The distorted wave born approximation is only valid for scattering at surfaces with a relatively small roughness or surface structure $k_y\sigma \ll 1$. If $k_y\sigma$ becomes of order one or larger this condition is no longer valid and the results of the previous section can no longer be applied. In that case one can try to calculate the intensity of the refracted or reflected beam by using the phase-object approximation as discussed here. In short it comes down to making an accurate enough estimate of the neutron wave function in and near the sample and use this estimate to calculate the scattered intensity (see also section 3.1). An example of such a sample is shown in figure 6.7. In this figure a Silicon grating is shown where the surface has been etched away, resulting in a variable height $H(x,z)$ of the surface.

Again, the estimate of the neutron wave function in the sample is based on the solution

of the one-dimensional Schrödinger equation for a smooth surface with a sharp or graded interface. However, now it is assumed that this interface varies in height as $H(x,z)$. The incident-wave function is the same as before. The scattering of the incident-wave function into the scattered-wave function is determined by an appropriate Green function and then the scattered mutual coherence function is established. For a surface with some roughness or structure the scattering potential $V(\vec{r})$ is given by:

$$V(\vec{r}) = \frac{\hbar^2 k_c^2}{2m} u(H(x,z) - y), \tag{6.119}$$

where $k_c^2 = 2mV_0/\hbar^2 = 4\pi\rho_b$. The Green function for scattered waves can be approximated by taking the Green function for scattered waves for the undisturbed potential at position (x,z) along the sample surface (see Appendix D):

$$G^{(+)}(\vec{r},\vec{r}_s) = \frac{1}{4\pi^2}\int_0^\infty e^{i\vec{p}\cdot(\vec{r}-\vec{r}_s)}\frac{1}{2ip_y}e^{ip_y(y_s-H(x_s,z_s))}\Psi_p(y_s - H(x_s,z_s))d^2p_\parallel, \tag{6.120}$$

where $\Psi_p(\vec{r})$ is the part of the Green function determined by the sample details. The scattered-wave function ψ_{sc} can be found using equation (3.4) inserting the above Green function and the incident-wave function given by equation (6.65):

$$\psi_{sc}(\vec{k},\vec{r}) = \psi_{in}(\vec{k},\vec{r}) - \frac{\rho_b\psi_0(\vec{k}_\parallel)}{\pi}\times \tag{6.121}$$

$$\int_0^\infty \frac{\tau(p_y)e^{i\vec{p}\cdot\vec{r}}}{2ip_y}\int e^{-i\vec{Q}_\parallel\cdot\vec{r}_{s,\parallel}}e^{i(p'_y-p_y)H(x_s,z_s)}\int_{-\infty}^{H(x_s,z_s)} e^{i(k_y-p'_y)y_s}dy_s d^2r_{s,\parallel}d^2p_\parallel,$$

where $\vec{Q}_\parallel$ is the wavevector transfer parallel to the surface defined as $\vec{Q}_\parallel = \vec{p}_\parallel - \vec{k}_\parallel$. The integral over y_s can be performed assuming a little absorption so that the lower limit vanishes, yielding

$$\psi_{sc}(\vec{k},\vec{r}) = \psi_{in}(\vec{k},\vec{r}) + \tag{6.122}$$

$$\frac{\rho_b\psi_0(\vec{k}_\parallel)}{\pi}\int_0^\infty \frac{\tau(p_y)e^{i\vec{p}\cdot\vec{r}}}{2p_y(k_y-p'_y)}\int e^{-i\vec{Q}_\parallel\cdot\vec{r}_{s,\parallel}}e^{-iQ_yH(x_s,z_s)}d^2r_{s,\parallel}d^2p_\parallel,$$

where Q_y is the wavevector transfer perpendicular to the surface defined as $Q_y = p_y - k_y$. This wave function can be inserted in the definition of the mutual coherence function (equation (2.6)) to find the scattered mutual coherence function close to the sample surface. After neglecting the interference between the incident beam and the reflected / refracted beam and assuming the scattered mutual coherence function close to the sample surface is homogeneous, the wavevector distribution of the scattered mutual coherence function becomes (using equation (C.12)):

$$W_{sc}(\vec{r}_1,\vec{p}) = \frac{1}{p_y^2 A_s}\int W_{in}(\vec{r}_1,\vec{k}_\parallel)S_k(\vec{p},\vec{k})d^2k_\parallel, \tag{6.123}$$

where

$$S_k(\vec{p},\vec{k}) = \frac{p_y^2 A_s}{4\pi^2}R_{PO}(\vec{p},\vec{k})\int e^{-i\vec{Q}_\parallel\cdot\vec{r}_\parallel}E[e^{-iQ_y(H(x_s+x,z_s+z)-H(x_s,z_s))}]d^2r_\parallel, \tag{6.124}$$

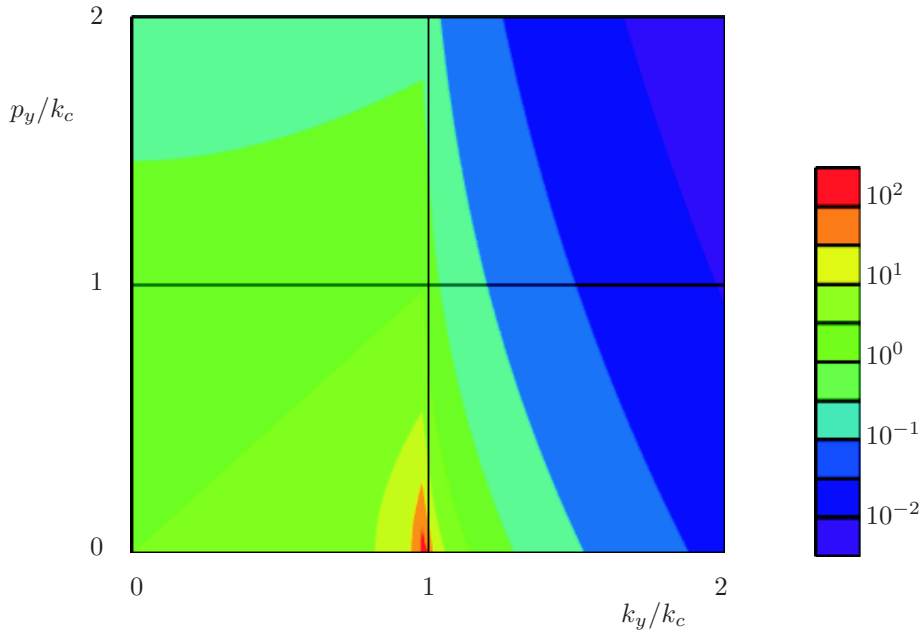

Figure 6.8: Phase-object enhancement coefficient as function of the reduced perpendicular component of the incident wavevector k_y/k_c and scattered wavevector p_y/k_c.

and

$$R_{PO}(\vec{p},\vec{k}) = \left|\frac{p_y - p'_y}{k_y - p'_y}\right|^2, \tag{6.125}$$

is the *phase-object enhancement coefficient* (see also figure 6.8).

For the specular part ($p_y = -k_y$) it is equal to the reflectivity of the flat sample surface. For $|k_y| \to 0$ and $|p_y| > |k_y|$ this factor goes to infinity, the total scattering however is limited as the neutron source area for $|k_y| \to 0$ also goes to 0. The sample surface structure factor is proportional to the two-dimensional Fourier transform of the expectation value of the relative phase shift acquired by a neutron wave function reflecting from the surface of the sample. This is shown schematically in figure 6.7. The count rate in the detector can be calculated by inserting this sample surface structure factor in equation (6.110).

6.6 Rough multi layers

Specular and diffuse scattering from rough multi layers can be described in the first Born approximation and in the distorted-wave Born approximation [53], [54], [55], [52]. As the Born approximation can be regarded as the small scattering limit of the (correct) distorted-wave Born approximation only this last approximation will be briefly discussed here.

The procedure for the distorted-wave Born approximation is essentially the same as for the single interface. First an estimate of the wave function in the sample and an appropriate Green function must be established. Then equation (6.73) can be applied to find the scattered-wave function. The final step is to use this scattered-wave function to create the mutual coherence function at the detector position and calculate the count rate in the detector. As before, most authors split the scattered intensity up in a specular part and a diffuse part. The result can be expressed in a form similar to equation (6.100), where the sample correlation function can be calculated analytically or numerically from the model used. Ψ_k, representing the incident beam, can be calculated using the matrix calculations or recursion relations as given in section 6.2.1. Ψ_p, representing the Green function, can be calculated in the same way, choosing either the time reversed solution (see section 6.4.3) or some other solution for the smooth interfaces, fit to be used for the problem at hand.

An important complication is the fact that the roughness for each interface in the multilayer *can* be correlated to the roughness of any other interface in the multilayer. To be able to calculate the effect of these types of correlations mostly some model for the correlation between the roughnesses is assumed. Because of these aspects the results are strongly dependent on the model used. In each specific case careful considerations must be made to avoid the use of wrong models or calculation methods.

Chapter 7

Spin echo neutron reflectometry

7.1 Introduction

Rekveldt was first to consider combining the neutron spin echo technique and reflectometry [56]. In the same way as in small angle neutron scattering (chapter 5) it is possible to use the precession of the neutron spin to code the angle of the neutron path through magnetic flux density regions. It is assumed that the magnetic flux density changes in such a way that within the (transversal) coherence length of the beam the magnetic flux density can be taken constant. Hence, beam splitting effects are ignored and the 2-shim neutron flux and 2-flip neutron flux are sufficient to fully describe the neutron flux and measured polarization (see section 4.7). Then, the influence of the magnetic flux density is described by means of its influence on the precession along the classical neutron path through the instrument.

To describe the neutron path in case of neutron reflectometry four angles are important: α_k, the angle between the path of the incident neutron (wavevector $\vec{k}$) and the sample surface and the same for the not-scattered or transmitted neutron. β_k, the angle the path of the incident neutron makes with the xy-plane. α_p the angle between the path of the off-specular scattered neutron (wavevector $\vec{p}$) and the sample surface and β_p the angle between the path of the off-specular scattered neutron and the xy-plane. These angles are schematically shown in figure 7.1. θ_s is the angle between the path of the off-specular scattered neutron and the path of the not-scattered neutron. Using these definitions, the wavevector of the incident neutron is represented by

$$\vec{k} = \bar{k} \begin{pmatrix} \cos\alpha_k \cos\beta_k \\ -\sin\alpha_k \\ \cos\alpha_k \sin\beta_k \end{pmatrix}, \tag{7.1}$$

and the wavevector of the scattered neutron by

$$\vec{p} = \bar{k} \begin{pmatrix} \cos\alpha_p \cos\beta_p \\ \sin\alpha_p \\ \cos\alpha_p \sin\beta_p \end{pmatrix}. \tag{7.2}$$

The polarization precession angle acquired by a neutron traveling through parallelogram shaped magnetic flux density regions is given by equations (5.1) and (5.2). The angle that

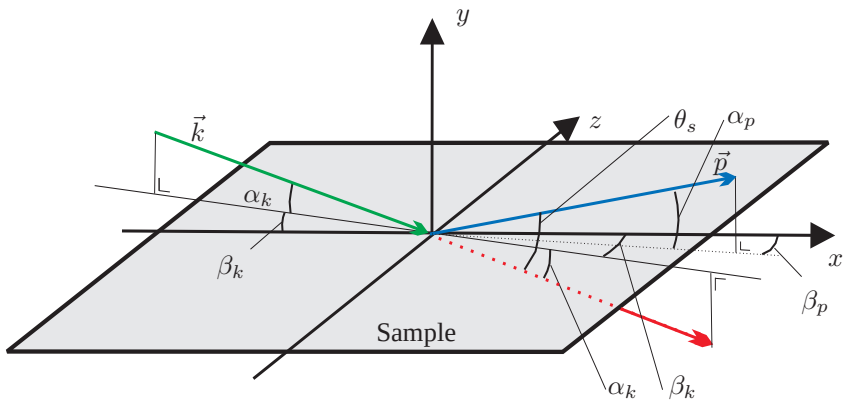

Figure 7.1: Definition of angles in spin echo neutron reflection geometry. α_k is the angle between the path of the incident neutron (represented by vector $\vec{k}$) and the sample surface and the same for the not-scattered or transmitted neutron. β_k is the angle the path of the incident neutron makes with the xy-plane. α_p the angle between the path of the off-specular scattered neutron (vector $\vec{p}$) and the sample surface and β_p is the angle between the path of the off-specular scattered neutron and the xy-plane. θ_s is the angle between the path of the off-specular scattered neutron and the path of the not-scattered neutron.

is coded by the precession angle (θ_I or θ_{II}) is the angle the neutron path makes with the x-axis in the plane of the parallelogram (see also figure 5.1). This angle can be adjusted by rotating the magnetic flux density regions around the beam direction. In figure 7.2 this is shown schematically. The angle of the neutron path can be coded to increase or decrease the precession angle by adjusting the sign of the magnetic flux density B_1 and/or B_2 (indicated by the color of the magnetic flux density region) or the inclination angles θ_1 and/or θ_2.

Figure 7.2 (A) shows the instrument if the coded angle before the sample is β_k and after the sample is either β_k or β_p depending on which neutron path is considered (the transmitted or the scattered one respectively). Here, for a not-scattered or specular reflected neutron the precession angle acquired in region I is exactly balanced by the one in region II, producing a perfect spin echo. If β_p is different from β_k by scattering in the z-direction this exact balance is canceled and a net precession angle remains. This enables the probing of the sample surface structure in the z direction.

Figure 7.2 (B) shows the instrument if the coded angle before the sample is α_k and after the sample is either α_k or α_p (the transmitted or the scattered one respectively). For the neutron path for which holds $\alpha_p = \alpha_k$ the precession angle acquired in region I is exactly balanced by the one in region II, producing a perfect spin echo. This is the case for the specular reflected neutron. Hence, it enables the possibility to separate (part of) the off-specular and specular reflection.

Figure 7.2 (C) shows the instrument if the coded angle before the sample is α_k and after the sample is either $-\alpha_k$ or $-\alpha_p$. For the neutron path for which holds $\alpha_p = -\alpha_k$ the precession angle acquired in region I is exactly balanced by the one in region II, producing a perfect spin echo. This is the case for the not-scattered or transmitted neutron. If α_p is different from $-\alpha_k$ by specular reflection the spin echo is canceled and a net precession angle remains, which for specular reflection is proportional to $2\alpha_k$. Hence, if the off-specular

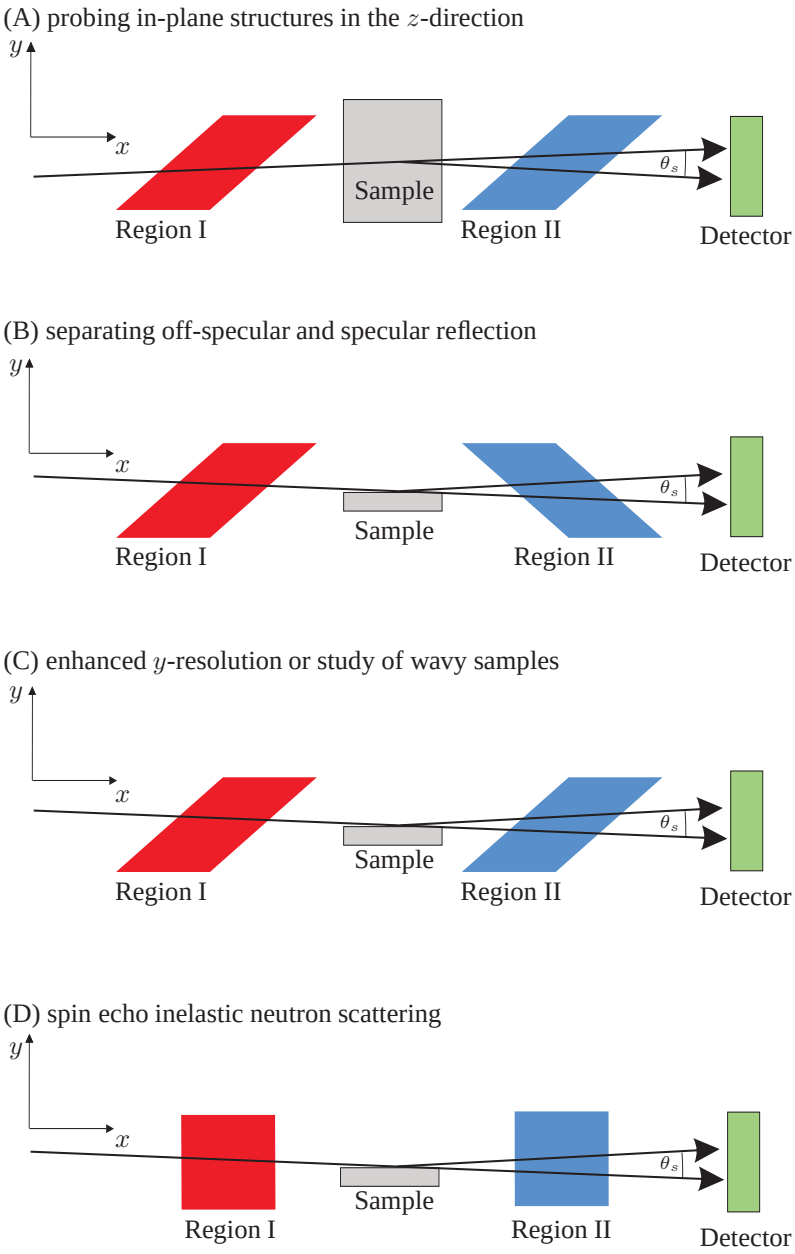

Figure 7.2: Principle of precession angle coding of a spin echo neutron reflectometer. (A) coding angle β_k before the sample and β_k or β_p after the sample; (B) coding angle α_k before the sample and α_k or α_p after the sample; (C) coding angle α_k before the sample and $-\alpha_k$ or $-\alpha_p$ after the sample; (D) coding the wavelength before and after the sample. See also figure 7.1. Region I has a magnetic flux density directed to the reader and region II a direction from the reader.

reflection can be neglected the y-resolution can be enhanced or one can study wavy samples without loss of resolution or intensity.

Figure 7.2 (D) shows the instrument if the precession angle is independent of the angle of the path through the regions, but only depends on the wavelength of the neutrons. This can be realized by making the inclination angles θ_1 and θ_2 equal to $\pi/2$. A perfect spin echo is produced if the precession angle acquired in region I is exactly balanced by the one in region II. Hence, if the wavelength of the neutron is not changed in the reflection or scattering process producing. If the wavelength is changed by a non-elastic scattering process, a net precession angle remains, which is proportional to the change in wavelength. This is the standard spin echo technique as introduced by Mezei in the 1970's [32]. In the following section the above instrument options A to C will be discussed in more detail.

7.2 In-plane structures

The in-plane structure of the sample can be determined by means of off-specular reflection as was discussed in the previous chapter. Then, the sample surface structure factor is determined from the measurement of the neutron count rate at the relevant detector positions. As all direct scattering techniques this is done in momentum transfer-space or Q-space. Using the spin echo technique this is converted to real-space by an appropriate Fourier transform using the precession angle coding of the momentum transfer. This was first experimentally tested by Felcher et al. [57] in 2002 and repeated in 2003 [58].

As only elastic scattering is addressed here, the momentum transfer is completely determined by the scattering angle θ_s, or the difference between α_k and α_p and between β_k and β_p. These are the angles which can be encoded by an appropriate choice of the alignment of the precession regions I and II. It is assumed that the coherence matrix can be split up in the mutual coherence function of the wave function when all magnetic flux densities were turned off, $\Gamma_0(\vec{r}_1, \vec{r}_2, \tau)$ and the reduced coherence matrix $\widehat{\gamma}_B(\vec{r}_1, \vec{r}_2, \tau)$ as defined in section 4.2:

$$\widehat{\Gamma}(\vec{r}_1, \vec{r}_2, \tau) = \Gamma_0(\vec{r}_1, \vec{r}_2, \tau)\widehat{\gamma}_B(\vec{r}_1, \vec{r}_2, \tau). \tag{7.3}$$

The propagation of the mutual coherence function, Γ_0 is discussed in the previous chapter and given by equation (6.94). Again, if the sample dimensions can not be neglected the sample should be split up in several smaller samples (each much larger than the coherence length) and the resulting mutual coherence function is the (incoherent) sum of all separate contributions. Under the conditions as discussed in the introduction of this chapter the propagation of the reduced coherence matrix is given by

$$\widehat{\gamma}_B(\vec{r}_1, \vec{r}_2, \tau) = \widehat{D}(\vec{r}_2, \vec{r_2'})\widehat{\gamma}_B(\vec{r_1'}, \vec{r_2'}, \tau)\widehat{D}(\vec{r}_1, \vec{r_1'})^\dagger, \tag{7.4}$$

the same form as equations (4.23) and (4.25), where the matrices $\widehat{D}$ are defined in equation (4.28) and describe the magnetic flux density interaction with the neutron wave function traveling from $\vec{r_1'}$ or $\vec{r_2'}$ on the neutron source to $\vec{r}_1$ or $\vec{r}_2$ on the detector via the sample surface. For a completely unpolarized neutron source the matrix $\widehat{\gamma}_B(\vec{r_1'}, \vec{r_2'}, \tau)$ reduces to $\widehat{I}/2$. As in section 5.1 the device matrix between polarizer and flipper for the spin echo instrument is given by:

$$\widehat{E}(\vec{r}, \vec{r'}) = \widehat{R}(\vec{r'}, \vec{r})^\dagger \widehat{T}_z(\phi_{II}(\vec{p}))\widehat{T}_z(\phi_I(\vec{k}))\widehat{R}(\vec{r'}, \vec{r}), \tag{7.5}$$

where $\widehat{R}(\vec{r'},\vec{r})$ is the device matrix of the rotator before region I and $\widehat{R}(\vec{r'},\vec{r})^\dagger$ the same for the rotator after region II and

$$\phi_I(\vec{k}) = -c\bar{\lambda}B_1L_1(1-\beta_k\tan\theta_1) \tag{7.6}$$

and

$$\phi_{II}(\vec{p}) = -c\bar{\lambda}B_2L_2(1-\beta_p\tan\theta_2). \tag{7.7}$$

If the sample scatters non-magnetic, $\theta_1 = \theta_2$ and $B_1L_1 = -B_2L_2$ the device matrix for region I, the sample and region II is just $\widehat{T}_z(\vec{l}_{se}\cdot\vec{q}_{se})$, where $\vec{q}_{se} = \vec{p}-\vec{k}$ is the wavevector transfer at the sample position, the direction of $\vec{l}_{se}$ is the coding direction (here $\vec{e}_z$) and $l_{se} = c\bar{\lambda}^2B_1L_1\tan\theta_1/2\pi$ is called the *spin echo length*. The polarizing factor of $\widehat{E}(\vec{r},\vec{r'})$ is:

$$P_E(\vec{r},\vec{r'}) = (1-P_R^2(\vec{r'},\vec{r}))\cos\left\{\vec{l}_{se}\cdot\vec{q}_{se}\right\} + P_R^2(\vec{r'},\vec{r}), \tag{7.8}$$

where P_R is the polarizing factor of $\widehat{R}(\vec{r'},\vec{r})$. For a perfect spin echo instrument the factor before the cosine must be maximal and the other term minimal, hence $P_R = 0$. The complete device matrix is found by including the polarizer, flipper and analyser:

$$\widehat{D}(\vec{r},\vec{r'}) = \widehat{D}_A(\vec{r},\vec{r'})\widehat{F}(\vec{r},\vec{r'})\widehat{E}(\vec{r},\vec{r'})\widehat{D}_P(\vec{r},\vec{r'}), \tag{7.9}$$

where $\widehat{D}_P$ corresponds to the device matrix of the polarizer, $\widehat{D}_A$ of the analyser (see equation (4.37)) and $\widehat{F}$ of the flipper just before the analyser (see also section 4.7). In the following it is assumed that these device matrices are constant. Hence $\widehat{D}$ only depends on $\vec{p}-\vec{k}$. The detector count rate can be found by integrating equation (4.9) over the detector area:

$$I_d = 2v_p\int_{A_d}\mathrm{Tr}(\widehat{\Gamma}(\vec{r}_d,\vec{r}_d,0))d^2r_d, \tag{7.10}$$

where A_d is the detector area perpendicular to $\vec{v}_p$ and assumed large enough to capture all scattered or reflected neutrons. Inserting equations (7.3), (7.4), (7.9), (6.94) and (C.28) this yields for a completely homogeneous, incoherent and unpolarized source with area A_0:

$$I_d = \int_{A_d}\int_{A_0}\frac{J_0}{4\pi r_{ds}^2r_{s0}^2}S_k(\vec{p},\vec{k})\Omega_d(\vec{p}-\vec{k})d^2r'd^2r_d, \tag{7.11}$$

where

$$\Omega_d(\vec{p}-\vec{k}) = \frac{1}{2}\mathrm{Tr}\left(\widehat{D}(\vec{p}-\vec{k})\widehat{D}(\vec{p}-\vec{k})^\dagger\right) \tag{7.12}$$

and $\vec{k} = \bar{k}(\vec{r}_{s0}-\vec{r'})/r_{s0}$, $\vec{p} = \bar{k}(\vec{r}_d-\vec{r}_{s0})/r_{ds}$ and $\vec{r'}$ is the source position. Again, if the sample dimensions can not be neglected the sample should be split up in several smaller parts (each much larger than the coherence length) and the resulting detector count rate is the sum of all separate contributions, yielding:

$$I_d = \int_{A_d}\int_{A_0}\int_{A_s}\frac{J_0}{4\pi r_{ds}^2r_{s0}^2A_s}S_k(\vec{p},\vec{k})\Omega_d(\vec{p}-\vec{k})d^2r_sd^2r'd^2r_d. \tag{7.13}$$

The 2-shim count rate can be determined by replacing Ω_d in the above equation by $T_PT_A/4$ where T_P and T_A are the transmissions of polarizer and analyser respectively:

$$I_s = \frac{T_PT_A}{4}\int_{A_d}\int_{A_0}\int_{A_s}\frac{J_0}{4\pi r_{ds}^2r_{s0}^2A_s}S_k(\vec{p},\vec{k})d^2r_sd^2r'd^2r_d. \tag{7.14}$$

The 2-flip count rate is found by replacing Ω_d by $T_P T_A P_P P_A P_E(\vec{p}-\vec{k})/4$, yielding:

$$I_f = \frac{T_P T_A P_P P_A}{4} \int_{A_d}\int_{A_0}\int_{A_s} \frac{J_0}{4\pi r_{ds}^2 r_{s0}^2 A_s} S_k(\vec{p},\vec{k}) P_E(\vec{p}-\vec{k}) d^2r_s d^2r' d^2r_d. \quad (7.15)$$

The integral over the detector area can be transformed to an integral over p_y and p_z and the integral over the source area can be transformed to an integral over k_y and k_z:

$$I_f = \frac{T_P T_A P_P P_A}{4} \frac{J_0}{A_s 4\pi \bar{k}^4} \int_{A_s}\int_{k_y}\int_{k_z}\int_{p_y}\int_{p_z} S_k(\vec{p},\vec{k}) P_E(\vec{p}-\vec{k}) dp_z dp_y dk_z dk_y d^2r_s. \quad (7.16)$$

This integral can be evaluated by realizing that in the case considered P_E only depends on the difference $p_z - k_z$. Further, the sample surface structure factor only depends on $\vec{p}-\vec{k}$ and k_y and p_y. If the detector is wide enough the integral over p_z goes from $-\infty$ to $+\infty$ and can be replaced by an integral over $Q_z = p_z - k_z$ and the same range:

$$I_f = \frac{T_P T_A P_P P_A}{4} \frac{J_0}{A_s 4\pi \bar{k}^4} \int_{A_s}\int_{k_z} dk_z \int_{Q_z} \left\{ \int_{p_y}\int_{k_y} S_k(\vec{p},\vec{k}) dk_y dp_y \right\} P_E(Q_z) dQ_z d^2r_s, \quad (7.17)$$

Furthermore, if it is assumed that the distances r_{s0} and r_{ds} are large compared to the sample, source and detector dimensions, then the argument of the integral over the sample surface is constant and the above equation is reduced to:

$$I_f = \frac{T_P T_A P_P P_A}{4} \frac{J_0}{4\pi \bar{k}^4} \int_{k_z} dk_z \int_{Q_z} \left\{ \int_{p_y}\int_{k_y} S_k(\vec{p},\vec{k}) dk_y dp_y \right\} P_E(Q_z) dQ_z, \quad (7.18)$$

and the measured polarization becomes:

$$P_m = P_P P_A \frac{\int_{Q_z} \left\{ \int_{p_y}\int_{k_y} S_k(\vec{p},\vec{k}) dk_y dp_y \right\} P_E(Q_z) dQ_z}{\int_{Q_z} \left\{ \int_{p_y}\int_{k_y} S_k(\vec{p},\vec{k}) dk_y dp_y \right\} dQ_z}. \quad (7.19)$$

The factor $P_E(Q_z)$ is given by equation (7.8). In the ideal spin echo instrument $P_R = 0$ and the integral over Q_z represents a cosine transform (or the real part of a Fourier transform) of the sample surface structure factor, hence the above equation becomes:

$$P_m = P_P P_A \frac{G_r(l_{se})}{G_r(0)}, \quad (7.20)$$

where

$$G_r(l_{se}) = \Re\left(\int_{Q_z} \left\{ \int_{p_y}\int_{k_y} S_k(\vec{p},\vec{k}) dk_y dp_y \right\} e^{i l_{se} Q_z} dQ_z \right), \quad (7.21)$$

comparable to equation (5.27). $G_r(r)$ is a one dimensional sample correlation function. For standard neutron reflection geometry (see figure 6.1) the range of integration of k_y is determined by position H and the width W_y of the entrance diaphragm and the range of integration of p_y by position H_d and the width D_y of the diaphragm before the detector. In general these ranges are quite small and the integration over k_y and p_y can be interpreted as a resolution effect.

One should realize that the validity of this last equation depends on several conditions, which were mentioned during its derivation. The most important ones are the quality of the spin echo instrument, which determines $P_E(Q_z)$ and the small size of the sample compared to the distance between sample and source and sample and detector. In (spin echo) small angle neutrons scattering instruments this condition is almost always met. For neutron reflectometers large sample sizes are more common. In case were the sample size is too large deviations might occur and one should use equation (7.13) instead. Another important condition is that the sample correlation length that is probed (l_{se}) is smaller than $\sqrt{r_{ds}/\bar{k}}$. Otherwise the equations used to calculate the scattered coherence function should be calculated using its definition and equation (6.89) for the scattered-wave functions, without neglecting the differences between the two vectors $\vec{p}$. Finally, the magnetic flux density should be homogeneous over the probed length, otherwise the way the coherence matrix propagates is not accurately described by equation (7.4). In that case no analytical solution has been found for the propagation of the mutual coherence matrix or (which is the same) polarization of the neutron beam.

If the sample surface structure factor can be calculated by means of the phase-object approximation (see section 6.5) the one dimensional sample correlation function becomes:

$$G_r(l_{se}) = \int_{p_y}\int_{k_y} \frac{p_y^2 A_s}{2\pi} R_{PO}(\vec{p},\vec{k}) G_r'(l_{se}) dk_y dp_y, \tag{7.22}$$

where

$$G_r'(l_{se}) = \Re\left(\int E[e^{-iQ_y(H(x_s+x,z_s+l_{se})-H(x_s,z_s))}]dx\right) \tag{7.23}$$

and it was assumed that $Q_x \approx 0$. Ignoring resolution effects the measured polarization reduces to:

$$P_m = P_P P_A \frac{G_r'(l_{se})}{G_r'(0)}, \tag{7.24}$$

Plomp et al. [59] used this formula to describe his measurements on a grating (the same as of Felcher et al. and Major et al. [57], [58]), explaining both theirs and his results.

7.3 Separating off-specular and specular reflection

It was first realized by Pynn et al. [60] that the specular reflected part could be separated from the off-specular part by changing the coded angle to α_k and $-\alpha_p$ as shown in figure 7.2 (B). Then it is possible to separate the neutrons that are reflected in the specular direction ($\alpha_p = -\alpha_k$) from the neutrons that are reflected or scattered in the diffuse or off-specular direction. If the sample scatters non-magnetic, $\theta_1 = -\theta_2$ and $B_1 L_1 = -B_2 L_2$ the device matrix for region I, the sample and region II is just $\widehat{T}_z(l_{se}(p_y+k_y))$, where p_y and k_y are the components perpendicular to the sample surface of the wavevector of the incident respectively the scattered-wave function. Again $l_{se} = c\bar{\lambda}^2 B_1 L_1 \tan\theta_1/2\pi$ is the spin echo length. Equations (7.14) and (7.16) are still valid because up to this point in the derivation in the previous section no assumptions were made for the coding direction. Now equation (7.16) can be evaluated by realizing that in the case considered P_E only depends on $k_y + p_y$:

$$I_f = \frac{T_P T_A P_P P_A}{4} \frac{J_0}{A_s 4\pi \bar{k}^4} \int_{A_s}\int_{k_y}\int_{p_y}\int_{k_z}\int_{p_z} S_k(\vec{p},\vec{k}) dp_z dk_z P_E(p_y+k_y) dp_y dk_y d^2 r_s. \tag{7.25}$$

If the sample size is small compared to detector-sample and source-sample distances this becomes:

$$I_f = \frac{T_P T_A P_P P_A}{4} \frac{J_0}{4\pi \bar{k}^4} \int_{k_y} \int_{p_y} \int_{k_z} \int_{p_z} S_k(\vec{p}, \vec{k}) dp_z dk_z P_E(p_y + k_y) dp_y dk_y. \quad (7.26)$$

Assume as before (equation (6.42)), the sample surface structure factor can be split in a specular and diffuse component, which are given by equations (6.112) and (6.113), then the specular part becomes:

$$I_f^s = \frac{T_P T_A P_P P_A}{4} \frac{J_0 \rho_b^2 A_s}{4\pi \bar{k}^4} \int_{k_y} \int_{p_y} \int_{k_z} \int_{p_z} S_s(\vec{p}, \vec{k}) dp_z dk_z dp_y dk_y \quad (7.27)$$

where it was used that for the specular part $p_y = -k_y$. Note that this part does not depend on the spin-echo length. The diffuse part becomes:

$$I_f^d = \frac{T_P T_A P_P P_A}{4} \frac{J_0 \rho_b^2 A_s}{4\pi \bar{k}^4} \int_{k_y} \int_{p_y} \int_{k_z} \int_{p_z} S_d(\vec{p}, \vec{k}) dp_z dk_z P_E(p_y + k_y) dp_y dk_y. \quad (7.28)$$

Hence, if now the spin-echo length is varied, the specular part is constant and the diffuse part changes according to the above equation. This enables the determination of the specular and diffuse part separately.

As an example, if the diffuse part varies slowly and the p_y and k_y range is limited, the diffuse part can be taken constant and the above equation for the diffuse part becomes:

$$I_f^d \approx Z \frac{T_P T_A P_P P_A}{4} \frac{J_0 \rho_b^2 A_s}{4\pi \bar{k}^4} \int_{k_z} \int_{p_z} S_d(\vec{p}, \vec{k}) dp_z dk_z, \quad (7.29)$$

where

$$Z = \int_{k_{min}}^{k_{max}} \int_{p_{min}}^{p_{max}} P_E(p_y + k_y) dp_y dk_y, \quad (7.30)$$

is determined by the instrument properties only. If P_E is given by equation (7.8) and $P_R(\vec{r'}, \vec{r})$ is taken constant, this becomes:

$$Z = P_R^2 \Delta k_y \Delta p_y + \frac{1 - P_R^2}{l_{se}^2} 4 \sin\left(l_{se} \frac{\Delta k_y}{2}\right) \sin\left(l_{se} \frac{\Delta p_y}{2}\right) \cos\left(l_{se}(\bar{k}_y + \bar{p}_y)\right), \quad (7.31)$$

where $\Delta k_y = k_{max} - k_{min}$, $\Delta p_y = p_{max} - p_{min}$, $\bar{k}_y = (k_{max} + k_{min})/2$ and $\bar{p}_y = (p_{max} + p_{min})/2$. Hence, if the spin-echo length is 0 then $Z = 1$ and when it is large enough ($l_{se} \gg \Delta k_y, \Delta p_y$), Z reduces to the first term, which for an ideal spin echo instrument is 0. Hence, the diffuse part averages to zero and the true specular part remains.

7.4 Enhanced resolution or wavy samples

Rekveldt [16] showed that by changing the coded angle to α_k and α_p as shown in figure 7.2 (C) it is possible to increase the resolution of the measurement of the specular reflectivity without reducing the intensity of the neutron beam. If the sample scatters non-magnetic, $\theta_1 = \theta_2$ and $B_1 L_1 = -B_2 L_2$ the device matrix for region I, the sample and region II is

just $\widehat{T}_z(l_{se}(p_y - k_y))$, where p_y and k_y are the components perpendicular to the sample surface of the wavevector of the incident respectively the scattered-wave function. Again $l_{se} = c\bar{\lambda}^2 B_1 L_1 \tan\theta_1/2\pi$ is the spin echo length. Equations (7.14) and (7.16) are still valid because up to this point in the derivation in the previous section no assumptions were made for the coding direction. Now equation (7.16) can be evaluated by realizing that in the case considered here P_E only depends on $p_y - k_y$. Both the specular and the diffuse part can be accounted for.

Further, if the diffuse part is ignored this method can be used to increase the resolution without a loss in intensity. For the specular part ($p_y = -k_y$) equation (6.104) is used:

$$S_k^{(0,0)}(\vec{p},\vec{k}) = R(p_y)p_y^2 A_s \delta^{(2)}(\vec{q}_\parallel), \tag{7.32}$$

which inserted in equation (7.15) yields:

$$I_f = \frac{T_P T_A P_P P_A}{4} \int_{A_d}\int_{A_0}\int_{A_s} \frac{J_0}{4\pi r_{ds}^2 r_{s0}^2} R(k_y)k_y^2 \delta^{(2)}(\vec{p}_\parallel - \vec{k}_\parallel) P_E(2k_y) d^2r_s d^2r' d^2r_d, \tag{7.33}$$

where $\vec{k} = \bar{k}(\vec{r}_s - \vec{r'})/r_s$, $\vec{p} = \bar{k}(\vec{r}_d - \vec{r}_s)/r_{ds}$ and $\vec{r'}$ is the source position. If, again the sample size can be neglected compared to the sample-source distance, this reduces to:

$$I_f = \frac{T_P T_A P_P P_A}{4} \frac{J_0 A_s}{4\pi r_{ds}^2 r_{s0}^2} \int_{A_d}\int_{A_0} R(k_y)k_y^2 \delta^{(2)}(\vec{p}_\parallel - \vec{k}_\parallel) P_E(2k_y) d^2r' d^2r_d. \tag{7.34}$$

The two-dimensional Dirac-delta function $\delta^{(2)}(\vec{p}_\parallel - \vec{k}_\parallel)$ represents that only specular reflection is taken into account. Therefor it is possible to take both a large detector area and a large source area (entrance diaphragm). The above equation then reduces further to:

$$I_f = \frac{T_P T_A P_P P_A}{4} \frac{J_0 A_s \Delta k_z}{4\pi \bar{k}^4} \int_0^\infty R(k_y)k_y^2 P_E(2k_y) dk_y, \tag{7.35}$$

where Δk_z is determined by the width of the entrance diaphragm ($\bar{k}W_z/r_s$) or the width of the detector diaphragm ($\bar{k}W_d/r_s$) or both. The function $P_E(2k_y)$ in the ideal case is $\cos(2k_y l_{se})$ so that the above formula represents the real part of the Fourier transform of $R(k_y)k_y^2$:

$$I_f(l_{se}) = \frac{T_P T_A P_P P_A}{4} \frac{J_0 A_s \Delta k_z}{4\pi \bar{k}^4} \int_0^\infty R(k_y)k_y^2 \cos(2l_{se}k_y) dk_y, \tag{7.36}$$

This Fourier transform can be back transformed to yield $R(q)$:

$$R(q) = \frac{1}{q^2} \frac{16\bar{k}^4}{T_P T_A P_P P_A J_0 A_s \Delta k_z} \int_0^\infty I_f(l_{se}) \cos(2l_{se}q) dl_{se}, \tag{7.37}$$

Hence, in principle it is possible to determine the reflectivity of the sample with an completely uncollimated beam.

However, practically a problem arises due to the properties of the back transform of the Fourier transformation. The spectrum $I_f(l_{se})$ is determined with a finite accuracy due to counting statistics. The law of error propagation for Fourier transforms roughly distributes the counting statistics evenly over the transformed spectrum. If the reflectivity changes from

1 to 10^{-3} in the interesting range this forces the statics for the whole measured spectrum to be better than 10^{-3}, which is rather impossible. This problem becomes even worse for larger reflectivity ranges. The solution for this problem is to limit the reflectivity range to be measured. This can be accomplished by either limiting the source area or the detector area. Then, the limits of the Fourier transform in the above equation do not extent from 0 to ∞ but from $q-\Delta q$ to $q+\Delta q$, where both q and Δq are determined by instrument parameters. For the geometry presented in chapter 6 and a source limiting situation $q = \bar{k}H/r_s$ and $\Delta q = \bar{k}W_y/2r_s$, while for a detector limiting situation $q = \bar{k}H_d/r_{ds}$ and $\Delta q = \bar{k}W_d/r_{ds}$:

$$I_f = \frac{T_P T_A P_P P_A}{4} \frac{J_0 A_s \Delta k_z}{4\pi \bar{k}^4} \int_{q-\Delta q}^{q+\Delta q} R(k_y) k_y^2 P_E(2k_y) dk_y, \tag{7.38}$$

which can be interpreted as the (real part) of the Fourier transform of $\tilde{R}(k_y)k_y^2$, where $\tilde{R}(k_y) = R(k_y)Res(k_y)$ where $Res(k_y)$ is a resolution function, in this case $Res(k_y) = u(k_y + q + \Delta q) - u(k_y - q - \Delta q)$ and $u(x)$ is the Heaviside step function: $u(x) = 1$ if $x \geq 0$ and $u(x) = 0$ if $x < 0$. If the sample is not perfectly flat but has a certain amount of waviness this can be translated into an adaptation of the resolution function. Further if the source is not exactly homogeneous or incoherent this results in a different resolution function also. The combination of all possible effects tends to Gaussian shaped resolution function.

In case a multi-detector or a position sensitive detector is used to determine the count rate I_f the above equation changes to:

$$I_f = \Sigma_i I_f^{(i)}, \tag{7.39}$$

where

$$I_f^{(i)} = \frac{T_P T_A P_P P_A}{4} \frac{J_0 A_s \Delta k_z}{4\pi \bar{k}^4} \int_{q_i}^{q_{i+1}} R(k_y) k_y^2 P_E(2k_y) dk_y \tag{7.40}$$

and the limits q_i are determined by the corresponding limits of the channel, i in which the counts are collected. For each channel the back Fourier transform can be done, resulting in:

$$R^{(i)}(q) = \frac{1}{q^2} \frac{16\bar{k}^4}{T_P T_A P_P P_A J_0 A_s \Delta k_z} \int_0^{\infty} I_f^{(i)}(l_{se}) \cos(2l_{se}q) dl_{se} \tag{7.41}$$

and all channels added together yield [16]:

$$R(q) = \Sigma_i R^{(i)}(q). \tag{7.42}$$

The advantage of this method is that in each channel the detector count rate due to low reflectivity is not blurred by the statistics of counts due to high reflectivity. Note that this method is independent of the actual values q_i and the scaling factor before the integral also does not depend on either i or q_i. Hence, all detector counts are used so that no intensity is lost and the division of the detector area in channels can be optimized for each experiment, depending on $R(q)$, the waviness of the sample and the available neutron counting statistics. A limitation of this method is that it should be possible to perform the back Fourier transform. Hence one should measure toward large spin-echo lengths (l_{se}) for the enhanced resolution and one might use an artificial filter to limit or reduce oscillations after the transform [61]. The wavevector transfer resolution will be of the order of $\pi/l_{se,max}$.

Chapter 8

Concluding remarks

It is possible to use coherence theory to describe propagation of neutrons through neutron scattering instruments. Coherence theory describes the propagation of the ensemble average of the neutron wave function. Coherence theory as adopted here, only considers neutron wave functions, having approximately an equal amount of total energy, denoted by *quasi-monochromatic* wave functions. This is due to the dispersion relation of matter-waves, and hence the interference between non-monochromatic wave functions, can in general be ignored.

One advantage using coherence theory over standard scattering theoretical considerations is the incorporation of instrumental and source effects. By means of coherence theory it is possible to accurately calculate scattered neutron intensities, given the full instrumental details. It was shown that in all scattering cases it is possible to retrieve the results as published in literature by introducing appropriate approximations. The introduced approximations are documented so one can asses when a particular approximation is valid and when it is not. Further it was shown that also neutron polarization effects can be described by using the coherence matrix approach. This enables understanding of beam splitting effects due to magnetic flux density variations and indicates when these effects will become really measurable in real neutrons scattering devices.

Another advantage of coherence theory is that in principle no conversion to *momentum space* (or q-space) is needed. All scattering phenomena can be described in *real space*. The Fourier transform to go from real space to momentum space and vice versa is contained in the propagation formula for the mutual coherence function or coherence matrix. This formula describes the propagation of the mutual coherence function through free space (vacuum or small interaction potential). It must be emphasized that scattering of neutrons is not incorporated in the coherence theory. It only deals with propagation of neutrons before interaction with an scattering object and after it.

Interaction with the object itself is described by means of the time-dependent Schrödinger equation for a (polarized) neutron wave function. Here, coherence lengths and time do not play any role because these are related to coherence properties only, not to the wave function. Hence, one should realize that a neutron wave function 'scatters' from the whole of the interaction potential, not just from the part of the interaction potential covered by the coherence lengths (coherence volume) and time of the neutron ensemble average (or neutron beam). Although this seems obvious at first, it can become confusing when trying

to understand the scattering of neutrons in real space.

In chapters 5 and 7 some aspects of the potential of neutron spin coding techniques are described. In these examples always the neutron spin is first rotated to some angle and then rotated backwards toward its starting position. This is why it is called *spin-echo* technique. Mezei was the first to apply this to the coding of the energy transfer of the neutron in a scattering process [32]. However, other applications are possible which are not to be ignored. In these applications the spin coding technique is used to label each neutron with a special property of the neutron. An example is the coding of the neutrons wavelength in neutron Larmor precession transmission experiments [62]. Another example is the coding of a specific component of the neutrons wavevector (for instance perpendicular to a Bragg-plane) in neutron diffraction experiments [63]. This enables high-resolution neutron diffraction experiments, yielding accurate information on crystal lattice spacings, comparable to X-rays. Hence, spin-echo coding techniques are expanding neutron scattering applications to limits never thought possible with conventional neutron scattering techniques.

Bibliography

[1] L. Mandel and E. Wolf. *Optical Coherence and Quantum Optics*. Cambridge University Press, first edition, 1995.

[2] V. Holý, U. Pietsch, and T. Baumbach. *High-resolution X-ray scattering from thin films and Multilayers*. Springer-Verlag, Berlin, 1999.

[3] S. K. Sinha, M. Tolan, and A. Gibaud. Effects of partial coherence on the scattering of x rays by matter. *Phys. Rev. B*, 57(5):2740–2758, Feb 1998.

[4] F. van der Veen and F. Pfeiffer. Coherent x-ray scattering. *J. Phys. Condens. Matter*, 16:5003–5030, 2004.

[5] V. F. Sears. *Neutron optics*. Oxford University Press, first edition, 1989.

[6] H. Rauch, H. Wölwitsch, H. Kaiser, R. Clothier, and S. A. Werner. Measurement and characterization of the three-dimensional coherence function in neutron interferometry. *Phys. Rev. A*, 53(2):902–908, Feb 1996.

[7] R. Gähler, J. Felber, F. Mezei, and R. Golub. Space-time approach to scattering from many-body systems. *Phys. Rev. A*, 58(1):280–295, Jul 1998.

[8] V. O. de Haan, J. Plomp, W. G. Bouwman, M. Trinker, M. Th. Rekveldt, C. P. Duif, E. Jericha, H. Rauch, and A. A. van Well. Phase-object approximation in small angle neutron scattering experiments on silicon gratings. *Journal of Applied Crystallography*, 40:151–157, 2007.

[9] F. Mezei. Coherent approach to neutron beam polarization. In M. Schlenker et al, editor, *Imaging processes and Coherence in Physics, Lecture Notes in Physics 112*, page 282, Springer-Verlag, Berlin, 1980.

[10] A. A. Michelson. *Phil. Mag.*, 30:1, 1890.

[11] L. I. Schiff. *Quantum mechanics*. McGraw-Hill Book company, New-York, 1968.

[12] L. Van Hove. Correlations in space and time and born approximation scattering in systems of interacting particles. *Phys. Rev.*, 95(1):249–262, Jul 1954.

[13] R. P. Feynman. Space-time approach to non-relativistic quantum mechanics. *Rev. Mod. Phys.*, 20(2):367–387, Apr 1948.

[14] B. K. Jap and R. M. Glaeser. The scattering of high-energy electrons. i. feynman path-integral formulation. *Acta Cryst. A*, 34:94–102, 1978.

[15] M. Th. Rekveldt. Novel SANS instrument using neutron spin echo. *Nucl. Instr. & Methods in Phys. Res. B*, 114:366–370, 1996.

[16] M. Th. Rekveldt. Spin-echo small-angle neutron scattering in neutron reflectometry. *Journal of Applied Crystallography*, 36(6):1301–1306, Dec 2003.

[17] M. Th. Rekveldt, W. G. Bouwman, W. H. Kraan, O. Uca, S. Grigoriev, S. Habicht, and T. Keller. *Neutron Spin Echo*, volume 601 of *Lecture Notes in Physics*, chapter Elastic neutron scattering measurements using Larmor precession of polarized neutrons, pages 87–99. Springer, Berlin, 2003. Ed. by F. Mezei, C. Pappas and T. Gutberlet.

[18] R. Gähler, R. Golub, K. Habicht, T. Keller, and J. Felber. Space-time description of neutron spin-echo spectrometry. *Physica B*, 229:1–17, 1996.

[19] E. Jericha, M. Baron, M. Hainbuchner, R. Loidl, M. Villa, and H. Rauch. Ultra-small-angle neutron scattering studies of artificial lattices. *Journal of Applied Crystallography*, 36(3 Part 1):778–782, Jun 2003.

[20] M. Agamalian, G. D. Wignall, and R. Triolo. Optimization of a Bonse–Hart Ultra-Small-Angle Neutron Scattering Facility by Elimination of the Rocking-Curve Wings. *Journal of Applied Crystallography*, 30(3):345–352, Jun 1997.

[21] J. G. Barker, C. J. Glinka, J. J. Moyer, M. H. Kim, A. R. Drews, and M. Agamalian. Design and performance of a thermal-neutron double-crystal diffractometer for USANS at NIST. *Journal of Applied Crystallography*, 38(6):1004–1011, Dec 2005.

[22] T. Krouglov, I. M. de Schepper, W. G. Bouwman, and M. Th. Rekveldt. Real-space interpretation of spin-echo small-angle neutron scattering. *Journal of Applied Crystallography*, 36(1):117–124, Feb 2003.

[23] J. Schelten and W. Schmatz. Multiple-scattering treatment for small-angle scattering problems. *Journal of Applied Crystallography*, 13(4):385–390, Aug 1980.

[24] H. Muller, H. Rose, and P. Schorsch. A coherence function approach to image simulation. *Journal of Microscopy*, 190(1-2):73–88, 1998.

[25] T. Krouglov. *Spin-echo small-angle neutron scattering applied to colloid systems*. Delft Universtiy of Technology, first edition, 2005. PhD thesis.

[26] M. Abramowitz and I. A. Stegun. *Handbook of mathematical functions*. National Bureau of Standards Applied Mathematics Series - 55, tenth edition, 1972.

[27] J. Plomp, J. G. Baker, V. O. de Haan, W. G. Bouwman, and A. A. van Well. Neutron refraction by cylindrical metal wires. *Nucl. Instr. & Methods in Phys. Res. B*, (Accepted).

[28] P. A. M. Dirac. *Rev. Mod. Phys.*, A 117:610, 1928.

[29] F. Mezei. Zeeman energy, interference and neutron spin echo: A minimal theory. *Physica B*, 151(1–2):74–81, 1988.

[30] W. H. Kraan. *Instrumentation to handle thermal polarized neutron beams*. Delft Universtiy of Technology, first edition, 2004. PhD thesis.

[31] C. Schwink and O. Schärpf. *Z. Physik B*, 21:305, 1975.

[32] F. Mezei. *Z. Phys.*, 255:146, 1972.

[33] R. Pynn. Neutron spin-echo and three-axis spectrometers. *J. Phys. E: Sci. Instrum.*, 11:1133–1140, 1978.

[34] T. Keller, R. Gähler, H. Kuntze, and R. Golub. *Neutron News*, 6(3):16–17, 1995.

[35] S. V. Grigoriev, W. H. Kraan, M. Th. Rekveldt, T. Kruglov, and W. G. Bouwman. Spin-echo small-angle neutron scattering for magnetic samples. *Journal of Applied Crystallography*, 39(2):252–258, Apr 2006.

[36] M. Th. Rekveldt, S. V. Grigoriev, W. H. Kraan, N. H. van Dijk, and W. G. Bouwman. *Rev. Sci. Instrum.*, 77:073902–1, 2006.

[37] M. Th. Rekveldt. *Z. Physik A*, 259:391, 1973.

[38] J. Leckner. *Theory of reflection*. Martinus Nijhoff publishers, Dordrecht, first edition, 1987.

[39] L. G. Parratt. Surface studies of solids by total reflection of x-rays. *Phys. Rev.*, 95(2):359–369, Jul 1954.

[40] S. K. Sinha, E. B. Sirota, S. Garoff, and H. B. Stanley. X-ray and neutron scattering from rough surfaces. *Phys. Rev. B*, 38(4):2297–2311, Aug 1988.

[41] G. Porod. *Kolloid Z*, 124(2):83, 1951.

[42] A. Braslau, P. S. Pershan, G. Swislow, B. M. Ocko, and J. Als-Nielsen. Capillary waves on the surface of simple liquids measured by x-ray reflectivity. *Phys. Rev. A*, 38(5):2457–2470, Sep 1988.

[43] A Steyerl. Effect of surface roughness on the total reflexion and transmission of slow neutrons. *Z. Physik*, 254:169–188, June 1972.

[44] R. Pynn. Neutron scattering by rough surfaces at grazing incidence. *Phys. Rev. B*, 45(2):602–612, Jan 1992.

[45] D. K. G. de Boer. Influence of the roughness profile on the specular reflectivity of x rays and neutrons. *Phys. Rev. B*, 49(9):5817–5820, Mar 1994.

[46] W. Weber and B. Lengeler. Diffuse scattering of hard x rays from rough surfaces. *Phys. Rev. B*, 46(12):7953–7956, Sep 1992.

[47] A. A. Maradudin and D. L. Mills. Scattering and absorption of electromagnetic radiation by a semi-infinite medium in the presence of surface roughness. *Phys. Rev. B*, 11(4):1392–1415, Feb 1975.

[48] M. Rauscher, T. Salditt, and H. Spohn. Small-angle x-ray scattering under grazing incidence: The cross section in the distorted-wave born approximation. *Phys. Rev. B*, 52(23):16855–16863, Dec 1995.

[49] Y. Yoneda. Anomalous surface reflection of x rays. *Phys. Rev.*, 131(5):2010–2013, Sep 1963.

[50] J. Daillant and O. Belorgey. Surface scattering of x rays in thin films. part i. theoretical treatment. *The Journal of Chemical Physics*, 97(8):5824–5836, 1992.

[51] L. Névot and P. Croce. Caractérisation des surfaces par réflexion rasante de rayons x. application à l'étude du polissage de quelques verres silicates. *Revue Phys. Appl.*, 15:761–779, 1980.

[52] D. K. G. de Boer. X-ray scattering and x-ray fluorescence from materials with rough interfaces. *Phys. Rev. B*, 53(10):6048–6064, Mar 1996.

[53] S. K. Sinha. Reflectivity using neutrons or x-rays? a critical comparison. *Physica B*, 173(1–2):25–34, Aug 1991.

[54] V. Holý, J. Kubéna, I. Ohlídal, K. Lischka, and W. Plotz. X-ray reflection from rough layered systems. *Phys. Rev. B*, 47(23):15896–15903, Jun 1993.

[55] V. Holý and T. Baumbach. Nonspecular x-ray reflection from rough multilayers. *Phys. Rev. B*, 49(15):10668–10676, Apr 1994.

[56] M. Th. Rekveldt. Neutron reflectometry and SANS by neutron spin echo. *Physica B*, 234-236:1135–1137, 1997.

[57] G. P. Felcher, S. G. E. te Velthuis, J. Major, A. Dosch, A. Anderson, A. Habicht, and T. Keller. Spin-echo resolved grazing incidence scattering (SERGIS) of cold neutrons. *Proc. SPIE*, 4785:164, 2002.

[58] J. Major, H. Dosch, G. P. Felcher, K. Habicht, T. Keller, S. G. E. te Velthuis, A. Vorobiev, and M. Wahl. Combining of neutron spin echo and reflectivity: a new technique for probing surface and interface order. *Physica B*, 336:8–15, 2003.

[59] J. Plomp, V. O. de Haan, R. M. Dalgliesh, S. Langridge, and A. A. van Well. Time-of-flight spin-echo small-angle neutron measurements. In *Polarized neutrons in condensed matter investigations*, page (in press), Berlin, september 2006.

[60] R. Pynn, M. R. Fitzsimmons, M. Th. Rekveldt, J. Major, H. Fritzsche, D. Weller, and E. C. Johns. Optimization of neutron scattering instrumentation using neutron spin echo: Application to the discrimination of diffuse scattering in neutron reflectivity experiments. *Review of Scientific Instruments*, 73(8):2948–2957, Aug 2002.

[61] A. Virjo. The fourier method in slow neutron time-of-flight spectrometry. *Nuclear Instruments and Methods*, 73(2):189–199, 1969.

[62] W. H. Kraan and M. Th. Rekveldt. Neutron larmor precession transmission experiments. *Nuclear Instruments and Methods in Physics Research Section A: Accelerators, Spectrometers, Detectors and Associated Equipment*, 276(3):521–528, 1989.

[63] M. T. Rekveldt, T. Keller, and R. Golub. Larmor precession, a technique for high-sensitivity neutron diffraction. *Europhysics Letters (EPL)*, 54(3):342–346, 2001.

[64] G. Palasantzas and J. Krim. Effect of the form of the height-height correlation function on diffuse x-ray scattering from a self-affine surface. *Phys. Rev. B*, 48(5):2873–2877, Aug 1993.

[65] W. E. Boyce and R. D. DiPrima. *Elementary differential equations and boundary value problems*, chapter Second order linear equations, pages 107–185. John Wiley & Sons, New-York, 4 edition, 1986.

[66] D. L. Mills. Attenuation of surface polaritons by surface roughness. *Phys. Rev. B*, 12(10):4036–4046, Nov 1975.

Appendix A

Rotation matrices

A rotation matrix is a multiplication of rotation or streaming matrices only and can be described with three real functions:

$$\widehat{H} = \frac{1}{\sqrt{2}} \begin{pmatrix} \sqrt{1+P}e^{i\alpha} & i\sqrt{1-P}e^{i\beta} \\ i\sqrt{1-P}e^{-i\beta} & \sqrt{1+P}e^{-i\alpha} \end{pmatrix}, \tag{A.1}$$

where $|P| \leq 1$ and α, β and P are all functions of $\vec{r}$ and $\vec{r'}$. P is called the *polarizing factor* of the matrix. This matrix can be interpreted as an effective rotation of the polarization vector over an angle 2θ around a normal $\vec{n}$ as shown in figure A.1, for which holds:

$$\widehat{H} = \widehat{I}\cos\theta - i\left(n_x\widehat{\sigma}_x + n_y\widehat{\sigma}_y + n_z\widehat{\sigma}_z\right)\sin\theta, \tag{A.2}$$

or because $\left(n_x\widehat{\sigma}_x + n_y\widehat{\sigma}_y + n_z\widehat{\sigma}_z\right)^2 = \widehat{I}$:

$$\widehat{H} = e^{-i\theta\left(n_x\widehat{\sigma}_x + n_y\widehat{\sigma}_y + n_z\widehat{\sigma}_z\right)}. \tag{A.3}$$

α, β and P can be expressed in terms of θ and $\vec{n}$:

$$P = 1 - 2(1-n_z^2)\sin^2\theta, \tag{A.4}$$

$$\tan\alpha = -n_z\tan\theta \quad , \tag{A.5}$$

$$\tan\beta = -n_y/n_x \quad , \tag{A.6}$$

or reversed:

$$n_x\sin\theta = -\sqrt{\frac{1-P}{2}}\cos\beta, \tag{A.7}$$

$$n_y\sin\theta = \sqrt{\frac{1-P}{2}}\sin\beta, \tag{A.8}$$

$$n_z\sin\theta = -\sqrt{\frac{1+P}{2}}\sin\alpha. \tag{A.9}$$

A typical property of rotation matrices is that the product of two rotation matrices is another rotation matrix. Further properties are:

$$\widehat{H}\widehat{H}^\dagger = \widehat{I}, \tag{A.10}$$

$$\det \widehat{H} = 1, \tag{A.11}$$

$$\mathrm{Tr}(\widehat{\sigma}_z \widehat{H} \widehat{\sigma}_z \widehat{H}^\dagger) = 2P. \tag{A.12}$$

Notice further that any rotation matrix can be transformed in a sum of a matrix $\widehat{T}_z$ and $\widehat{F}_z$:

$$\widehat{H} = \sqrt{\frac{1+P}{2}}\widehat{T}_z(2\alpha) + \sqrt{\frac{1-P}{2}}\widehat{F}_z(2\beta), \tag{A.13}$$

where

$$\widehat{F}_z(\tau) = \begin{pmatrix} 0 & ie^{i\tau/2} \\ ie^{-i\tau/2} & 0 \end{pmatrix} \tag{A.14}$$

is a *flipping matrix*. This matrix can be interpreted as an effective rotation of the polarization vector over an angle π along a normal $\vec{n}$ in the (x, y) plane as shown in figure A.2. Some special matrices and their properties are shown below:

$$\widehat{F}_z(\beta)\widehat{T}_z(\alpha) = \widehat{F}_z(\beta - \alpha), \tag{A.15}$$

$$\widehat{T}_z(\beta)\widehat{F}_z(\alpha) = \widehat{F}_z(\beta + \alpha), \tag{A.16}$$

$$\widehat{F}_z(\beta)\widehat{F}_z(\alpha) = -\widehat{T}_z(\beta - \alpha), \tag{A.17}$$

$$\widehat{T}_z(\beta)\widehat{T}_z(\alpha) = \widehat{T}_z(\beta + \alpha), \tag{A.18}$$

$$\widehat{F}_z(\alpha)\widehat{\sigma}_y = -\widehat{\sigma}_y\widehat{F}_z(-\alpha), \tag{A.19}$$

$$\widehat{T}_z(\alpha)\widehat{\sigma}_y = \widehat{\sigma}_y\widehat{T}_z(-\alpha) \tag{A.20}$$

and

$$\mathrm{Tr}(\widehat{\sigma}_y\widehat{T}_z(\alpha)) = 0, \tag{A.21}$$

$$\mathrm{Tr}(\widehat{F}_z(\alpha)) = 0, \tag{A.22}$$

$$\mathrm{Tr}(\widehat{T}_z(\alpha)) = 2\cos\frac{\alpha}{2}. \tag{A.23}$$

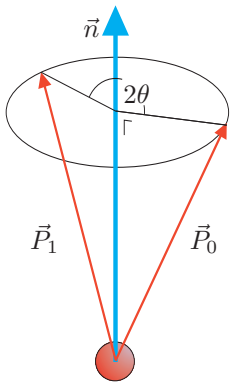

Figure A.1: Effect of rotation or streaming matrix on rotation of polarization vector from $\vec{P}_0$ to $\vec{P}_1$.

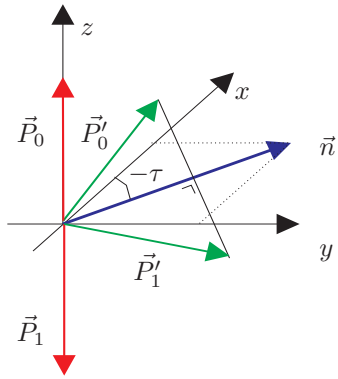

Figure A.2: Effect of flipping matrix on rotation of polarization vector from $\vec{P}_0$ to $\vec{P}_1$ if the polarization is parallel to the z-axis and from $\vec{P}_0'$ to $\vec{P}_1'$ otherwise.

Appendix B

Rough surfaces

Roughness of surfaces can be described in several ways. Here, it is important to model the optical potential at the interface as changes in this potential causes neutrons to scatter. Let the height of the surface above the xz-plane be given by a function $H(x,z)$ (see figure B.1).The height-height correlation function is given by:

$$C(x,z) = \frac{1}{A_s}\int_{A_s} H(x_s,z_s)H(x_s+x,z_s+z)dx_s dz_s, \tag{B.1}$$

where the integration is over the sample surface area, A_s. In the following it is assumed that $H(x,z)$ has a Gaussian random distribution. The first moment (or average) of $H(x,z)$ is 0. The second moment (or variance) of $H(x,z)$ is defined as: $\sigma^2 = C(0,0)$. The expectation value of $e^{iqH(x,z)}$, known as the *characteristic function* of $H(x,z)$, is given by:

$$E[e^{iqH(x,z)}] = e^{-q^2\sigma^2/2}. \tag{B.2}$$

Further it is assumed that $H(x_1,z_1) - H(x_2,z_2)$ has a Gaussian random distribution with zero mean too and its variance only depends on $x_1 - x_2$ and $z_2 - z_1$:

$$g(x,z) = \left\langle [H(x_s,z_s) - H(x_s+x,z_s+z)]^2 \right\rangle_{A_s}, \tag{B.3}$$

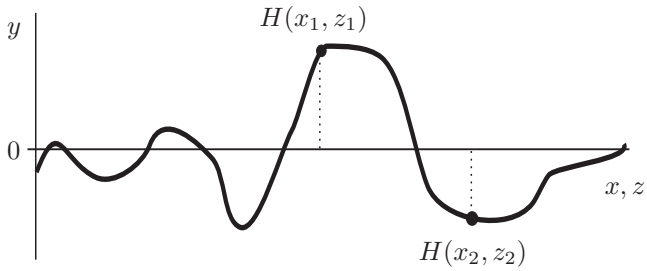

Figure B.1: Height distribution of a rough surface. $H(x,z)$ is the height above the xz-plane. The average of $H(x,z)$ is 0.

where the average is taken over the whole sample area. Note that $g(x, z)$ can be reduced to:

$$g(x, z) = 2(C(0, 0) - C(x, z)). \tag{B.4}$$

Note that the expectation value of $e^{iq(H(x_s,z_s)-H(x_s+x,z_s+z))}$ is given by:

$$E[e^{iq(H(x_s,z_s)-H(x_s+x,z_s+z))}] = e^{-q^2 g(x,z)/2}. \tag{B.5}$$

For a discussion of possible height-height correlation functions see for instance [40] and [64].

The optical potential of the sample is modeled as:

$$V(x, y, z) = u(y + d)u(H(x, z) - y)V_0, \tag{B.6}$$

where V_0 is the optical potential of the (homogeneous) sample material (see also section 3.3), d is the thickness of the sample in the y-direction and $u(y)$ is the Heaviside step function. Note that it is assumed that the interface at $y = -d$ is completely flat.

Appendix C

Scattering at surfaces

The scattering at a smooth surface results in a change of the *incident* mutual coherence function into the *scattered* mutual coherence function at the scattering position. In general a mutual coherence function describes the correlations between two wave functions propagating through free space according to its definition as given by equation (2.6). To find out what happens in the scattering process the Schrödinger equation must be solved. Depending on the problem at hand (the optical potential distribution and the scattering geometry) sometimes a general solution can be derived from this wave equation, coupling the scattered-wave function to the incident-wave function. In the case considered here (specular and off-specular reflection at a smooth sample surface) under certain conditions the general solution can be expressed in terms of wavevector distributions. Here, the incident-wave function is assumed to be a distribution over plane wave components and each component is scattered in its own special way. After scattering all components are added, forming the scattered-wave function. Hence, in the following the relation between a mutual coherence function to the desired components of the wave function is discussed first. Then, the incident mutual coherence function is transformed to the scattered one by applying the solution of the Schrödinger equation to each of the components and adding them. Finally, this is applied to find the scattered mutual coherence function at the detector position.

C.1 Wavevector distribution of mutual coherence function

Let $\Psi(\vec{r},t)$ denote a neutron wave function characterizing the field at point $\vec{r}$ at time t. The neutron wave function $\Psi(\vec{r},t)$ is constructed by its constituting monochromatic plane-wave components (see also section 2.1):

$$\Psi(\vec{r},t) = e^{-i\omega_k t}\int \psi(\vec{k},\vec{r})d^3k, \tag{C.1}$$

where $\vec{k}$ is the wavevector, $\omega_k = \hbar k^2/2m$ and m the neutron mass. If further it is assumed that the beam is directed to positive value's of x and z only, the wavevector $\vec{k} = \vec{k}_{\|} + k_y\vec{e}_y$, where $k_y = \vec{k}\cdot\vec{e}_y$ so that $k_y = -\sqrt{\vec{k}^2 - k_{\|}^2}$. The negative sign denotes that the plane wave is traveling in the $-y$ direction. The plane-wave components can be described by:

$$\psi(\vec{k},\vec{r}) = \psi_0(\vec{k}_{\|})e^{i\vec{k}\cdot\vec{r}}. \tag{C.2}$$

Hence, the neutron wave function can be described by:

$$\Psi(\vec{r},t) = e^{-i\omega_k t}\int e^{i\vec{k}\cdot\vec{r}}\psi_0(\vec{k}_\parallel)d^2k_\parallel. \tag{C.3}$$

Note that the mutual coherence function can be described by the above variables using its definition (2.6):

$$\Gamma(\vec{r}_1,\vec{r}_2,\tau) = e^{-i\omega_k\tau}\int\int\left\langle\psi(\vec{k}_1,\vec{r}_1)^*\psi(\vec{k}_2,\vec{r}_2)\right\rangle d^2k_{1,\parallel}d^2k_{2,\parallel}, \tag{C.4}$$

which can be reduced to:

$$\Gamma(\vec{r}_1,\vec{r}_2,\tau) = e^{-i\omega_k\tau}\int\int\left\langle\psi_0(\vec{k}_{1,\parallel})^*\psi_0(\vec{k}_{2,\parallel})\right\rangle e^{i\vec{k}_2\cdot\vec{r}_2-i\vec{k}_1\cdot\vec{r}_1}d^2k_{1,\parallel}d^2k_{2,\parallel}. \tag{C.5}$$

From this equation it follows by inverse Fourier transformation:

$$\left\langle\psi_0(\vec{k}_{1,\parallel})^*\psi_0(\vec{k}_{2,\parallel})\right\rangle = \frac{1}{16\pi^4}\int\int e^{i\vec{k}_1\cdot\vec{r}_1-i\vec{k}_2\cdot\vec{r}_2}\Gamma(\vec{r}_1,\vec{r}_2,0)d^2r_{1,\parallel}d^2r_{2,\parallel}. \tag{C.6}$$

If the mutual coherence function is homogeneous (only depending on $\vec{r}_2-\vec{r}_1$), then this reduces to:

$$\left\langle\psi_0(\vec{k}_{1,\parallel})^*\psi_0(\vec{k}_{2,\parallel})\right\rangle = \frac{\delta^{(2)}(\vec{k}_{1,\parallel}-\vec{k}_{2,\parallel})}{4\pi^2}W(\vec{r}_1,\vec{k}_{2,\parallel}), \tag{C.7}$$

where

$$W(\vec{r}_1,\vec{k}_\parallel) = \int e^{-i\vec{k}_\parallel\cdot\vec{r}_\parallel}\Gamma(\vec{r}_1,\vec{r}_1+\vec{r}_\parallel,0)d^2r_\parallel, \tag{C.8}$$

is the wavevector distribution.

C.2 Scattering at a smooth sample surface

The incident-wave function at the sample surface can be represented by:

$$\Psi_{in}(\vec{r},t) = e^{-i\omega_k t}\int e^{i\vec{k}\cdot\vec{r}}\psi_0(\vec{k}_\parallel)d^2k_\parallel. \tag{C.9}$$

and following the derivation given in section 6.2.1 the scattered-wave function in the far-zone can be expressed as:

$$\Psi_{sc}^{(0)}(\vec{r},t) = e^{-i\omega_k t}\int\rho(k_y)e^{-2ik_y y}e^{i\vec{k}\cdot\vec{r}}\psi_0(\vec{k}_\parallel)d^2k_\parallel, \tag{C.10}$$

where $k_y = -\sqrt{k^2-k_\parallel^2}$. By taking $\vec{p}_\parallel = \vec{k}_\parallel$ and $p_y = -k_y$ this equation can be rewritten as:

$$\Psi_{sc}^{(0)}(\vec{r},t) = e^{-i\omega_k t}\int\rho(p_y)e^{i\vec{p}\cdot\vec{r}}\psi_0(\vec{p}_\parallel)d^2p_\parallel. \tag{C.11}$$

If it is assumed that *close to the sample surface* both the incident mutual coherence function and the scattered one are homogeneous, the wavevector distribution of the scattered mutual coherence function is defined by:

$$W_{sc}(\vec{r}_1,\vec{p}_\parallel) = \int e^{-i\vec{p}_\parallel\cdot\vec{r}_\parallel}\Gamma_{sc}(\vec{r}_1,\vec{r}_1+\vec{r}_\parallel,0)d^2r_\parallel. \tag{C.12}$$

Using the definition of the mutual coherence function and after inserting equations (C.10) and (C.7) this becomes:

$$W_{sc}^{(0,0)}(\vec{r}_1, \vec{p}_\parallel) = R(p_y) W_{in}(\vec{r}_1, \vec{p}_\parallel), \tag{C.13}$$

where $R(p_y) = \rho(p_y)^* \rho(p_y)$. The mutual coherence function can be determined by a Fourier transform of equation (C.13):

$$\Gamma_{sc}^{(0,0)}(\vec{r}_1, \vec{r}_1 + \vec{r}_\parallel, 0) = \frac{1}{4\pi^2} \int e^{i\vec{p}_\parallel \cdot \vec{r}_\parallel} R(p_y) W_{in}(\vec{r}_1, \vec{p}_\parallel) d^2 p_\parallel. \tag{C.14}$$

Inserting W_{in} this becomes at the sample position:

$$\Gamma_{sc}^{(0,0)}(\vec{r}_s, \vec{r}_s + \vec{r}_\parallel, \tau) = \frac{1}{4\pi^2} \int \int e^{i\vec{p}_\parallel \cdot (\vec{r}_\parallel - \vec{s}_\parallel)} \Gamma_{in}(\vec{r}_s, \vec{r}_s + \vec{s}_\parallel, \tau) R(p_y) d^2 p_\parallel d^2 s_\parallel. \tag{C.15}$$

C.3 Mutual coherence function at detector position

Equation (6.10) can be used to calculate the propagation of the mutual coherence function to the detector:

$$\Gamma_{sc}(\vec{r}_d, \vec{r}_d, 0) = \int_{y=0} \frac{\cos^2 \phi_1}{r_{d1}^2 \bar{\lambda}^2} \int_{y=0} e^{-i\vec{p}\cdot\vec{r}} \Gamma_{sc}(\vec{r}_1, \vec{r}_1 + \vec{r}, 0) d^2 r d^2 r_1, \tag{C.16}$$

where $\vec{p} = \bar{k}(\vec{r}_d - \vec{r}_1)/r_{d1}$. The inner-integral of this formula is the Fourier transform of the mutual coherence function at position $\vec{r}_1$ on the sample plane, the same as equation (C.12), so that:

$$\Gamma_{sc}(\vec{r}_d, \vec{r}_d, 0) = \int_{y=0} \frac{\cos^2 \phi_1}{r_{d1}^2 \bar{\lambda}^2} W_{sc}(\vec{r}_1, \vec{p}) d^2 r_1. \tag{C.17}$$

Hence, the mutual coherence function at the detector position is proportional to the sample average of the scattered wavevector distribution, when it is assumed that at the sample position the mutual coherence function of incident and scattered wave are homogeneous and the sample correlation lengths are not too large. If these conditions are not fulfilled a more elaborate derivation is needed, based directly on the derivation of the propagation of the mutual coherence function as given by Mandel [1]. According to equations (C.10) and (C.5) the scattered mutual coherence function is given by:

$$\Gamma_{sc}^{(0,0)}(\vec{r}_1, \vec{r}_2, \tau) = e^{-i\omega_k \tau} \times \tag{C.18}$$

$$\int \int \rho(p_{1,y})^* \rho(p_{2,y}) \left\langle \psi_0(\vec{p}_{1,\parallel})^* \psi_0(\vec{p}_{2,\parallel}) \right\rangle e^{i\vec{p}_2 \cdot \vec{r}_2 - i\vec{p}_1 \cdot \vec{r}_1} d^2 p_{1,\parallel} d^2 p_{2,\parallel}.$$

Inserting equation (C.6) yields:

$$\Gamma_{sc}^{(0,0)}(\vec{r}_1, \vec{r}_2, \tau) = \int \int \Xi(\vec{r'}_1, \vec{r'}_2) \Gamma_{in}(\vec{r'}_1, \vec{r'}_2, \tau) d^2 r'_{1,\parallel} d^2 r'_{2,\parallel}, \tag{C.19}$$

where

$$\Xi(\vec{r'}_1, \vec{r'}_2) = \int \int e^{-i\vec{p}_1 \cdot \vec{r}_1 + i\vec{p}_2 \cdot \vec{r}_2} \frac{\rho(p_{1,y})^* \rho(p_{2,y})}{16\pi^4} e^{i\vec{p}_1 \cdot \vec{r'}_1 - i\vec{p}_2 \cdot \vec{r'}_2} d^2 p_{1,\parallel} d^2 p_{2,\parallel} \tag{C.20}$$

To solve this integral equation the *Weyl representation of a diverging spherical wave* is used [1]. This transforms an integral over $\vec{k}_{\|}$ into a Green function:

$$\int_{-\infty}^{\infty} \frac{e^{i\vec{k}\cdot\vec{r}}}{k_y} d^2k_{\|} = 2\pi \frac{e^{i\bar{k}r}}{ir}. \tag{C.21}$$

If both sides of this formula are differentiated with respect to y and interchanging the order of differentiation and integration this becomes:

$$\int_{-\infty}^{\infty} e^{i\vec{k}\cdot\vec{r}} d^2k_{\|} = 2\pi \frac{\partial}{\partial y}\left[\frac{e^{i\bar{k}r}}{ir}\right]. \tag{C.22}$$

In the far-zone the differential at the right-hand side becomes:

$$\frac{\partial}{\partial y}\left[\frac{e^{i\bar{k}r}}{ir}\right] = \bar{k}\cos\theta \frac{e^{i\bar{k}r}}{r}, \tag{C.23}$$

where $\cos\theta = \vec{e}_y \cdot \vec{r}/r$ and hence

$$\int_{-\infty}^{\infty} e^{i\vec{k}\cdot\vec{r}} d^2k_{\|} = 2\pi\bar{k}\cos\theta \frac{e^{i\bar{k}r}}{r}. \tag{C.24}$$

Inserting this result in equation (C.20) and assuming that $\rho(p_{1,y})$ and $\rho(p_{2,y})$ are constant, yields:

$$\Xi(\vec{r'}_1, \vec{r'}_2) = \rho(p_{1,y})^* \rho(p_{2,y}) \cos\theta_1 \cos\theta_2 \frac{e^{i\bar{k}(R_2 - R_1)}}{R_1 R_2 \bar{\lambda}^2}, \tag{C.25}$$

where $R_i = \left|\vec{r'}_i - \vec{r}_i\right|$ and $\cos\theta_i = \vec{e}_y \cdot (\vec{r'}_i - \vec{r}_i)/R_i$ and $\vec{p}_i$ is a wavevector with length $\bar{k}$ and a direction that corresponds to the direction of $\vec{r'}_i - \vec{r}_i$. Note that for the derivation of this formula it was used that the incident mutual coherence function was known on the sample plane. Instead of using the sample plane any plane will do as long as one takes care of the correct values for $\rho(p_{1,y})$ and $\rho(p_{2,y})$.

C.4 Wavevector distribution for an incoherent source

Equation (2.31) and equation (2.36) can be used to calculate the incident mutual coherence function for a completely homogeneous and incoherent source with area A_0:

$$\Gamma_{in}(\vec{r}_1, \vec{r}_1 + \vec{r}, 0) = \frac{J_0}{2v_p 4\pi r_1^2} \int_{A_0} e^{i\bar{k}\vec{r}\cdot(\vec{r}_1 - \vec{r'})/r_1} d^2r', \tag{C.26}$$

so that

$$W_{in}(\vec{r}_1, \vec{k}_{\|}) = \frac{J_0}{2v_p 4\pi r_1^2} \int_{A_0} \int e^{i\vec{r}_{\|}\cdot((\vec{r}_1 - \vec{r'})\bar{k}/r_1 - \vec{k}_{\|})} d^2r_{\|} d^2r', \tag{C.27}$$

which can be reduced to:

$$W_{in}(\vec{r}_1, \vec{k}_{\|}) = \frac{J_0\pi}{2v_p r_1^2} \int_{A_0} \delta^{(2)}\left(\bar{k}\frac{\vec{r}_{1,\|} - \vec{r'}_{\|}}{r_1} - \vec{k}_{\|}\right) d^2r'. \tag{C.28}$$

Appendix D

Scattering at rough or structured sample surfaces

Following the derivation given in section 6.4 the scattered-wave function can be expressed as (equation (6.73)):

$$\psi_{sc}(\vec{k},\vec{r}) = \psi_{sc}^{(0)}(\vec{k},\vec{r}) - \frac{2m}{\hbar^2}\int G^{(+)}(\vec{r},\vec{r}_s)V^{(1)}(\vec{r}_s)\psi_{sc}^{(0)}(\vec{k},\vec{r}_s)d^3r_s. \tag{D.1}$$

To solve this equation a precise estimate of the Green function and the undisturbed scattered-wave function is needed.

D.1 Green function

The Green function for scattered waves can be approximated by taking the Green function for scattered waves for the undisturbed potential [43], [47], [48] defined by:

$$\left(\nabla^2 + \bar{k}^2 - \frac{2mV^{(0)}(\vec{r}_s)}{\hbar^2}\right) G^{(+)}(\vec{r},\vec{r}_s) = \delta(\vec{r}-\vec{r}_s), \tag{D.2}$$

where the ∇^2 operator represents the derivatives to $\vec{r}_s$. It can be solved by supposing the Green function can be factorized (see section 6.2):

$$G^{(+)}(\vec{r},\vec{r}_s) = \frac{1}{4\pi^2}\int_0^\infty e^{i\vec{p}_\parallel\cdot(\vec{r}-\vec{r}_s)} g(p_y,y,y_s)d^2p_\parallel, \tag{D.3}$$

where $\vec{p}$ is a wavevector with length $\bar{k}$ and $g(p_y,y,y_s)$ is a one-dimensional Green function perpendicular to the surface. Note, that if $g(p_y,y,y_s)$ would be equal to $e^{ip_y(y-y_s)}/2ip_y$ this formula can be converted to Weyls representation of a spherical wave, which in the far-zone reduces to (conform equation (C.21)):

$$G^{(+)}(\vec{r},\vec{r}_s) = G_0(\vec{r}-\vec{r}_s) = \frac{e^{i\bar{k}|\vec{r}-\vec{r}_s|}}{4\pi\,|\vec{r}-\vec{r}_s|}. \tag{D.4}$$

Inserting the factorized Green function in equation (D.2) and inverse Fourier transforming, yields:

$$\frac{\partial^2 g(p_y,y,y_s)}{\partial y^2} + p_y^2 g(p_y,y,y_s) = \delta(y-y_s) \quad y \geq y_0, \tag{D.5}$$

$$\frac{\partial^2 g(p_y,y,y_s)}{\partial y^2} + (p_y')^2 g(p_y,y,y_s) = \delta(y-y_s) \quad y < y_0, \tag{D.6}$$

where y_0 is the position of the interface, $p_y' = +\sqrt{p_y^2 - k_c^2}$ and $k_c^2 = 2mV_0/\hbar^2$. The accent denotes the value of the variable in the sample material and the positive sign is taken as p_y is also positive. The method of variation of parameters can be used to find the particular solution of these in-homogeneous linear second-order differential equations [65]:

$$g_p(p_y,y,y_s) = \begin{array}{ll} \frac{1}{2ip_y}\int_{-\infty}^{y}\left(e^{-ip_y(t-y)} - e^{ip_y(t-y)}\right)\delta(t-y_s)dt & y \geq y_0 \\ \frac{1}{2ip_y'}\int_{-\infty}^{y}\left(e^{-ip_y'(t-y)} - e^{ip_y'(t-y)}\right)\delta(t-y_s)dt & y < y_0 \end{array}, \tag{D.7}$$

which if $y_s < y_0$ can be reduced to :

$$g_p(p_y,y,y_s) = \begin{array}{ll} \frac{1}{2ip_y'}\left(e^{ip_y'(y_s-y)} - e^{-ip_y'(y_s-y)}\right) & y \geq y_s \\ 0 & y < y_s \end{array} \tag{D.8}$$

and if $y_s \geq y_0$

$$g_p(p_y,y,y_s) = \begin{array}{ll} \frac{1}{2ip_y}\left(e^{-ip_y(y_s-y)} - e^{ip_y(y_s-y)}\right) & y \geq y_s \\ 0 & y < y_s \end{array}. \tag{D.9}$$

The complete solution for the in-homogeneous differential equation can be found by adding the particular solution to the solution of the homogeneous differential equation. If $y_s < y_0$ the Green function for $y > y_0$ should only have a component away from the surface in the $+y$-direction. For $y < y_s$ it should only have a component in the $-y$-direction, hence:

$$g(p_y,y,y_s) = \begin{array}{ll} c_1 e^{ip_y y} & y \geq y_0 \\ c_2' e^{-ip_y' y} + \frac{1}{2ip_y'}\left(e^{ip_y'(y_s-y)} - e^{-ip_y'(y_s-y)}\right) & y_s \leq y < y_0 \\ c_2' e^{-ip_y' y} & y < y_s \end{array} \tag{D.10}$$

and if $y_s \geq y_0$ the Green function for $y > y_s$ should only have a component away from the surface in the $+y$-direction. For $y < y_0$ it should only have a component in the $-y$-direction, hence:

$$g(p_y,y,y_s) = \begin{array}{ll} d_1 e^{ip_y y} + \frac{1}{2ip_y} e^{ip_y(y-y_s)} & y \geq y_s \\ d_1 e^{ip_y y} + \frac{1}{2ip_y} e^{ip_y(y_s-y)} & y_0 \leq y < y_s \\ d_2' e^{-ip_y' y} & y < y_0 \end{array}. \tag{D.11}$$

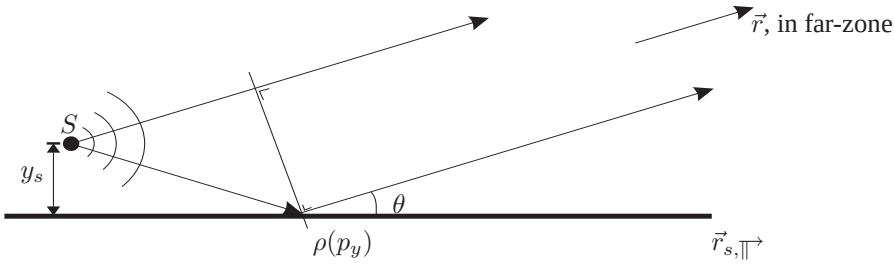

Figure D.1: Propagation of Green function from a source, S of disturbance above the sample surface to an observation point in the far-zone.

These solutions and their derivatives to y must be continuous at $y = y_0$, hence if $y_s < y_0$:

$$g(p_y, y, y_s) = \begin{cases} \frac{1}{2ip'_y}\tilde{\tau}(p_y)e^{ip_y(y-y_0)-ip'_y(y_s-y_0)} & y \geq y_0 \\ \frac{1}{2ip'_y}\left(e^{ip'_y|y_s-y|} - \rho(p_y)e^{-ip'_y(y_s+y-2y_0)}\right) & y < y_0 \end{cases} \tag{D.12}$$

and if $y_s \geq y_0$

$$g(p_y, y, y_s) = \begin{cases} \frac{1}{2ip_y}\left(\rho(p_y)e^{ip_y(y_s+y-2y_0)} + e^{ip_y|y-y_s|}\right) & y \geq y_0 \\ \frac{1}{2ip_y}\tau(p_y)e^{ip_y(y_s-y_0)-ip'_y(y-y_0)} & y < y_0 \end{cases}, \tag{D.13}$$

where $\rho(p_y) = (p_y - p'_y)/(p_y + p'_y)$, the reflection coefficient of the wave reflecting at the sample surface, $\tau(p_y) = 2p_y/(p_y + p'_y)$, the transmission of the wave function traversing the sample surface from outside to inside and $\tilde{\tau}(p_y) = 2p'_y/(p_y + p'_y)$, the transmission of the wave field traversing the sample surface from inside to outside. The Green function can be seen as the propagation of a disturbance starting from the source point, $\vec{r}_s$ toward the observation point, $\vec{r}$. If the disturbance starts above the sample, there are two possible paths for the disturbance to reach the observation point (see figure D.1). One directly and one reflected by the plane surface. The phase difference between these paths obviously depends on the distance to the surface and for small scattering angles and in the far-zone is just $2p_y y_s$. If the disturbance is in the sample there is only one way to reach the observation point, where the disturbance first propagates through the sample until it reaches the surface and is partly transmitted with a transmission coefficient $\tilde{\tau}(p_y) = 2p'_y/(p_y + p'_y)$ depending on the angle (see figure D.2). The transmission coefficient is actually the one of a plane wave traveling from the inside to the outside, but after constructing the Green function it is transformed to the one of a plane wave traveling from the outside to the inside, which in this case are closely related. After the transmission the disturbance propagates further to the observation point. The phase difference with the wave supposedly transmitted from the starting position if the sample was omitted is just $(p_y - p'_y)y_s$. If $p_y < k_c\ p'_y$ will become completely imaginary and the propagation of the disturbance in the sample is a phase-less damped exponential wave function. In the case considered here $y_s, y_0 \ll y$ and hence the

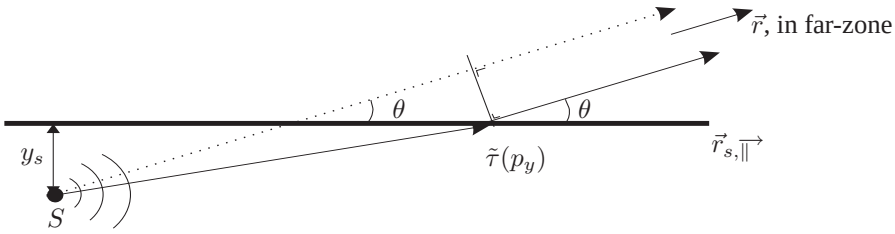

Figure D.2: Propagation of Green function from a source, S of disturbance below the sample surface to an observation point in the far-zone.

one-dimensional Green function becomes:

$$g(p_y, y, y_s) = \frac{1}{2ip_y} e^{ip_y(y-y_s)} e^{ip_y(y_s-y_0)} \Psi_p(y_s - y_0), \tag{D.14}$$

where

$$\Psi_p(y) = \begin{cases} e^{-ip_y y} + \rho(p_y) e^{ip_y y} & y \geq 0 \\ \tau(p_y) e^{-ip'_y y} & y < 0 \end{cases} \tag{D.15}$$

and it was used that $\tilde{\tau}(p_y)/p'_y = \tau(p_y)/p_y$. Assuming $e^{ip_y(y_s-y_0)}\Psi_p(y_s - y_0)$ is constant or a slowly varying function of $\vec{p}$, the Green function for large distances ($|\vec{r} - \vec{r}_s| >> \bar{\lambda}$) becomes [66]:

$$G^{(+)}(\vec{r}, \vec{r}_s) = G_0(\vec{r} - \vec{r}_s) e^{ip_y(y_s-y_0)} \Psi_p(y_s - y_0), \tag{D.16}$$

where now $\vec{p} = \bar{k}(\vec{r} - \vec{r}_s)/\left|\vec{r} - \vec{r}_s\right|$. If $y_s < y_0$ the condition for a constant or slowly varying value of $e^{ip_y(y_s-y_0)}\Psi_p(y_s - y_0)$, comes down to $\left|(p_y - p'_y)(y_s - y_0)\right| \ll 1$, so that either the sample surface structure should not be too high $p_y(y_s - y_0) < 1$ or $p_y(y_s - y_0) > k_c^2$. These conditions start to overlap when $k_c(y_s - y_0) \approx 1$, hence as long as $k_c(y_s - y_0) \ll 1$ these conditions are fulfilled for all p_y. This condition will certainly not hold for the non-diffuse component of the scattering as then the integral over $y_s - y_0$ extends from $-\infty$ to 0. The same result under the same conditions can be derived by using the method of *stationary phase for double integrals* as discussed by Mandel [1].

D.2 Wavevector distribution of scattered mutual coherence function

The scattered-wave function given by equation (D.1) due to the undisturbed potential $V^{(0)}$ becomes:

$$\psi_{sc}^{(0)}(\vec{k}, \vec{r}) = \int \psi_0(\vec{k}_\parallel) \rho(k_y) e^{i\vec{k}_\parallel \cdot \vec{r}} e^{-ik_y y} d^2 k_\parallel, \tag{D.17}$$

where in the far-zone the interference between the incident beam and the scattered beam is ignored. Using the wavevector representation of the Green function derived in the previous section and equation (6.74) for the incident-wave function, the scattered-wave function

given by equation (D.1) due to the disturbed potential $V^{(1)}$ becomes

$$\psi_{sc}^{(1)}(\vec{k},\vec{r}) = -\frac{m}{i\hbar^2 4\pi^2}\int\int \psi_0(\vec{k}_\parallel)e^{i(\vec{k}_\parallel-\vec{p}_\parallel)\cdot\vec{r}_s}e^{i\vec{p}\cdot\vec{r}}\frac{\Psi_k(y_s)\Psi_p(y_s)}{p_y}V^{(1)}(\vec{r}_s)d^3r_s d^2p_\parallel, \tag{D.18}$$

and integrated over all possible contributions:

$$\psi_{sc}^{(1)}(\vec{r},t) = \frac{ime^{-i\omega_k t}}{\hbar^2 4\pi^2}\times \tag{D.19}$$

$$\int\int\int \psi_0(\vec{k}_\parallel)e^{i\vec{p}\cdot\vec{r}+i(\vec{k}_\parallel-\vec{p}_\parallel)\cdot\vec{r}_s}\frac{\Psi_p(y_s)\Psi_k(y_s)}{p_y}V^{(1)}(\vec{r}_s)d^3r_s d^2p_\parallel d^2k_\parallel.$$

If it is assumed that *close to the sample surface* both the incident mutual coherence function and the scattered one are homogeneous, the wavevector distribution of the scattered mutual coherence function is defined by:

$$W_{sc}(\vec{r}_s,\vec{p}_\parallel) = \int e^{-i\vec{p}_\parallel\cdot\vec{r}_\parallel}\Gamma_{sc}(\vec{r}_s,\vec{r}_s+\vec{r}_\parallel,0)d^2r_\parallel. \tag{D.20}$$

Using the definition of the mutual coherence function and equation (C.7) and inserting the above equation results in:

$$W_{sc}(\vec{r}_s,\vec{p}_\parallel) = W_{sc}^{(0,0)}(\vec{r}_s,\vec{p}_\parallel)+W_{sc}^{(1,0)}(\vec{r}_s,\vec{p}_\parallel)+W_{sc}^{(0,1)}(\vec{r}_s,\vec{p}_\parallel)+W_{sc}^{(1,1)}(\vec{r}_s,\vec{p}_\parallel), \tag{D.21}$$

where

$$W_{sc}^{(a,b)}(\vec{r}_s,\vec{p}_\parallel) = \frac{1}{p_y^2 A_s}\int W_{in}(\vec{r}_s,\vec{k}_\parallel)S_k^{(a,b)}(\vec{p},\vec{k})d^2k_\parallel, \tag{D.22}$$

where the *sample surface structure factors* are defined as:

$$S_k^{(a,b)}(\vec{p},\vec{k}) = \int e^{-i\vec{Q}_\parallel\cdot\vec{r}_\parallel}G_s^{(a,b)}(\vec{p},\vec{k},\vec{r})d^2r_\parallel \tag{D.23}$$

where $\vec{Q}_\parallel = \vec{p}_\parallel - \vec{k}_\parallel$ equals the wavevector transfer parallel to the sample surface. The *sample correlation functions* are defined as:

$$G_s^{(0,0)}(\vec{p},\vec{k},\vec{r}_\parallel) = \frac{R(k_y)p_y^2 A_s}{4\pi^2}, \tag{D.24}$$

$$G_s^{(1,0)}(\vec{p},\vec{k},\vec{r}_\parallel) = \left(\frac{im}{2\pi\hbar^2}\right)^2 V_0\frac{\tau(p_y)^2}{2p_y}\int \Psi_p(y_s)^*\Psi_k(y_s)^*V^{(1)}(\vec{r}_s)^*d^3r_s, \tag{D.25}$$

$$G_s^{(0,1)}(\vec{p},\vec{k},\vec{r}_\parallel) = G_s^{(1,0)}(\vec{p},\vec{k},\vec{r}_\parallel)^* \tag{D.26}$$

and

$$G_s^{(1,1)}(\vec{p},\vec{k},\vec{r}_\parallel) = \left(\frac{m}{2\pi\hbar^2}\right)^2\times \tag{D.27}$$

$$\int\int \Psi_p(y_s)^*\Psi_k(y_s)^*\Psi_p(y_s+y)\Psi_k(y_s+y)V^{(1)}(\vec{r}_s)^*V^{(1)}(\vec{r}_s+\vec{r}_\parallel)d^3r_s dy,$$

D.3 Mutual coherence function at detector position

Using equations (C.17) and (D.22) the mutual coherence function at the detector position becomes:

$$\Gamma_{sc}(\vec{r}_d, \vec{r}_d, 0) = \frac{1}{A_s} \int_{A_s} \frac{1}{4\pi^2 r_{ds}^2} \int W_{in}(\vec{r}_s, \vec{k}_\parallel) S_k(\vec{p}, \vec{k}) d^2k_\parallel d^2r_s. \tag{D.28}$$

This formula is derived under the condition of homogeneous incident and scattered mutual coherence function at the sample position. The homogeneousness must extend over the sample correlation length determined by G_s.

Summary

This book starts with an introduction to coherence theory as applied to neutron scattering. Further, it discusses application of this theory to some neutron scattering techniques. Especially it describes the application to small angle neutron scattering and neutron reflectometry. An extension is given of coherence theory for neutrons to incorporate neutron polarization effects. This extension is used to describe neutron spin echo coding techniques which are the basis for the mentioned applications.

Acknowledgments

This work was financially supported by the *Nederlandse Organisatie voor Wetenschappelijk Onderzoek (NWO)*. This research project has been supported in part by the European Commission under the 6th Framework Program through the Key Action: Strengthening the European Research Area, Research Infrastructures (Contract No. RII3-CT-2003-505925) and by the Austrian Science Fund (Project F 1514).

Further, many thanks to all people at the department of Radiation, Radionuclides and Reactor of Delft University of Technology who have stimulated and encouraged me to write this book.

Index

Published April 2007 by

BonPhysics Research and Investigations B.V.

Laan van Heemstede 38 · P.O. Box 5629

3297 ZG Puttershoek · The Netherlands

to commemorate its establishment 10 years ago.

BonPhysics was founded by Dr. ir. ing. Victor de Haan in 1997.

He observed a growing need for small scale R & D activities.

Companies and government agencies unable to perform these activities themselves

can be confronted with fundamental and/or technical problems.

BonPhysics is able to solves these problems for them.

more information on www.bonphysics.nl